ON SIMPLE AND ACCURATE FINITE ELEMENT MODELS FOR NONLINEAR BENDING ANALYSIS OF BEAMS AND PLATES

A Dissertation

by

YETZIRAH YKSYA URTHALER LAPEIRA

Submitted to the Office of Graduate Studies of
Texas A&M University
in partial fulfillment of the requirements for the degree of

DOCTOR OF PHILOSOPHY

May 2007

Major Subject: Mechanical Engineering

ON SIMPLE AND ACCURATE FINITE ELEMENT MODELS FOR NONLINEAR BENDING ANALYSIS OF BEAMS AND PLATES

A Dissertation

by

YETZIRAH YKSYA URTHALER LAPEIRA

Submitted to the Office of Graduate Studies of
Texas A&M University
in partial fulfillment of the requirements for the degree of

DOCTOR OF PHILOSOPHY

Approved by:

Chair of Committee,	J.N. Reddy
Committee Members,	Steve Suh
	Harry Hogan
	Goong Chen
Head of Department,	Dennis O'Neal

May 2007

Major Subject: Mechanical Engineering

ABSTRACT

On Simple and Accurate Finite Element Models for
Nonlinear Bending Analysis of Beams and Plates. (May 2007)
Yetzirah Yksya Urthaler Lapeira, B.S., Universidad Simon Bolivar;
M.S., Universidad Simon Bolivar
Chair of Advisory Committee: Dr. J.N. Reddy

This study is concerned with the development of simple and accurate alternative finite element models to displacement finite element models for geometrically nonlinear bending analysis of beams and plates. First, a unified corotational beam finite element that incorporates the kinematics of classical as well as refined beam theories, including the Timoshenko and Reddy beam theories, is developed in a single finite element. The governing equations are written in a "corotational" local frame that rotates with the element and with respect to which the standard linear engineering relations between strains and internal forces are valid. The element is based on Lagrange interpolation of the axial displacement, Hermite cubic interpolation of the transverse displacement, and related quadratic interpolation of the rotation, and it does not experience shear locking. The model is verified by comparisons with exact and/or approximate solutions available in the literature. Very good agreement is found in all cases.

Next, a finite element model is developed using a mixed formulation of the first-order shear deformation theory of laminated composite plates. A p-type Lagrangian basis is used to approximate the nodal degrees of freedom that consist of three displacements, two rotations, and three moment resultants. The geometric nonlinearity, in the sense of the von Kàrman, is included in the plate theory. The mixed plate element developed herein is employed in the linear and nonlinear bending analy-

sis of a variety of layered composite rectangular plates. The effects of transverse shear deformation, material anisotropy, and bending-stretching coupling on deflections and stresses are investigated. The predictive capability of the present model is demonstrated by comparison with analytical, experimental, and numerical solutions available in the literature. The model provides an accurate prediction of the global bending response of thin and moderately thick plates subjected to moderate and moderately large rotations. The inclusion of the bending moments at the nodes results in increased accuracy in the computation of stresses over those determined by conventional displacement-based finite element models. The many results presented here for geometrically nonlinear bending analysis of beams and plates should serve as reference for future investigations.

To my own self: You made it, Yetzi!

ACKNOWLEDGMENTS

First of all, I would like to thank God, for giving me life, health and intelligence, for providing me the educational opportunity of studying for a PhD in the United States, and for supplying the necessary support and help through the people I am about to mention.

I cannot fully express my gratitude to my advisor, Professor Reddy, for his constant support during the course of my education. His expert advice as a teacher and researcher, guidance and assistance as a friend, and his example of patience, generosity and selfless concern for his students will always be a source of inspiration in my personal and professional life. I will not forget his words of encouragement when I felt the PhD demands were too overwhelming: 'Yetzi, do not give up on your dreams, you have a bright future in front of you'. I am so fortunate to be counted as one of his students. Thank you Dr. Reddy.

I wish to thank Dr. Steve Suh, Dr. Harry Hogan and Dr. Goong Chen for serving on my PhD committee. Their advice and assistance is greatly appreciated. Special thanks to Dr. Peter Vàlko for giving me the opportunity of working as research assistant in the Petroleum Engineering Department at Texas A & M University, during a semester when my funding sources were scarce. I would also like to acknowledge the financial support of Universidad Simon Bolivar, Venezuela, and the Department of Mechanical Engineering at Texas A & M University.

I am forever indebted to my mother, Delia, and sisters, Carola and Ana for their love, support and sacrifices that have enabled me to walk this journey. They are the engine behind my success and accomplishments. I would also like to extend special thanks to Lorenzo 'papi' Castro, Cristina, Kurt and Tirso, for their continuous support and encouragement.

It is also a pleasure to acknowledge the support of the many wonderful friends who were cheering me up during difficult times: Pedro Viggiani, Rebecca Hernandez, Carissa Randolph, Gisela Lin, Steve Wilson, Sheetal Desai, Peter Popov, Lino and Saudah Hidajat, and Larry and Yanelys Villasmil.

The completion of this work would have not been possible without the love and persistent support of Burak Basaran. Thanks to my BeBe for believing in me, and for bringing balance, perspective, joy and humor into my life.

TABLE OF CONTENTS

CHAPTER Page

LIST OF TABLES

TABLE Page

LIST OF FIGURES

FIGURE Page

FIGURE Page

FIGURE Page

FIGURE Page

CHAPTER I

INTRODUCTION

I.1. Preliminary comments

All physical structures exhibit nonlinear behavior to some extent. They may be made of rubber or plastic materials that do not have a constant elasticity modulus, they may be operating over a range of temperatures where the material behavior is very different from that at ambient temperature (material nonlinearity); or they may be subjected to large displacements and rotations (geometric nonlinearity). In such cases, linear finite element models are not able to predict the structural response accurately. Hence, the development of efficient and accurate nonlinear finite element models becomes crucial.

The present study deals with the development of efficient, simple and accurate finite element models for geometrically nonlinear bending analysis of beams and plates. Firstly, attention is given to the development of corotational shear-deformable beam finite elements with high-rotation capability. Since beams provide simple models for understanding the fundamentals of plate elements, the conducted research should serve as future reference for the derivation of new corotational plate elements. In the second part of the study, focus is given to the formulation of a new mixed plate bending finite element for the analysis of laminated composite beams and plates undergoing moderately large rotations. The following review of literature provides a background for the present study.

The journal model is *Communications in Numerical Methods in Engineering*.

I.2. Corotational finite element models for beams

I.2.1. Background and literature review

Beam structures that undergo large displacements and rotations require a nonlinear analysis. The design of failure-free installation procedures for submarine pipelines [1], dynamic analysis of marine pipes during operation [2], flight simulation of flexible aircraft [3]), and stability analysis of frame structures [4–8], are examples of such applications. The development of accurate and efficient computational procedures to accommodate large rotation capability of beams and frame structures has therefore become a subject of considerable interest among researchers. These procedures can be based on either the classical Lagrangian descriptions of motion [9–13] or they can be derived by using the so-called corotational description of motion [1, 3, 6–8, 14–22]. The attractiveness of the latter resides in the fact that it can be applied to simplify the Lagrangian formulations for large displacements and small strains problems without significant loss of accuracy.

Nonlinear finite element models for thin beams can be formulated using either the continuum approach [9, 23] or the beam-column-theory [4–8, 24, 25], depending on magnitudes of strains and displacements to be accounted for in the formulation. In the latter case (i.e., beam-column theory) it is assumed that the geometric changes are negligible, so that no distinction is made between the Piola-Kirchhoff and Cauchy stresses. The geometric nonlinearity is treated by including the rotation-related quadratic terms in the strain-displacement equations (i.e., the von Kármán nonlinear strains; see Reddy [25, 26]). However, the beam-column finite element in large rotation problems suffers from one inherent drawback: it is restricted to small rotations between two successive load increments during the deformation process. The corotational approach overcomes the aforementioned drawback and provides a

nonlinear framework in which standard linear beam finite elements can be utilized locally.

The origin of the corotational description of motion has its roots in the polar decomposition theorem. According to this theorem, the total deformation of a continuous body can be decomposed into rigid body motion and relative deformation. In the derivation of the finite element, this decomposition is achieved by attaching a local coordinate system to each element so that it rotates with the average rigid body rotation of the element. In this way, the finite rigid body motion part is eliminated from the total displacements. The remaining relative deformation, which is assumed to be small with respect to the local frame, is used for the calculation of strains and element internal nodal forces. As a consequence, the linear beam theory can be used for describing the relative deformation, endowing the method with significant advantages in computational speed and programming simplicity. The nonlinearity is introduced via the coordinate transformation of the local displacements in terms of the displacement components associated with a fixed global coordinate system.

The development of the "corotational" approach has been underway since the early 60's. Argyris [14] introduced this rigid-plus-deformational decomposition concept, which he termed "natural approach", for the calculation of the geometrical stiffness matrices of wings and flanges under membrane and bending stresses. A comprehensive publication on the theory and other applications of this method can be found in [16]. Wempner [27] also applied the same idea for the study of finite rotations of flexible shells. Some initial contributions using the corotational approach are also reported by Belytschko [15] on nonlinear transient analysis of beams, and by Oran [6, 7] on large deformation and stability analysis of frame structures. In a later paper, Belytschko and Glaum [17] introduce the term 'corotational' to refer to the motion of the local coordinate system attached to the element. Afterwards, most of

the articles published on the subject have adopted the same terminology.

I.2.2. Present study

In the derivation of corotational beam elements, the Euler-Bernoulli beam theory has been commonly used to model the kinematics of the beam. However, the Euler-Bernoulli beam theory fails to give accurate results when the length-to-thickness ratio is relatively small. This is because the effect of transverse shear strains, neglected in the classical theory, becomes significant in deep beams. Very few publications on corotational formulations based on shear deformation beam theories have been reported. Crisfield [28] outlines the procedure to calculate the tangent stiffness matrix and residual force vector for a corotational two-dimensional Timoshenko beam element; however numerical tests to validate the method were not provided therein. More recently, Iura and Suetake [20] have published a paper on the accuracy of three-dimensional Timoshenko beam elements using the corotational approach.

Motivated by the above considerations, the derivation of a new corotational finite element model for nonlinear bending analysis of beams is also undertaken in the present study [22]. The significant and novel contributions of the proposed model can be summarized as follows:

- Three different theories to model the kinematic behavior of beams are considered: The classical Euler-Bernoulli beam theory (EBT), the Timoshenko beam theory (TBT) [26, 29], and the simplified Reddy beam theory (RBT) [30, 31].
- The unified linear finite element model of beams developed by Reddy [32] is extended to nonlinear analysis.
- The shear-locking is resolved by using appropriate approximation functions for the generalized displacements, i.e. Lagrange interpolation of the axial displace-

ment, Hermite cubic interpolation of the transverse displacement, and interdependent quadratic interpolation of the rotation.

- The model is applied in problems with severe geometric nonlinearity (large rotations).

I.3. Mixed finite element models of laminated composites

I.3.1. Background and literature review

Fiber-reinforced composite materials are widely used in many engineering structures. The applications range from medical prosthetic devices to sports equipment, electronics, automotive parts, to light-weight aircraft structures. Composite structures offer many advantages over conventional materials, owing to their high strength-to-weight and stiffness-to-weight ratios.

The analysis of laminated plates is a non-trivial task and it can still be considered an open research problem. Their complex structural behavior is attributed to their anisotropic response, significant shear deformation in the thickness direction and extension-bending coupling. A satisfactory laminate theory and a reliable finite element model have to capture all these effects.

Based on geometrical considerations, concerning the small dimension of the thickness in comparison with the in-plane dimensions, composite plates are usually analyzed through two-dimensional models, also known as *laminated plate theories or equivalent single-layer theories*(ESL). In a laminated plate theory, the laminate is assumed to be in a state of plane stress and the individual laminae are assumed to be elastic and perfectly bonded. The laminate properties are obtained by integrating the lamina properties through the thickness. Accordingly, the laminate is reduced to a single-layer plate with an equivalent anisotropic response.

A simple equivalent single-layer laminated plate theory is the classical laminate plate theory (CLPT) [33–35]. It represents an extension of the classical Kirchhoff-Love plate theory to anisotropic laminated plates. Despite its simple formulation, the CLPT theory does not account for transverse shear strains, and therefore results inadequate for the prediction of the global response of thick plates. The transverse shear deformation effects are even more pronounced in the case of composite plates, due to the low transverse shear modulus relative to the in-plane Young's moduli. A reliable prediction of the response characteristics of high modulus composite plates requires the use of shear deformable theories.

Several shear deformation plate theories are available in the literature [36–38]. The Reissner-Mindlin theory, also known as the first-order shear deformation theory (FSDT), assumes a constant state of transverse shear strains along the plate thickness and allows the use of C^0 approximation functions. A generalization of this theory to arbitrarily laminated anisotropic plates is due to Yang et al. [39] and Whitney and Pagano [40] . When using FSDT to model a plate, shear correction factors are introduced to correct for the discrepancy between the actual parabolic transverse shear stress distribution and those computed using the kinematics assumptions of the FSDT. Higher-order plate theories (HSDT) [41, 42] provide a slight increase in accuracy relative to the FSDT solution, at the expense of a significant increase in computational effort. Furthermore, finite element models of high-order theories require C^1 interpolation functions to satisfy the continuity requirements and the vanishing condition of transverse shear stresses on the top and bottom surfaces of the plate. Of all the equivalent-single layer theories, FSDT provides the best compromise between economy, simplicity and accuracy in the prediction of the global response of thin to moderately thick laminates [43–45].

A number of analytical solutions of classical and refined laminated plate theories

have been proposed by several authors [45–52]. Nevertheless, exact solutions cannot be developed when complex geometries, arbitrary boundary conditions and lamination schemes or nonlinearities are involved. The use of approximate solutions, such as the finite element method, becomes mandatory in such cases.

Finite element formulations for the bending of laminated plates have been traditionally derived from the principle of virtual displacements or the principle of minimum total potential energy. Displacement-based finite element models of the classical plate theory require the use of C^1 interpolation functions, which are computationally expensive, in order to guarantee continuity of transverse deflections and its derivatives across the element boundaries.

To overcome the stringent continuity requirements placed by the conventional variational formulations, the so-called "*mixed variational formulations*" are often used as an alternate approach (see [53–57] for an exhaustive review). The phrase "mixed" is used to imply the fact that both displacement and force variables are given equal importance in the variational formulation. In finite element models constructed under mixed variational principles, displacements and stress resultants are treated as independent variables, thus allowing the use of C^0 interpolation functions. The superiority of C^0-formulated plate elements in linear and non-linear analysis has been shown in many published papers [58–60].

The advantages of the mixed formulations over traditional variational formulations include the relaxation of inter-element continuity requirements, accurate representation of stresses, reduced formulative effort and the ease with which the model can be applied to non-linear and other complicated problems [43, 61].

The use of independent approximation of displacements and bending moments in plate bending elements was first proposed independently by Herrmann [62] and Hellan [63]. Following Herrmann's work, a number of papers were published in the

literature on mixed finite element models [64–67]. Reddy and Tsay [68, 69] used rectangular elements based on Reissner-type variational principles to analyze bending, stability and vibration of linear isotropic and orthotropic plates. The aforementioned models were based on the kinematic assumptions of the classical plate theory, and the effect of shear strains was not considered therein.

Several mixed finite elements have been successfully derived and applied in the bending analysis of shear deformable plates. Putcha and Reddy [70] derived a mixed shear flexible finite element consisting of three displacements, two rotations and three bending moments. Results were presented for linear bending analysis of laminated anisotropic plates. Pinsky and Jasti [71] proposed the use of additional bubble functions in the approximation of displacements and transverse shear stresses, in order to eliminate the effect of shear locking. Bathe and Dvorkin [72] derived a mixed plate bending element, also known in the literature as the "MITC" element, which included the transverse displacement, section rotations and transverse shear strains as nodal degrees of freedom. However, the results presented therein were limited to isotropic plates. Pontaza and Reddy [73] developed a finite element formulation for the bending of thin and thick orthotropic plates based on a least-squares variational principle. In a recent article [74], Auricchio and co-workers have discussed the application of a mixed FSDT finite element in the analysis of monoclinic plates, based on a mixed-enhanced formulation derived earlier by the same author for laminated composites [75].

The models mentioned above did not take into account geometric nonlinearities. To the best of the author's knowledge, only the following attempts can be cited with regards to the use of mixed finite elements in nonlinear bending analysis of laminated plates in the context of ESL shear deformation theories. The first account is that by Putcha and Reddy [61, 76] who formulated a mixed finite element based on a refined

high-order shear deformation theory HSDT for laminated composite plates developed by the second author [41, 42]. The geometric nonlinearity was incorporated via the von Kàrman strains and reduced integration was used to alleviate the shear-locking effect. The formulation yielded an accurate representation of the transverse shear stresses through the thickness, at the expense of an increase in the number of degrees of freedom (i.e. three displacements, two rotations and six moment resultants) when compared to classical plate elements (three displacements, two rotations and three moment resultants). A similar formulation for laminated beams based on a high-order shear deformation theory was proposed by Singh et. al [77]. In their work, both in-plane and shear strains were included as field variables resulting in a element with twelve degrees of freedom per node.

Apparently, there are no reports on the use of the first-order shear theory in the development of mixed finite elements for nonlinear bending analysis of laminated plates. One of the objectives of this work is to derive such an element.

I.3.2. Present work

The bibliographic review discussed above reveals that FSDT gives the best compromise between prediction capability and computational costs for a wide class of problems. The literature also shows that finite elements based on mixed variational formulations have the advantage of yielding accurate bending moments and stresses, when compared to the displacement finite elements. The present study, motivated by these findings, deals with the development of a new mixed finite element for the nonlinear bending analysis of laminated plates based on the first-order shear deformation theory.

The proposed formulation allows the use of C^0 interpolation functions in the finite

element model. The element has eight degrees of freedom per node, which include three displacement components, two shear rotations and three moment resultants. Geometrical nonlinearities in the von Kàrman sense are included in the governing equations, thus allowing analysis of moderately large rotations problems. Attention herein is restricted to plates made of linear-elastic materials and subjected to static conservative loads.

In recent years high-order finite elements have been introduced and successfully applied to eliminate the locking in the numerical solution of plate bending problems [73, 78–80]. This shortcoming can also be remedied by using low-order elements and reduced integration techniques. In this work both approaches are implemented and the behavior of the element is compared under both cases.

The performance of the element in terms of convergence and accuracy is assessed via several numerical tests. The solution of the nonlinear system of equations is carried out using a Newton-Raphson iterative scheme. The effect of length-to-thickness ratio, lamination scheme, number of layers, lamination angle and boundary conditions on the mechanical behavior of anisotropic plates and beams is investigated. Results are compared with closed-form solutions and displacement-based finite element models available in the scientific literature.

The model presented here differs from previous mixed FE models for laminated plates in the following ways:

- The development of mixed plate finite elements based on FSDT is extended to nonlinear bending problems of anisotropic laminated plates.
- The proposed model offers the flexibility of improving the accuracy of displacements and stresses by using h- and p-refinement.
- The numerical shear locking is resolved using low-order elements with reduced

integration and high-order elements with full integration. A comparison of the performance of the element under both cases is carried out.

- The formulation is simple and has a greater physical appeal when compared with formulations that neglect the transverse shear strains, such as those based on CLPT.

- Another desirable feature of the present finite element is the reduction of nodal degrees of freedom per node in comparison with mixed finite elements based on HSDT. Moreover, the additional unknowns introduced by higher-order theories are often difficult to interpret in physical terms.

The dissertation is organized as follows. Details on the corotational formulation for beams and corresponding numerical results are given in Chapters II and III, respectively. Chapter IV provides a complete description of the mixed finite element formulation for laminated composite plates. Linear and nonlinear results obtained with the aforementioned formulation are presented in Chapter V. Conclusions derived from this study and guidelines for future research are discussed in Chapter VI.

CHAPTER II

A COROTATIONAL BEAM FINITE ELEMENT

II.1. Preliminary comments

In the linear description of the motion of beams it is assumed that the displacements are very small and that the material is linearly elastic. In addition, the equilibrium equations are derived using the undeformed configuration of the body due to the fact that geometry does not change with the loading. However, in geometrically nonlinear analysis of structures, geometric changes are significant and the geometry of the body must be updated during the deformation process. Consequently, it becomes necessary to distinguish between various measures of stress and strain, and description of motion. In the *Lagrangian description*, the motion of the body is either referred to the initial undeformed configuration (*total Lagrangian description*) or to the latest known configuration (*updated Lagrangian description*). On the other hand, in the *Corotational description*, the motion of the body is decomposed into rigid body motion and relative deformation. The latter approach provides a nonlinear framework in which linear measures of stress and strain can be applied locally (i.e. Cauchy stress and linearized strain, respectively), thus simplifying the Lagrangian governing equations without significant loss in accuracy. For this reason, the corotational is gaining popularity among the engineering community for the nonlinear analysis of both planar and spatial beam structures.

In this chapter a two-dimensional corotational beam finite element will be derived using a linear unified beam model (see Reddy [32]). The present development is based on the assumption that the material is linearly elastic and the displacements and rotations are arbitrarily large.

II.2. A review of beam theories

Several theories can be found in the literature to represent the kinematic behavior of beams. The classical Euler-Bernoulli beam theory (EBT) which neglects the effect of transverse shear strain is the simplest of such theories. However, the EBT fails to provide accurate results when the thickness-to-length ratio is relatively large. In such cases, the shear deformation theories, namely, the first-order shear deformation beam theory of Timoshenko (TBT) and the third-order beam theory of Reddy (RBT) exhibit more accurate solutions. In addition, RBT des nt require the shear correction factor.

The corotational beam finite element formulation derived in the present work is based on both classical and shear deformation theories. Towards this end we present a summary of the aforementioned beam theories, their inter-relationships and the unified beam finite element model developed by Reddy [32].

II.2.1. Governing equations

The simplest and most commonly used beam theory is the classical Euler-Bernoulli beam theory(EBT), which is based on the displacement field

$$\begin{aligned} u^E(x,z) &= -z\frac{dw_0^E}{dx} \\ w^E(x,z) &= w_0^E(x) \end{aligned} \tag{2.1}$$

where w_0 is the transverse deflection of the point $(x,0)$ of a point on the mid-plane and the superscript "E'' denotes the quantities in the Euler-Bernoulli beam theory. The x-coordinate is taken along the length of the beam,z-coordinate along the height of the beam and the y-coordinate is taken along the width of the beam. The displacement field (2.1) implies that straight lines normal to the mid-plane before deformation

remain straight and normal to the mid-plane after deformation, as shown in Figure 1a. These assumptions amount to neglecting both transverse shear and transverse normal effects, i.e., deformation is due to bending and in-plane stretching.

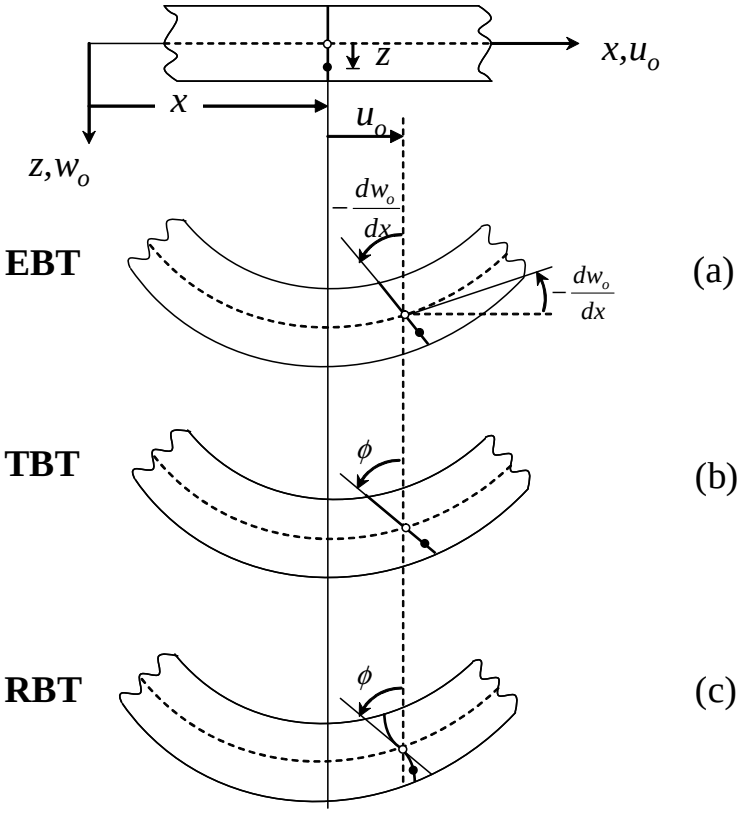

Fig. 1. Deformation of a transverse normal line in various beam theories.

The next theory in the hierarchy is the first-order shear deformation beam theory of Timoshenko(TBT), which is based on the displacement field

$$u^T(x,z) = z\phi^T(x)$$
$$w^T(x,z) = w_0^T(x) \tag{2.2}$$

where ϕ denotes the rotation of the cross section and the superscript "T" denotes the

quantities in the Timoshenko beam theory. In this theory the normality assumption of the Euler-Bernoulli beam theory is relaxed by assuming that the rotation is independent of the slope of the beam (see Figure 1b). In addition, the shear strain state is assumed to be constant with respect to the height of the beam. Therefore, the Timoshenko beam theory requires a shear correction factor to compensate for errors due to this assumption.

Next, we consider the third-order beam theory of Reddy. The corresponding displacement field accommodates quadratic variation of the transverse shear strain and stresses and removes the straightness assumption of the Euler-Bernoulli beam theory (see Figure 1c)

$$\begin{aligned} u^R(x,z) &= z\phi^R(x) - z^3\alpha\left(\phi^R + \frac{dw_0}{dx}\right) \\ w^R(x,z) &= w_0^R(x) \end{aligned} \tag{2.3}$$

where the superscript "R" denotes the quantities in the Reddy beam theory (RBT)and $\alpha = 4/(3h^2)$. For this theory there is no need to use shear correction factors.

The bending equations of equilibrium and stress resultant-displacement relations of the three beam theories considered in this study are summarized below for constant material and geometric properties:

- *The Euler-Bernoulli Beam Theory* (EBT)

$$\frac{d^2M_{xx}^E}{dx^2} = -q(x), \qquad M_{xx}^E = -D_{xx}\frac{d^2w_0^E}{dx^2} \tag{2.4}$$

- *The Timoshenko Beam Theory* (TBT)

$$\begin{aligned} \frac{dM_{xx}^T}{dx} &= Q_x^T, & \frac{dQ_{xx}^T}{dx} &= -q(x) \\ M_{xx}^T &= D_{xx}\frac{d\phi^T}{dx}, & Q_x^T &= A_{xz}K_s\left(\phi^T + \frac{dw_0^T}{dx}\right) \end{aligned} \tag{2.5a}$$

- *The Reddy Beam Theory* (RBT)

$$\frac{dM_{xx}^R}{dx} = Q_x^R + \alpha\frac{dP_{xx}}{dx} - \beta R_x \tag{2.6a}$$
$$\frac{dQ_x^R}{dx} = q(x) + \beta\frac{dR_{xx}}{dx} - \alpha\frac{d^2P_{xx}}{dx^2} \tag{2.6b}$$
$$M_{xx}^R = D_{xx}\frac{d\phi^R}{dx} - \alpha F_{xx}\left(\frac{d\phi^R}{dx} + \frac{d^2w_0^R}{dx^2}\right) \tag{2.6c}$$
$$Q_x^R = \bar{A}_{xz}\left(\phi^R + \frac{dw_0^R}{dx}\right) \tag{2.6d}$$
$$P_{xx} = F_{xx}\frac{d\phi^R}{dx} - \alpha H_{xx}\left(\frac{d\phi^R}{dx} + \frac{d^2w_0^R}{dx^2}\right) \tag{2.6e}$$
$$R_x = \bar{D}_{xz}\left(\phi^R + \frac{dw_0^R}{dx}\right) \tag{2.6f}$$

where the stiffness parameters are defined as

$$D_{xx} = E_x I_{yy}^{(2)}, \qquad F_{xx} = E_x I_{yy}^{(4)} \tag{2.7a}$$
$$H_{xx} = E_x I_{yy}^{(6)}, \qquad A_{xz} = G_{xz}A \tag{2.7b}$$
$$D_{xz} = G_{xz} I_{yy}^{(2)}, \qquad F_{xz} = G_{xz} I_{yy}^{(4)} \tag{2.7c}$$
$$\hat{D}_{xx} = D_{xx} - \gamma F_{xx}, \qquad \hat{F}_{xx} = F_{xx} - \gamma H_{xx} \tag{2.7d}$$
$$\hat{A}_{xz} = A_{xz} - \beta D_{xz}, \qquad \hat{D}_{xz} = D_{xz} - \beta F_{xz} \tag{2.7e}$$
$$\bar{D}_{xx} = \hat{D}_{xx} - \gamma \hat{F}_{xx}, \qquad \bar{A}_{xz} = \hat{A}_{xz} - \beta \hat{D}_{xz} \tag{2.7f}$$
$$\gamma = \frac{4}{3h^2}, \qquad \beta = 3\gamma = \frac{4}{h^2} \tag{2.7g}$$

where $I_{yy}^{(i)}$ denotes the ith area moment of inertia about the y-axis, A is the area of the cross section, h is the thickness of the beam, E_x is the elasticity modulus, G_{xz} the shear modulus and K_s the shear correction coefficient. For beams made of an isotropic material, we have $D_{xx} = EI$, $A_{xx} = EA$.

The Euler-Bernoulli beam theory (EBT) and the Timoshenko beam theory (TBT) are fourth-order theories whereas the Reddy beam theory (RBT) is a sixth-order the-

ory. Therefore, the relationships between the exact solutions of these theories can only be found by solving an additional second order differential equation (see [44]). A simplification of RBT can be made by reducing the order of the theory from sixth to fourth which is achieved by dropping the second-derivative term in the additional differential equation for w_0^R. In the following section a summary of the relations between the EBT, TBT and simplified RBT is presented.

II.2.2. Summary of the bending relations between the EBT, TBT and RBT

The relationships between TBT and simplified RBT in terms of the EBT developed by Reddy et.al [44], can be expressed in one set of equations as follows

$$V_x^U(x) = Q_x^E(x) + C_1 \tag{2.8}$$

$$M_{xx}^U(x) = M_{xx}^E(x) + C_1 x + C_2 \tag{2.9}$$

$$D_{xx}\theta^U(x) = -D_{xx}\frac{dw_0^E}{dx} + C_1\frac{x^2}{2} + C_2 x + C_3 \tag{2.10}$$

$$\begin{aligned} D_{xx}w_0^U(x) = {} & D_{xx}w_0(x) + \mathcal{A}M_{xx}^E(x) \\ & - C_1\left(\frac{x^3}{6} - \mathcal{A}x\right) - C_2\left(\frac{x^2}{2} - \mathcal{B}\right) - C_3 x - C_4 \end{aligned} \tag{2.11}$$

where the superscript "U" denotes the quantities belonging to either the Timoshenko beam theory ($\alpha = 0$) or the Reddy-Bickford beam theory ($\alpha \neq 0$). The slope θ^U has a different meaning for each theory, as defined below

$$\theta^U = \begin{cases} \psi^T & \text{for TBT} \\ \theta^U = \dfrac{\bar{D}_{xx}\phi_R}{D_{xx}} - \alpha F_{xx}\dfrac{dw_0^R}{dx} & \text{for simplified RBT} \end{cases} \tag{2.12}$$

$$\mathcal{A} = \begin{cases} \dfrac{D_{xx}}{A_{xz}K_s} & \text{for TBT} \\ \\ \dfrac{\hat{D}_{xx}}{A_{xz}} & \text{for simplified RBT} \end{cases} \tag{2.13}$$

$$\mathcal{B} = \begin{cases} 0 & \text{for TBT} \\ \\ \dfrac{\hat{D}_{xx}}{\hat{A}_{xz}} & \text{for simplified RBT} \end{cases} \tag{2.14}$$

II.2.3. A unified finite element model of beams

Based on the foregoing relationships, Reddy derived the stiffness matrix of a unified beam element (UBE) that incorporates the kinematics of all three theories. This amounts to using Hermit cubic interpolation for the transverse deflection w_0 and a dependent interpolation for the slope ϕ, resulting in a efficient and accurate locking-free finite element for the analysis of beams. Note that the Timoshenko beam element derived from this procedure corresponds to the *Interdependent Interpolation Element* (IIE) (see [31]).

The complete unified beam finite element model is given by

$$\frac{2D_{xx}}{\mu L^3}\begin{bmatrix} 6 & 3L & -6 & 3L \\ 3L & 2L^2\lambda & -3L & L^2\xi \\ -6 & -3L & 6 & -3L \\ 3L & L^2\xi & -3L & 2L^2\lambda \end{bmatrix}\begin{Bmatrix} \Delta_1 \\ \Delta_2 \\ \Delta_3 \\ \Delta_4 \end{Bmatrix} = \begin{Bmatrix} q_1 \\ q_2 \\ q_3 \\ q_4 \end{Bmatrix} + \begin{Bmatrix} Q_1 \\ Q_2 \\ Q_3 \\ Q_4 \end{Bmatrix} \tag{2.15}$$

where

$$\Omega = \frac{\mathcal{A}}{L^2 - 6\mathcal{B}}, \qquad \mu = 1 + 12\Omega \tag{2.16}$$

$$\lambda = 1 + 3\Omega, \qquad \xi = 1 - 6\Omega \tag{2.17}$$

and the load vector due to the distributed load $q(x)$

$$q_i^e = \int_0^L q(x)\varphi_i(x)dx \tag{2.18}$$

with $\varphi_i(x)$ being the Hermite interpolation functions.

Figure 2 shows the sign convention used for the generalized displacements and forces, which are defined as

$$w_0(x) = \Delta_1, \qquad \theta(0) = \Delta_2 \tag{2.19a}$$

$$w_0(L) = \Delta_3, \qquad \theta(L) = \Delta_4 \tag{2.19b}$$

$$Q_1 \equiv -V_x^U(0), \qquad Q_2 \equiv -M_{xx}^U(0) \tag{2.19c}$$

$$Q_3 \equiv -V_x^U(L), \qquad Q_4 \equiv -M_{xx}^U(L) \tag{2.19d}$$

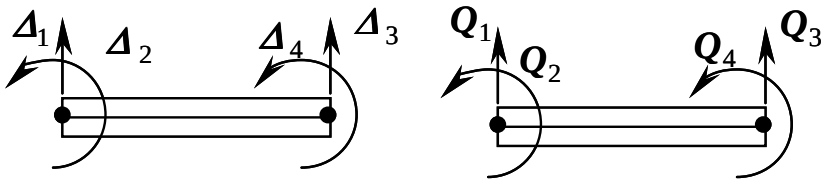

(a) Nodal Displacements (b) Nodal Forces

Fig. 2. Generalized displacements and forces of a typical unified beam finite element.

For frame structures the element stiffness matrix corresponds to the superposition of the bar element with the unified beam element, which gives

$$\mathbf{K} = \frac{2D_{xx}}{\mu L^3}\begin{bmatrix} \kappa & 0 & 0 & -\kappa & 0 & 0 \\ 0 & 6 & 3L & 0 & -6 & 3L \\ 0 & 3L & 2L^2\lambda & 0 & -3L & L^2\xi \\ -\kappa & 0 & 0 & \kappa & 0 & 0 \\ 0 & -6 & -3L & 0 & 6 & -3L \\ 0 & 3L & L^2\xi & 0 & -3L & 2L^2\lambda \end{bmatrix}, \quad \kappa = \frac{\mu A_{xx} L^2}{2D_{xx}} \tag{2.20}$$

II.3. The corotational formulation

II.3.1. Geometric considerations

We consider a plane, straight, prismatic beam with two nodes. The element is assumed to be initially aligned with the global x axis. The key concept of the corotational description is the decomposition of the the total motion of a continuous body into rigid body motion and relative deformation. In the derivation of the finite element, this decomposition is achieved by attaching a local coordinate system to each element so that it rotates with the average rigid body rotation of the element. In this way, the finite rigid body motion part is eliminated from the total displacements. The remaining relative deformation, which is assumed to be small with respect to the local frame, is used for the calculation of strains and element internal nodal forces. Hence, standard small-strain measures can be applied to obtain simplified governing equations which in turn provide significant computational advantages. The local or

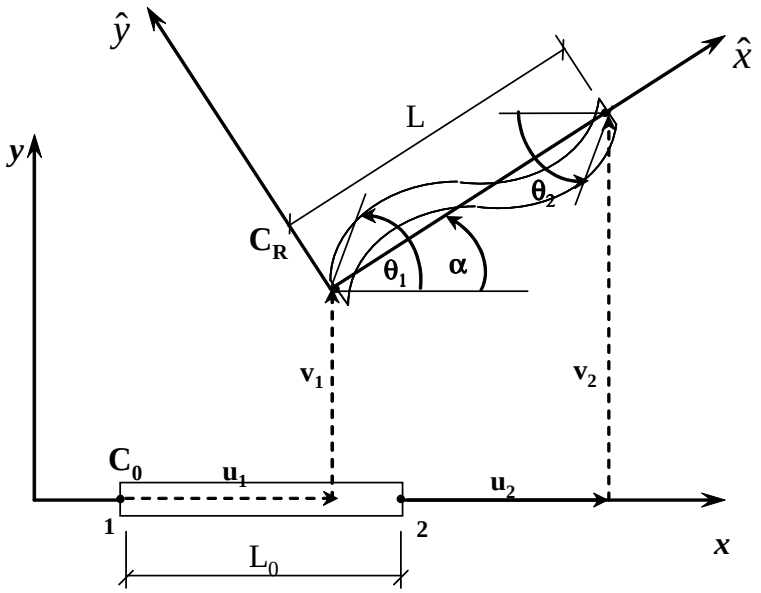

Fig. 3. Kinematics of the corotational Euler-Bernoulli beam element

corotated coordinate system $(\hat{x}, \hat{y})$ for the beam element is attached to the element and defined so that the $\hat{x}$ axis remains coincident with a line joining the end points of the element, as shown in Figure 3. Quantities with a "hat" will be used throughout this work to denote quantities measured in the corotated coordinate system. The position of the corotated frame is updated with the nodal displacements of the last known deformed configuration by using trigonometric relations as follows

$$c_\alpha = \cos(\alpha) = \frac{L_0 + u_2 - u_1}{L}, \quad s_\alpha = \sin(\alpha) = \frac{v_2 - v_1}{L} \tag{2.21}$$

where L_0 is the original length of the undeformed element and L is the current length.

For a linear unified beam element, the axial displacement $\hat{u_0}(\hat{x})$ and transverse deflection $\hat{w_0}(\hat{x})$ are interpolated as

$$\hat{u_0}(\hat{x}) = \sum_{j=1}^{2} \hat{u}_j \psi_j(\hat{x}) \quad \hat{w_0}(\hat{x}) = \sum_{j=1}^{4} \Delta_j \phi_j(\hat{x}), \hat{u}_1 = \hat{u_0}(\hat{x_1}), \quad \hat{u}_2 = \hat{u_0}(\hat{x_2}) \tag{2.22a}$$

$$\Delta_1 = \hat{w_0}(\hat{x_1}), \quad \Delta_2 = \theta(\hat{x_1}), \quad \Delta_3 = \hat{w_0}(\hat{x_2}), \quad \Delta_4 = \theta(\hat{x_2}) \tag{2.22b}$$

where ψ_j are the linear Lagrange interpolation functions, and ϕ_j are the Hermite interpolation functions. For our choice of local coordinate system, the axial displacement of node 1 and the transverse displacements at both nodes will be equal to zero. The global and local displacements are collected in vectors $\mathbf{u}$ and $\hat{\mathbf{u}}$, where u_l is the local elongation of the neutral axis of the beam

$$\hat{\mathbf{u}} = \begin{Bmatrix} 0 \\ 0 \\ \hat{\theta_1} \\ u_l \\ 0 \\ \hat{\theta_2} \end{Bmatrix}, \quad \mathbf{u} = \begin{Bmatrix} u_1 \\ w_1 \\ \theta_1 \\ u_2 \\ w_2 \\ \theta_2 \end{Bmatrix} \tag{2.23}$$

The sign convention used for the beam global displacements is shown in Figure 4,

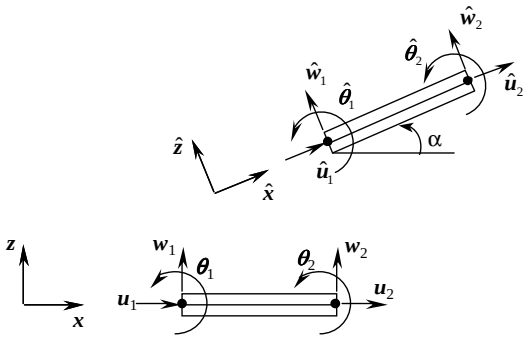

Fig. 4. Nodal displacements in the global frame.

and the relationship between the global and local degrees of freedom is found to be

$$\hat{\mathbf{u}} = \begin{bmatrix} c_\alpha & s_\alpha & 0 & 0 & 0 & 0 \\ -s_\alpha & c_\alpha & 0 & 0 & 0 & 0 \\ 0 & 0 & 1 & 0 & 0 & 0 \\ 0 & 0 & 0 & c_\alpha & s_\alpha & 0 \\ 0 & 0 & 0 & -s_\alpha & c_\alpha & 0 \\ 0 & 0 & 0 & 0 & 0 & 1 \end{bmatrix} \begin{Bmatrix} 0 \\ 0 \\ \theta_1 \\ u_{21} \\ w_{21} \\ \theta_2 \end{Bmatrix} + \begin{Bmatrix} 0 \\ 0 \\ -\alpha \\ L_0(c_\alpha - 1) \\ s_\alpha u_{21} - c_\alpha w_{21} \\ -\alpha \end{Bmatrix} \tag{2.24}$$

where $u_{21} = u_2 - u_1$ and $w_{21} = w_2 - w_1$ and

$$\begin{bmatrix} c_\alpha & s_\alpha & 0 & 0 & 0 & 0 \\ -s_\alpha & c_\alpha & 0 & 0 & 0 & 0 \\ 0 & 0 & 1 & 0 & 0 & 0 \\ 0 & 0 & 0 & c_\alpha & s_\alpha & 0 \\ 0 & 0 & 0 & -s_\alpha & c_\alpha & 0 \\ 0 & 0 & 0 & 0 & 0 & 1 \end{bmatrix} \tag{2.25}$$

denotes the transformation matrix from the local to the global coordinate system.

II.3.2. Equilibrium equations

The finite element approximation of the nonlinear equilibrium equations of geometrically nonlinear problems can be written in the general form

$$\mathbf{p} = \mathbf{K}(\mathbf{u})\mathbf{u} = \mathbf{f} \tag{2.26}$$

where $\mathbf{p}$ is the internal force vector, $\mathbf{f}$ the external force vector and $\mathbf{K}$ the direct stiffness matrix which is a function of the displacement vector $\mathbf{u}$. The geometric nonlinearity is fully introduced by the coordinate transformation between the local and global nodal degrees of freedom.

An incremental iterative procedure based on the Newton-Raphson method is adopted in this work. Therefore, (2.26) is linearized, yielding the following set of tangent stiffness equations

$$\mathbf{K}_T(\mathbf{u})\Delta\mathbf{u} = \mathbf{r} \tag{2.27}$$

where $\mathbf{K}_T$ is the so-called tangent stiffness matrix and $\mathbf{r}$ corresponds to the residual force vector.

For a beam element, which is regarded as a conservative system, there exists a potential energy function (see [57]) such that

$$\Pi(\mathbf{u}) = U(\mathbf{u}) - W(\mathbf{u}) \tag{2.28}$$

where U and W denote the internal (strain) energy and the external work function in the global frame, respectively. Differentiation of (2.28) with respect to $\mathbf{u}$ yields the residual force vector $\mathbf{r}$

$$\mathbf{r} = \frac{\partial \Pi}{\partial \mathbf{u}} = \frac{\partial U}{\partial \mathbf{u}} - \frac{\partial W}{\partial \mathbf{u}} = \mathbf{p} - \mathbf{f} \tag{2.29}$$

The tangent stiffness matrix $\mathbf{K}_T$ can be expressed in terms of the energy potential as

$$\mathbf{K}_T = \frac{\partial \mathbf{r}}{\partial \mathbf{u}} = \frac{\partial^2 \Pi}{\partial \mathbf{u} \partial \mathbf{u}} \tag{2.30}$$

The next step consists on relating the global residual equilibrium equations (2.27) to the local level where the linear equilibrium equations are valid. The basic assumption is that the energy is invariant with respect to rigid body motions, i.e. $\Pi(\mathbf{u}) = \Pi(\hat{\mathbf{u}})$, where $\hat{\mathbf{u}} = \hat{\mathbf{u}}(\mathbf{u})$. Therefore

$$\mathbf{r} = \frac{\partial \Pi}{\partial \mathbf{u}} = \frac{\partial \Pi}{\partial \hat{\mathbf{u}}} \frac{\partial \hat{\mathbf{u}}}{\partial \mathbf{u}} = \mathbf{T}^T \hat{\mathbf{r}} = \mathbf{p} - \mathbf{f} \tag{2.31}$$

where $\mathbf{T}$ is the transformation matrix defined by

$$T_{ij} = \frac{\partial \hat{u_i}}{\partial u_j} \tag{2.32}$$

The relationship between the local and global internal and external force vectors can be found in a similar fashion

$$\mathbf{p} = \frac{\partial U}{\partial \mathbf{u}} = \frac{\partial U}{\partial \hat{\mathbf{u}}} \frac{\partial \hat{\mathbf{u}}}{\partial \mathbf{u}} = \mathbf{T}^T \hat{\mathbf{p}} \tag{2.33}$$

$$\mathbf{f} = \frac{\partial W}{\partial \mathbf{u}} = \frac{\partial W}{\partial \hat{\mathbf{u}}} \frac{\partial \hat{\mathbf{u}}}{\partial \mathbf{u}} = \mathbf{T}^T \hat{\mathbf{f}} \tag{2.34}$$

The global tangent stiffness matrix corresponds to the sum of the material stiffness matrix, $\mathbf{K}_{T_M}$ and geometric matrix $\mathbf{K}_{T_G}$

$$\mathbf{K}_T = \frac{\partial \mathbf{r}}{\partial \mathbf{u}} = \frac{\partial}{\partial \mathbf{u}} \left[\frac{\partial \Pi}{\partial \hat{\mathbf{u}}} \frac{\partial \hat{\mathbf{u}}}{\partial \mathbf{u}} \right] = \mathbf{T}^T \hat{\mathbf{K}}_T \mathbf{T} + \hat{\mathbf{r}} \cdot \mathbf{G} = \mathbf{K}_{T_M} + \mathbf{K}_{T_G} \tag{2.35}$$

where $\hat{\mathbf{K}}_T$ and $\mathbf{G}$ are second order and third order tensors, respectively, defined as

$$\hat{K}_{Tij} = \frac{\partial^2 \Pi}{\partial \hat{u_i} \partial \hat{u_j}}, \quad G_{ijk} = \frac{\partial^2 \hat{u_i}}{\partial u_i \partial u_j} \tag{2.36}$$

II.3.2.1. Stiffness matrix

The material tangent stiffness matrix can be computed through Equation (2.35) using the transformation matrix $\mathbf{T}$ and the unified linear stiffness matrix given by Reddy [32]

$$\mathbf{K}_{T_M} = \frac{2D_{xx}}{\mu L^3}\begin{bmatrix} c_\alpha^2\kappa + 6s_\alpha^2 & c_\alpha s_\alpha\kappa - 6s_\alpha c_\alpha & -3s_\alpha L \\ c_\alpha s_\alpha\kappa - 6s_\alpha c_\alpha & s_\alpha^2\kappa + 6c_\alpha^2 & 3c_\alpha L \\ -3s_\alpha L & 3c_\alpha L & 2L^2\lambda \\ -c_\alpha^2\kappa - 6s_\alpha^2 & -c_\alpha s_\alpha\kappa + 6s_\alpha c_\alpha & 3s_\alpha L \\ -c_\alpha s_\alpha\kappa + 6s_\alpha c_\alpha & -s_\alpha^2\kappa - 6c_\alpha^2 & -3c_\alpha L \\ -3s_\alpha L & 3c_\alpha L & L^2\xi \end{bmatrix}$$

$$\begin{bmatrix} -c_\alpha^2\kappa - 6s_\alpha^2 & -c_\alpha s_\alpha\kappa + 6s_\alpha c_\alpha & -3s_\alpha L \\ -c_\alpha s_\alpha\kappa + 6s_\alpha c_\alpha & -s_\alpha^2\kappa - 6c_\alpha^2 & 3c_\alpha L \\ 3s_\alpha L & -3c_\alpha L & L^2\xi \\ c_\alpha^2\kappa + 6s_\alpha^2 & c_\alpha s_\alpha\kappa - 6s_\alpha c_\alpha & 3s_\alpha L \\ c_\alpha s_\alpha\kappa - 6s_\alpha c_\alpha & s_\alpha^2\kappa + 6c_\alpha^2 & -3c_\alpha L \\ 3s_\alpha L & -3c_\alpha L & 2L^2\lambda \end{bmatrix}, \quad \kappa = \frac{\mu A_{xx}L^2}{2D_{xx}} \tag{2.37}$$

where

$$\begin{aligned} \Omega &= \frac{\mathcal{A}}{L^2 - 6\mathcal{B}}, & \mu &= 1 + 12\Omega \\ \lambda &= 1 + 3\Omega, & \xi &= 1 - 6\Omega \end{aligned} \tag{2.38}$$

$$\mathcal{A} = \begin{cases} \dfrac{D_{xx}}{A_{xz}K_s} & \text{for TBT} \\ \\ \dfrac{\hat{D}_{xx}}{\bar{A}_{xz}} & \text{for simplified RBT} \end{cases}, \quad \mathcal{B} = \begin{cases} 0 & \text{for TBT} \\ \\ \dfrac{\hat{D}_{xx}}{\bar{A}_{xz}} & \text{for simplified RBT} \end{cases} \tag{2.39}$$

The stiffness parameters are defined as

$$\begin{aligned}
D_{xx} &= E_x I_{yy}^{(2)}, & F_{xx} &= E_x I_{yy}^{(4)} \\
H_{xx} &= E_x I_{yy}^{(6)}, & A_{xz} &= G_{xz} A \\
D_{xz} &= G_{xz} I_{yy}^{(2)}, & F_{xz} &= G_{xz} I_{yy}^{(4)} \\
\hat{D}_{xx} &= D_{xx} - \gamma F_{xx}, & \hat{F}_{xx} &= F_{xx} - \gamma H_{xx} \\
\hat{A}_{xz} &= A_{xz} - \beta D_{xz}, & \hat{D}_{xz} &= D_{xz} - \beta F_{xz} \\
\bar{D}_{xx} &= \hat{D}_{xx} - \gamma \hat{F}_{xx}, & \bar{A}_{xz} &= \hat{A}_{xz} - \beta \hat{D}_{xz} \\
\gamma &= \frac{4}{3h^2}, & \beta &= 3\gamma = \frac{4}{h^2}
\end{aligned} \tag{2.40}$$

where $I_{yy}^{(i)}$ denotes the ith area moment of inertia about the y-axis, A is the area of the cross section, h is the thickness of the beam, E_x is the elasticity modulus, G_{xz} the shear modulus and K_s the shear correction coefficient.For beams made of an isotropic material, we have $D_{xx} = EI$, $A_{xx} = EA$.

The expression for the geometric stiffness matrix can be found similarly using Equation (2.35) and the definitions given in (2.29)

$$\mathbf{K}_{T_G} = \frac{V}{L} \begin{bmatrix}
\sin 2\alpha & -\cos 2\alpha & 0 & -\sin 2\alpha & \cos 2\alpha & 0 \\
-\cos 2\alpha & -\sin 2\alpha & 0 & \cos 2\alpha & \sin 2\alpha & 0 \\
0 & 0 & 0 & 0 & 0 & 0 \\
-\sin 2\alpha & \cos 2\alpha & 0 & \sin 2\alpha & -\cos 2\alpha & 0 \\
\cos 2\alpha & \sin 2\alpha & 0 & -\cos 2\alpha & -\sin 2\alpha & 0 \\
0 & 0 & 0 & 0 & 0 & 0
\end{bmatrix} \tag{2.41}$$

where the shear force V can be found through the equilibrium equations in the corotated frame

$$V = 3\frac{2D_{xx}}{\mu L^2}(\hat{\theta_1} + \hat{\theta_2}) \tag{2.42}$$

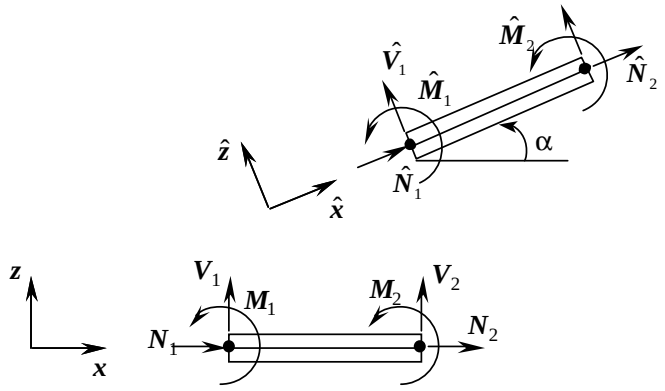

Fig. 5. Internal forces of the beam element in the global frame. The orientation of the arrows depicts positive sign convention.

The internal force vector $\mathbf{p}$ for the corotational element is then obtained by using relation (2.33),

$$\mathbf{p}^a = \left\{ \begin{array}{c} N_1 c_\alpha - V_1 s_\alpha \\ N_1 s_\alpha + V_1 c_\alpha \\ M_1 \\ N_2 c_\alpha - V_2 s_\alpha \\ N_2 s_\alpha + V_2 c_\alpha \\ M_2 \end{array} \right\} \tag{2.43}$$

where N is the axial load, V the shear force and M the bending moment. The axial force N and the shear force V are assumed to be constant along the length of the beam, whereas the bending moment M can vary linearly. The corresponding convention sign is shown in Figure 5.

CHAPTER III

A COROTATIONAL BEAM FINITE ELEMENT: NUMERICAL RESULTS

III.1. Preliminary comments

Several well established benchmark problems are solved to demonstrate the prediction capability of the corotational formulation derived in Chapter II. The effect of shear deformation and boundary conditions in the beam nonlinear response is studied, and a comparison of the numerical performance of classical and shear deformable corotational beam elements is carried out. The corotational beam elements developed on the kinematic assumptions of the EBT, TBT and RBT are denoted by CR-EBT, CR-TBT and CR-RBT, respectively.

The nonlinear system of equations is solved using a Newton-Raphson iteration procedure. Using the Euclidean norm,$\| \, . \, \|_{l^2}$, of a vector $\mathbf{u}$, defined by

$$\| \mathbf{u} \|_{l^2} = \sqrt{\sum_{i=1}^{M} |u_i|^2} \tag{3.1}$$

we terminate the iteration when the Euclidean norm of the relative error between two consecutive solutions $U_i^{(r)}$ and $U_i^{(r-1)}$ drops below a given tolerance ϵ. Thus, the converge criterion is given by

$$\sqrt{\frac{\sum_{i=1}^{N} |U_i^{(r)} - U_i^{(r-1)}|^2}{\sum_{i=1}^{M} |U_i^{(r)}|^2}} \leq \epsilon \tag{3.2}$$

where $U_i^{(r)}$ and $U_i^{(r-1)}$ are the solution vectors from the (r)st and $(r-1)$st iterations, respectively; and M is the number of total nodes in the domain.

The total applied load is divided into load increments of equal size. A tolerance of $\epsilon = 10^{-3}$ and maximum allowable iterations of 30 (per load step) are used in all the numerical examples unless otherwise stated. The initial solution vector is chosen to be the zero vector, in order to recover the linear solution in the first iteration.

III.2. Small strains and moderately large deflections

III.2.1. Beam under uniformly distributed load

Consider a beam of length $L = 100$ in., 1 in.$\times$ 1 in. cross sectional dimensions, made of steel ($E = 30$ msi, $\nu = 0.3$) and subjected to uniformly distributed load of intensity q_0 lb/in. Using the symmetry about $x = L/2$, one half of the domain is used as the computational domain. The following set of geometric boundary conditions are tested:

1. *Hinged at both ends*
$$w_0(0) = u_0(L/2) = \frac{dw_0}{dx}(L/2) = 0. \tag{3.3}$$
2. *Pinned at both ends*
$$u_0(0) = w_0(0) = u_0(L/2) = \frac{dw_0}{dx}(L/2) = 0 \tag{3.4}$$
3. *Clamped at both ends*
$$u_0(0) = w_0(0) = \frac{dw_0}{dx}(0) = u_0(L/2) = \frac{dw_0}{dx}(L/2) = 0 \tag{3.5}$$

The first type of boundary conditions are included in the numerical experimentation in order to verify that the element does not experience membrane locking. The results for this case are compared with the deflections of a pinned-pinned and a clamped-clamped beam, in order to study the effect of the boundary conditions on the nonlinear behavior of the beam.

Table 1 contains the corresponding finite element results for the deflections of all three cases. These results agree reasonably well with the numerical solution reported by Reddy [25] using finite element models based on the Euler-Bernoulli beam theory with the von Karmán nonlinear strain. Figure 6 shows the corotational finite element

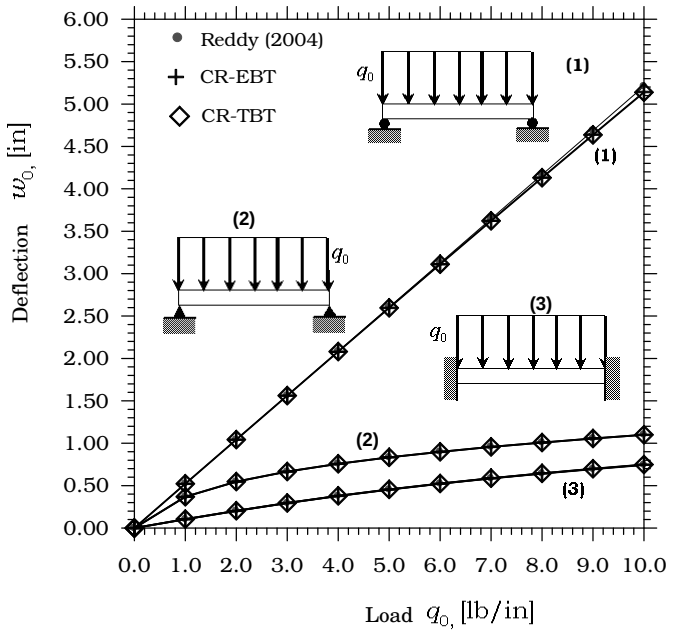

Fig. 6. Comparison of the center deflections of beams subjected to distributed load and with three different boundary conditions.

results for the deflections of the beam for the three aforementioned types of boundary conditions. The hinged-hinged beam exhibit larger transverse displacements than the pinned-pinned and clamped-clamped beams. For this boundary condition, the beam does not have any end constraint on the axial displacement u_0, and hence does not experience axial strain. On the other hand, the pinned-pinned and clamped-clamped beams are constrained from axial movement. As a result, they develop axial strain to accommodate the transverse deflection thus offering larger axial stiffness to stretching.

Table 1. Finite element results for the maximum deflections, w_{max}, of a beam under uniformly distributed load and three different boundary conditions.

Load, q_0	Reddy [25]	CR-EBT	CR-TBT	CR-RBT
		Hinged-hinged		
1.0	0.52083 (3)*	0.52076 (3)	0.52089 (3)	0.52097 (3)
2.0	1.04167 (3)	1.04111 (3)	1.04136 (3)	1.04151 (3)
3.0	1.56250 (3)	1.56061 (3)	1.56100 (3)	1.56121 (3)
4.0	2.08333 (3)	2.07885 (3)	2.07937 (3)	2.07966 (2)
5.0	2.60417 (2)	2.59581 (2)	2.59547 (2)	2.59582 (2)
6.0	3.12500 (2)	3.11045 (2)	3.10972 (2)	3.11013 (2)
7.0	3.64583 (2)	3.62260 (2)	3.62143 (2)	3.62190 (2)
8.0	4.16667 (2)	4.13191 (2)	4.13023 (2)	4.13076 (2)
9.0	4.68750 (2)	4.63803 (2)	4.63576 (2)	4.63635 (2)
10.0	5.20833 (2)	5.14059 (2)	5.13769 (2)	5.13834 (2)
		Pinned-pinned		
1.0	0.36848 (5)	0.36858 (5)	0.36862 (5)	0.36864 (5)
2.0	0.54545 (4)	0.54562 (4)	0.54564 (4)	0.54566 (4)
3.0	0.66407 (3)	0.66426 (4)	0.66426 (3)	0.66428 (3)
4.0	0.75569 (3)	0.75587 (3)	0.75587 (3)	0.75588 (3)
5.0	0.83148 (3)	0.83163 (3)	0.83163 (3)	0.83164 (3)
6.0	0.89673 (3)	0.89684 (3)	0.89683 (3)	0.89684 (3)
7.0	0.95440 (3)	0.95447 (3)	0.95446 (3)	0.95447 (3)
8.0	1.00632 (3)	1.00635 (3)	1.00633 (3)	1.00634 (3)
9.0	1.05372 (3)	1.05369 (3)	1.05367 (3)	1.05367 (3)
10.0	1.09744 (3)	1.09736 (3)	1.09734 (3)	1.09734 (3)
		Clamped-clamped		
1.0	0.10336 (3)	0.10337 (3)	0.10349 (3)	0.10356 (3)
2.0	0.20228 (3)	0.20232 (3)	0.20256 (3)	0.20269 (3)
3.0	0.29394 (3)	0.29405 (3)	0.29437 (3)	0.29455 (3)
4.0	0.37740 (3)	0.37762 (3)	0.37799 (3)	0.37821 (3)
5.0	0.45298 (3)	0.45331 (3)	0.45373 (3)	0.45397 (3)
6.0	0.52152 (3)	0.52198 (3)	0.52242 (3)	0.52267 (3)
7.0	0.58396 (3)	0.58455 (3)	0.58501 (3)	0.58528 (3)
8.0	0.64121 (3)	0.64191 (3)	0.64239 (3)	0.64267 (3)
9.0	0.69402 (3)	0.69484 (3)	0.69532 (3)	0.69561 (3)
10.0	0.74303 (3)	0.74395 (3)	0.74444 (3)	0.74474 (3)

*Number of iterations taken to converge.

Next, we consider the effect of the shear strain energy on the behavior of the CR-TBT beam finite elements developed herein. Table 2 contains nonlinear deflections, $\bar{w} = w_{max}EH^3/\Delta q_0 L^4$, of a pinned-pinned and clamped-clamped beam for various length-to-thickness ratios L/H, respectively. The effect of shear deformation is clear from the results. As the thickness of the beam becomes larger, the stiffness, shear strains and deflections $\bar{w}$ increase.

Table 2. Effect of length-to-thickness ratio on the deflections $\bar{w} = w_{max}EH^3/\Delta q_0 L^4$ of a pinned-pinned and clamped-clamped beam under uniformly distributed load.

pinned-pinned	**CR-EBT**		**CR-TBT**	
	Length-to-thickness ratio, L/H			
q_0	10	100	10	100
1.0	0.1562	0.1106	0.1602	0.1106
2.0	0.3125	0.1637	0.3204	0.1637
3.0	0.4688	0.1993	0.4806	0.1993
4.0	0.6250	0.2268	0.6408	0.2268
5.0	0.7813	0.2495	0.8010	0.2495
6.0	0.9375	0.2691	0.9612	0.2691
7.0	1.0937	0.2863	1.1214	0.2863
8.0	1.2500	0.3019	1.2816	0.3019
9.0	1.4063	0.3161	1.4418	0.3161
10.0	1.5625	0.3292	1.6020	0.3292
clamped-clamped	**CR-EBT**		**CR-TBT**	
	Length-to-thickness ratio, L/H			
q_0	10	100	10	100
1.0	0.0313	0.0310	0.0352	0.0311
2.0	0.0625	0.0607	0.0703	0.0608
3.0	0.0938	0.0882	0.1055	0.0883
4.0	0.1250	0.1133	0.1408	0.1134
5.0	0.1562	0.1360	0.1760	0.1361
6.0	0.1875	0.1566	0.2112	0.1567
7.0	0.2188	0.1754	0.2464	0.1755
8.0	0.2500	0.1926	0.2816	0.1927
9.0	0.2813	0.2085	0.3168	0.2086
10.0	0.3125	0.2232	0.3520	0.2233

On the other hand, thicker beams also exhibit less geometric nonlinearity, as can be seen from Figure 7. Results are compared with those obtained using CR-EBT beam elements. The deflections predicted by using TBT are very close to those predicted by the EBT when $L/H > 100$.

III.3. Small strains and large deflections

III.3.1. Cantilever beam with a concentrated load at the free end.

A cantilever beam, subjected to a concentrated load at the free end, was analyzed. Results for dimensionless vertical, w_0/L, and horizontal, $(L - u_0)/L$, end displacements as a function of the dimensionless load PL^2/D_{xx} are shown in Figure 8. The domain was divided into ten finite elements of equal size. Results from a closed form solution based on elliptical integrals developed by Bisshop and Drucker [81] are also shown in Figure 8 for comparison. Good agreement is indicated.

III.3.2. Cantilever beam with uniformly distributed load.

A cantilever beam subjected to uniformly distributed load was analyzed. Results for the maximum dimensionless axial and transverse displacements as a function of the load parameter qL^3/EI are shown in Figure 9. For this problem, the differential equations do not lead to any direct solution. Only approximate solutions are possible. Therefore, finite element results are compared with the approximate solution reported by Rohde [82]. For the previous two examples, a *relative nodal error* is used to measure the error between the approximate finite element solution, $\bar{w}(L)$, and the exact solution, $\bar{w}^*(L)$, at the point where the maximum deflection takes place.

Figures 10 (a) and (b) depict log-log plots of the error measures versus the mesh size. The rate of convergence is given by the slope of the lines.

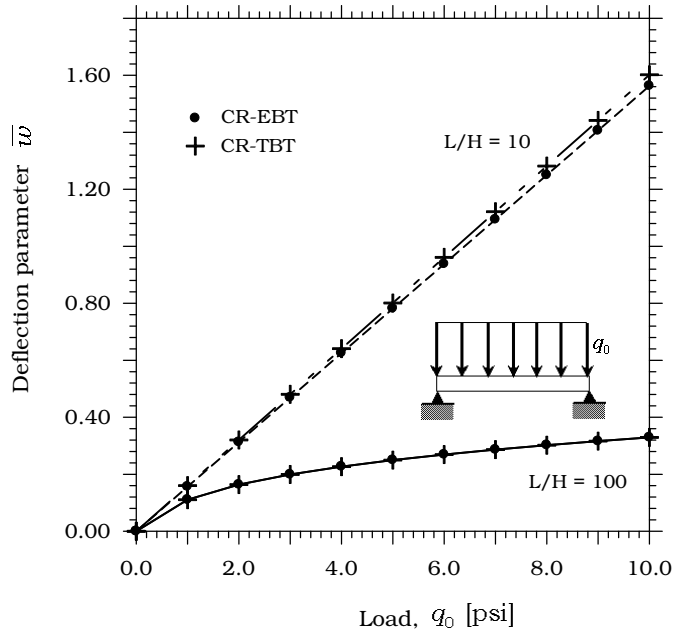

(a)

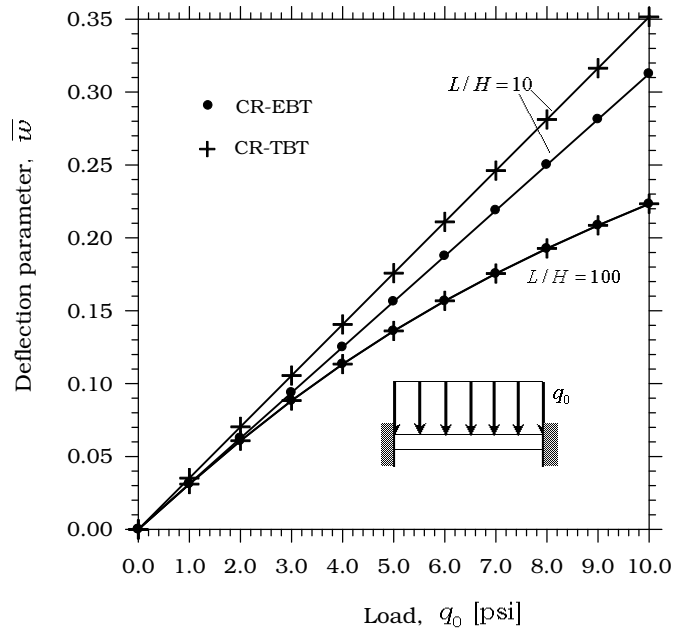

(b)

Fig. 7. Load-deflection response for thin ($L/H = 100$) and thick ($L/H = 10$)beams: (a) pinned-pinned, (b) clamped-clamped.

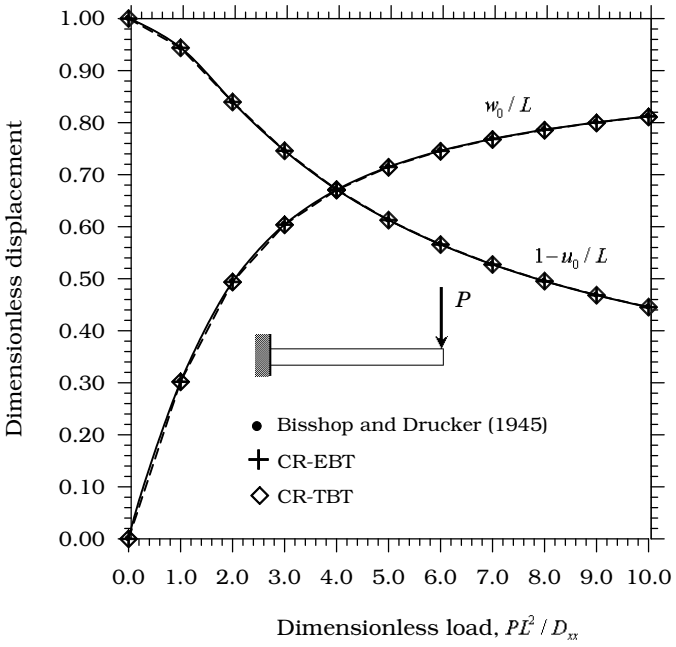

Fig. 8. Free-end axial and transverse dimensionless displacements of a cantilever beam subjected to a concentrated load.

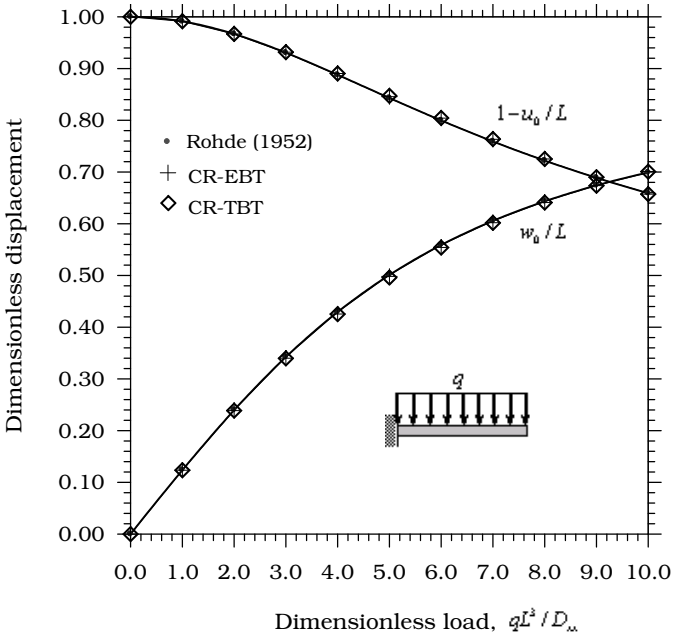

Fig. 9. Free-end axial and transverse dimensionless displacements of a cantilever beam subjected to distributed load.

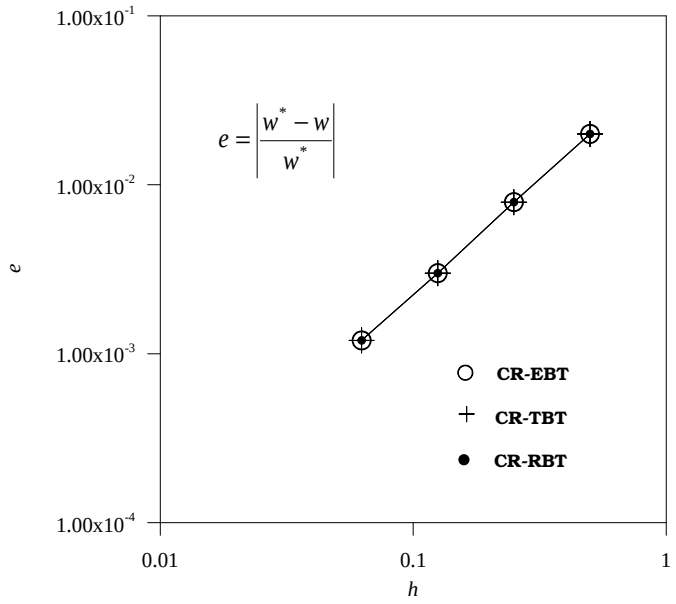

(a)

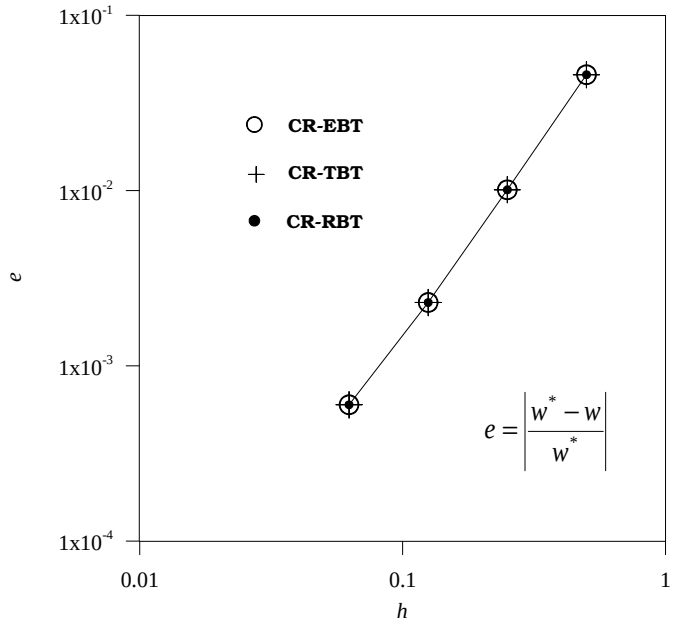

(b)

Fig. 10. h-convergence study of the center deflection for a cantilever beam subjected to: (a) uniform distributed load, (b) concentrated load.

III.3.3. Cantilever beam with an end moment.

Next, we analyze a cantilever beam subjected to a concentrated moment at the free end. This numerical example is studied in order to demonstrate the efficiency and large rotation capability of the corotational formulation and iterative solution scheme implemented in this work. The beam was also discretized into ten elements as in the previous examples.

The relationship between the bending moment M and the radius of curvature ρ, according to the EBT is given by

$$\frac{1}{\rho} = \frac{M}{EI} \tag{3.6}$$

A similar bending moment-curvature equation can be obtained for the TBT by using the relationships between the two theories described in detail in [44]. This relation is determined by the type of boundary conditions. For a clamped-free beam, both CR-EBT and CR-TBT have the same shear force, bending moment and slopes. Therefore, the resulting displacements are equal in both cases. The curvature radius ρ of a beam curled into an exact complete circle, and the dimensionless load parameter M^* required to reach this configuration are

$$\rho = \frac{L}{2\pi}, \quad M^* = \frac{ML}{2\pi EI} = 1.0 \tag{3.7}$$

Figure 11 shows the axial and transverse dimensionless displacements, $\bar{u} = u_0/L$ and $\bar{w} = w_0/L$, respectively. The results are obtained by using ten load increments. Figure 12 shows the deformed configuration of the beam for different values of the dimensionless load parameter M^*. Figure 13 depicts the values of the relative nodal error as a function of the mesh size in a logarithmic scale. The convergence of the finite element solution $\bar{w}$ to the analytical solution $\bar{w}^*$, with mesh refinement, is apparent from the results.

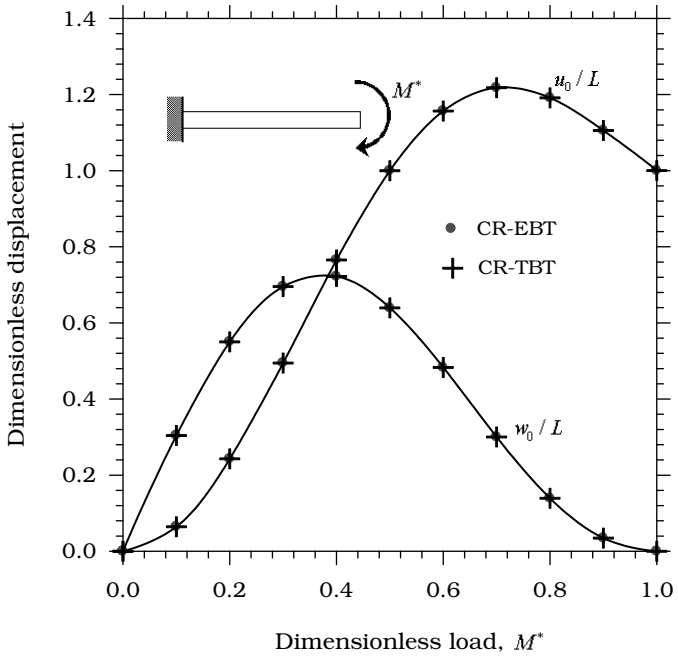

Fig. 11. Free-end dimensionless displacements $\bar{u}$ and $\bar{w}$ of a cantilever beam subjected to an end moment load.

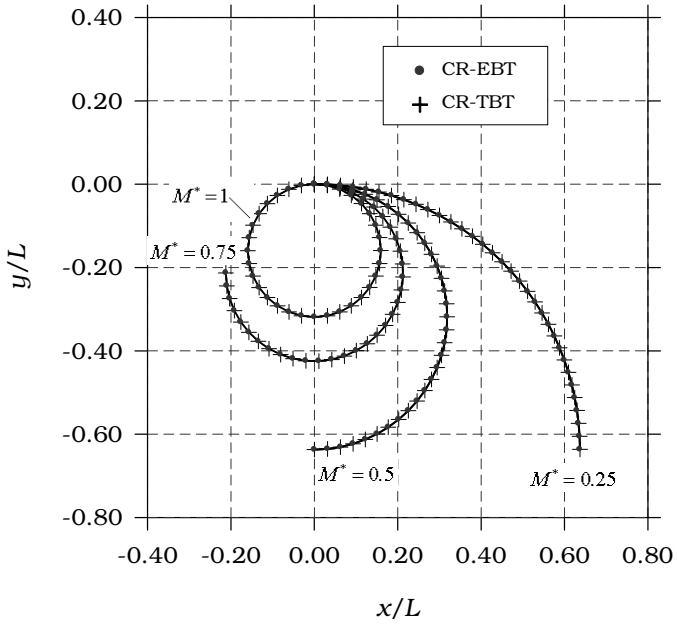

Fig. 12. Deformed configuration of a cantilever beam subjected to an end moment for different values of dimensionless load M^*

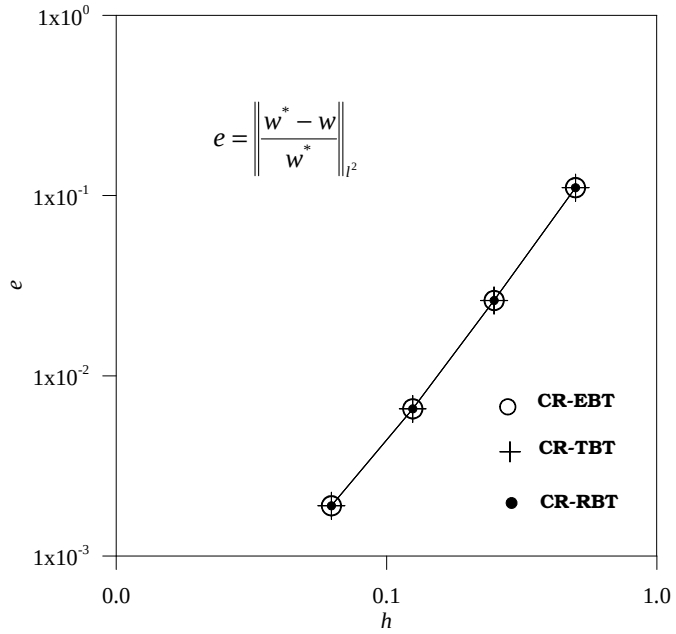

Fig. 13. h-convergence study of the transverse displacement $w(x)$ of a cantilever beam subjected to an end moment.

CHAPTER IV

MIXED FINITE ELEMENT MODEL OF THE FIRST-ORDER PLATE THEORY

IV.1. Preliminary comments

Consider a laminate of total thickness h composed of N_l orthotropic layers with the principal material coordinates (x_1^k, x_2^k, x_3^k) of the kth lamina oriented at an angle θ_k to the laminate coordinate x. The xy-plane is taken to be the undeformed midplane of the laminate, as shown in Figure 14.

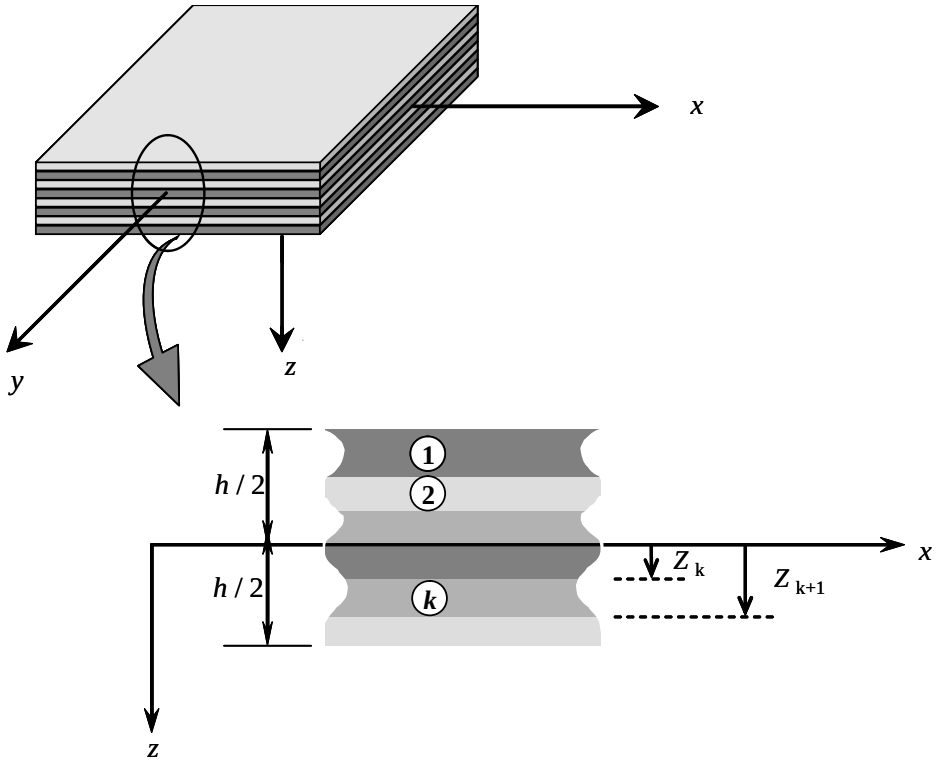

Fig. 14. Coordinate system and layer numbering used for a laminated plate.

The z-axis is taken positive downward from the midplane. The k-th layer is located between the points $z = z_k$ and $z = z_{k+1}$ in the thickness direction.

In formulating the mathematical model we make the following assumptions:

- The transverse normals remain straight after deformation
- The transverse normals do not experience elongation
- The transverse normals do not remain perpendicular to the midsurface after deformation
- The layers of the composite plate are perfectly bonded
- The material of each layer is linearly elastic and orthotropic
- Each layer is of uniform thickness
- The strains are small and the rotations are assumed to be moderately large
- The transverse shear stresses at the top and bottom surfaces are zero

The first three kinematic assumptions correspond to the Mindlin-Reissner hypotheses. These differ from the Kirchoff assumptions in that the normality condition is relaxed, thus allowing the inclusion of transverse shear strains in the theory.

IV.2. Governing equations

The displacement field for the Mindlin-Reissner plate theory, also known as *First-Order Shear Deformation Theory* (FSDT), is of the form

$$\begin{aligned} u(x,y,z) &= u_0(x,y) + z\phi_x(x,y) \\ v(x,y,z) &= v_0(x,y) + z\phi_y(x,y) \\ w(x,y,z) &= w_0(x,y) \end{aligned} \tag{4.1}$$

where (u_0, v_0, w_0) are the displacements along the coordinate lines of a material point on the midplane, and ϕ_x, ϕ_y are the rotations of a transverse normal about the x- and y-axes, respectively (see Figure 15).

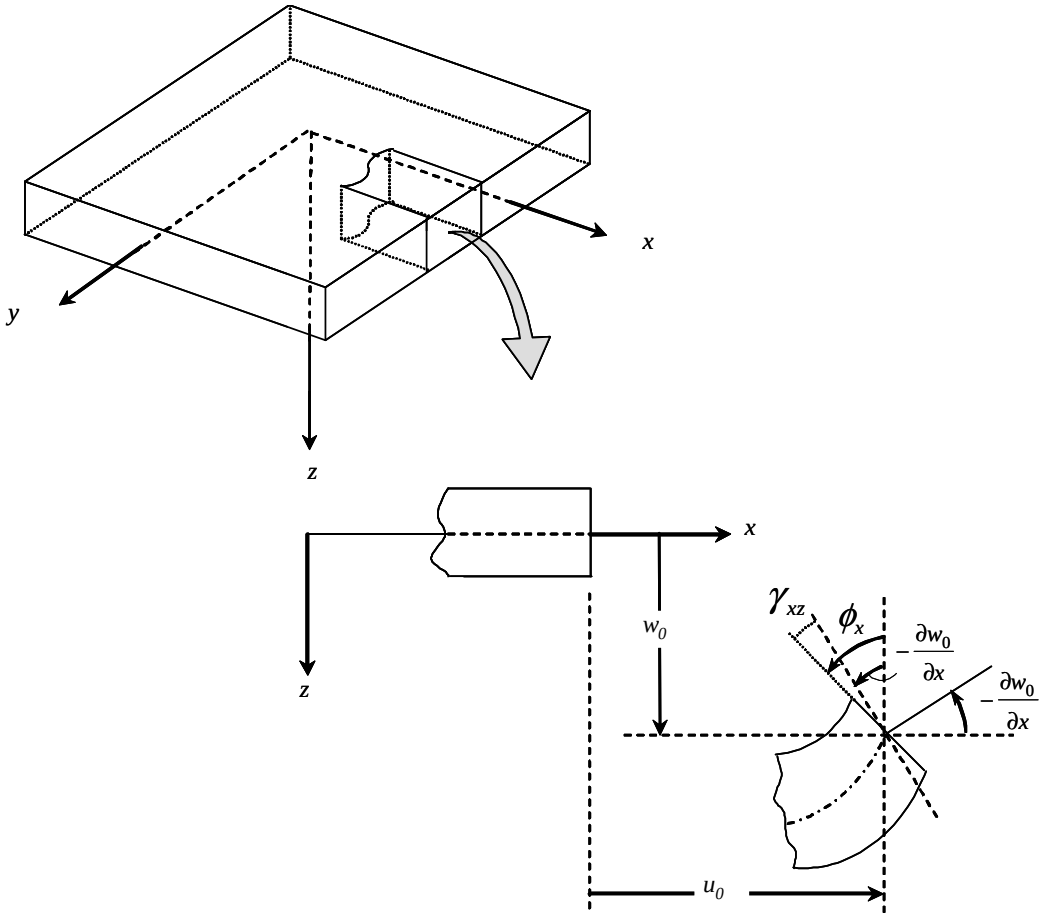

Fig. 15. Undeformed and deformed geometries of an edge of a plate under the assumptions of the first-order plate theory FSDT.

The assumed form of the displacement field of Eq. (4.1) allows reduction of the 3-D problem to one of studying the deformation of the midplane (2-D problem). Once $(u_0, v_0, w_0, \phi_x, \phi_y)$ are known, the displacements of any arbitrary point (x, y, z) in the 3-D continuum can be determined using Eq.(4.1).

In view of the small strain but moderate rotations assumption, the nonlinear Green strains reduce to

$$\varepsilon^0 = \left\{ \begin{array}{c} \varepsilon^0_{xx} \\ \varepsilon^0_{yy} \\ \gamma^0_{xy} \end{array} \right\} = \left\{ \begin{array}{c} \frac{\partial u_0}{\partial x} + \frac{1}{2}\left(\frac{\partial w_0}{\partial x}\right)^2 \\ \frac{\partial v_0}{\partial y} + \frac{1}{2}\left(\frac{\partial w_0}{\partial y}\right)^2 \\ \frac{\partial u_0}{\partial y} + \frac{\partial v_0}{\partial x} + \frac{\partial w_0}{\partial x}\frac{\partial w_0}{\partial y} \end{array} \right\} \tag{4.2}$$

$$\varepsilon^1 = \left\{ \begin{array}{c} \varepsilon^1_{xx} \\ \varepsilon^1_{yy} \\ \gamma^1_{xy} \end{array} \right\} = \left\{ \begin{array}{c} \frac{\partial \phi_x}{\partial x} \\ \frac{\partial \phi_y}{\partial y} \\ \frac{\partial \phi_x}{\partial y} + \frac{\partial \phi_y}{\partial x} \end{array} \right\} \tag{4.3}$$

$$\gamma^0 = \left\{ \begin{array}{c} \gamma^0_{xz} \\ \gamma^0_{yz} \end{array} \right\} = \left\{ \begin{array}{c} \frac{\partial w_0}{\partial x} + \phi_x \\ \frac{\partial w_0}{\partial y} + \phi_y \end{array} \right\} \tag{4.4}$$

where $(\varepsilon^0_{xx}, \varepsilon^0_{yy}, \varepsilon^0_{xy})$ are the membrane strains, $(\varepsilon^1_{xx}, \varepsilon^1_{yy}, \varepsilon^1_{xy})$ are the bending strains (curvatures) and $(\gamma^0_{xz}, \gamma^0_{yz})$ are the shear strains. The strains can be written in matrix form as follows

$$\varepsilon^0 = \mathcal{D}_1 \mathbf{u} + \varepsilon^0_{(NL)}, \quad \varepsilon^1 = \mathcal{D}_1 \mathbf{\Phi}, \quad \gamma^0 = \mathcal{D}_2 w_0 + \mathbf{\Phi} \tag{4.5}$$

where the in-plane displacement vector $\mathbf{u}$ and the differential operators $\mathcal{D}_1$ and $\mathcal{D}_2$ are given by

$$\mathbf{u} = \left\{ \begin{array}{c} u_0 \\ v_0 \end{array} \right\}, \quad \mathbf{\Phi} = \left\{ \begin{array}{c} \phi_x \\ \phi_y \end{array} \right\}, \quad \mathcal{D}_1 = \left[\begin{array}{cc} \frac{\partial}{\partial x} & 0 \\ 0 & \frac{\partial}{\partial y} \\ \frac{\partial}{\partial y} & \frac{\partial}{\partial x} \end{array} \right], \quad \mathcal{D}_2 = \left\{ \begin{array}{c} \frac{\partial}{\partial x} \\ \frac{\partial}{\partial y} \end{array} \right\} \tag{4.6}$$

and the nonlinear membrane strain ε^0_{NL} is defined as

$$\varepsilon^0_{(NL)} = \begin{Bmatrix} \frac{1}{2}\left(\frac{\partial w_0}{\partial x}\right)^2 \\ \frac{1}{2}\left(\frac{\partial w_0}{\partial y}\right)^2 \\ \frac{\partial w_0}{\partial x}\frac{\partial w_0}{\partial y} \end{Bmatrix} \tag{4.7}$$

The equations of motion associated with the theory are

$$\begin{aligned} \frac{\partial N_{xx}}{\partial x} + \frac{\partial N_{xy}}{\partial y} &= 0 \\ \frac{\partial N_{xy}}{\partial x} + \frac{\partial N_{yy}}{\partial y} &= 0 \\ \frac{\partial Q_x}{\partial x} + \frac{\partial Q_y}{\partial y} + q &= 0 \\ \frac{\partial M_{xx}}{\partial x} + \frac{\partial M_{xy}}{\partial y} - Q_x &= 0 \\ \frac{\partial M_{xy}}{\partial x} + \frac{\partial M_{yy}}{\partial y} - Q_y &= 0 \end{aligned} \tag{4.8}$$

where (N_{xx}, N_{yy}, N_{xy}) are the in-plane force resultants, (M_{xx}, M_{yy}, M_{xy}) are the moment resultants, (Q_x, Q_y) denote the transverse force resultants and q corresponds to the total transverse load. All stress resultants are measured per unit length (e.g. N_i and Q_i in lb/in and M_i in lb-in/in) and the positive sign convention is depicted in Figure 16.

The laminate constitutive equations that relate the force and moment resultants in Eq. (4.8) to the strains of Eq. (4.5), in laminate coordinates, are given by

$$\begin{Bmatrix} N_{xx} \\ N_{yy} \\ N_{xy} \end{Bmatrix} = \begin{bmatrix} A_{11} & A_{12} & A_{16} \\ A_{12} & A_{22} & A_{26} \\ A_{16} & A_{26} & A_{66} \end{bmatrix} \begin{Bmatrix} \varepsilon^0_{xx} \\ \varepsilon^0_{yy} \\ \gamma^0_{xy} \end{Bmatrix} + \begin{bmatrix} B_{11} & B_{12} & B_{16} \\ B_{12} & B_{22} & B_{26} \\ B_{16} & B_{26} & B_{66} \end{bmatrix} \begin{Bmatrix} \varepsilon^1_{xx} \\ \varepsilon^1_{yy} \\ \gamma^1_{xy} \end{Bmatrix} \tag{4.9}$$

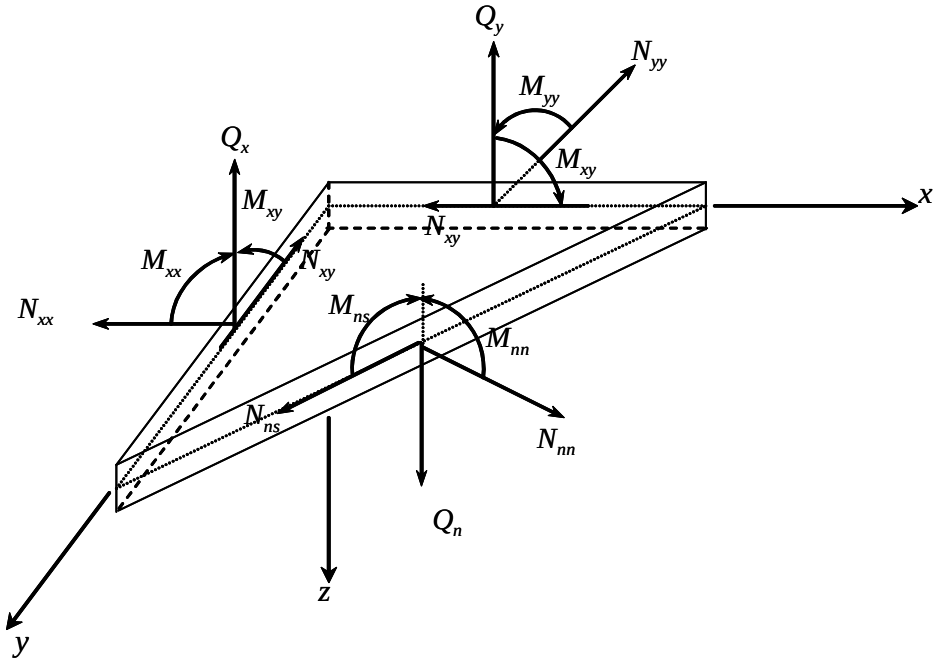

Fig. 16. Force and moment resultants on a plate element.

$$\begin{Bmatrix} M_{xx} \\ M_{yy} \\ M_{xy} \end{Bmatrix} = \begin{bmatrix} B_{11} & B_{12} & B_{16} \\ B_{12} & B_{22} & B_{26} \\ B_{16} & B_{26} & B_{66} \end{bmatrix} \begin{Bmatrix} \varepsilon^0_{xx} \\ \varepsilon^0_{yy} \\ \gamma^0_{xy} \end{Bmatrix} + \begin{bmatrix} D_{11} & D_{12} & D_{16} \\ D_{12} & D_{22} & D_{26} \\ D_{16} & D_{26} & D_{66} \end{bmatrix} \begin{Bmatrix} \varepsilon^1_{xx} \\ \varepsilon^1_{yy} \\ \gamma^1_{xy} \end{Bmatrix} \tag{4.10}$$

$$\begin{Bmatrix} Q_x \\ Q_y \end{Bmatrix} = K_s \begin{bmatrix} A_{55} & A_{45} \\ A_{45} & A_{44} \end{bmatrix} \begin{Bmatrix} \gamma^0_{xz} \\ \gamma^0_{yz} \end{Bmatrix} \tag{4.11}$$

where A_{ij} are the *extensional stiffnesses*, D_{ij} the *bending stiffnesses*, and B_{ij} the *bending-extensional stiffnesses*, which are defined in terms of the lamina stiffnesses $\bar{Q}^{(k)}_{ij}$ as

$$\begin{gathered} A_{ij} = \sum_{k=1}^{N_l} \bar{Q}^{(k)}_{ij}(z_{k+1} - z_k), \quad B_{ij} = \frac{1}{2}\sum_{k=1}^{N_l} \bar{Q}^{(k)}_{ij}(z^2_{k+1} - z^2_k) \\ D_{ij} = \frac{1}{3}\sum_{k=1}^{N_l} \bar{Q}^{(k)}_{ij}(z^3_{k+1} - z^3_k) \end{gathered} \tag{4.12}$$

Since the laminate is made of several orthotropic layers, with their material axes oriented arbitrarily with respect to the laminate coordinates (Figure 17), the $\bar{Q}_{ij}$ coefficients are computed in terms of the *plane stress-reduced stiffnesses* Q_{ij} using the following transformation equations

$$\bar{Q}_{11} = Q_{11}\cos^4\theta + 2(Q_{12}+Q_{66})\sin^2\theta\cos^2\theta + Q_{22}\sin^4\theta \tag{4.13a}$$

$$\bar{Q}_{12} = (Q_{11}+Q_{22}-4Q_{66})\sin^2\theta\cos^2\theta + Q_{12}(\sin^4\theta+\cos^4\theta) \tag{4.13b}$$

$$\bar{Q}_{22} = Q_{11}\sin^4\theta + 2(Q_{12}+2Q_{66})\sin^2\theta\cos^2\theta + Q_{22}\cos^4\theta \tag{4.13c}$$

$$\bar{Q}_{16} = (Q_{11}-Q_{12}-2Q_{66})\sin\theta\cos^3\theta + (Q_{12}-Q_{22}+2Q_{66})\sin^3\theta\cos\theta \tag{4.13d}$$

$$\bar{Q}_{26} = (Q_{11}-Q_{12}-2Q_{66})\sin^3\theta\cos\theta + (Q_{12}-Q_{22}+2Q_{66})\sin\theta\cos^3\theta \tag{4.13e}$$

$$\bar{Q}_{66} = (Q_{11}+Q_{22}-2Q_{12}-2Q_{66})\sin^2\theta\cos^2\theta + Q_{66}(\sin^4\theta+\cos^4\theta) \tag{4.13f}$$

$$\bar{Q}_{44} = Q_{44}\cos^2\theta + Q_{55}\sin^2\theta \tag{4.13g}$$

$$\bar{Q}_{45} = (Q_{55}-Q_{44})\cos\theta\sin\theta \tag{4.13h}$$

$$\bar{Q}_{55} = Q_{44}\sin^2\theta + Q_{55}\cos^2\theta \tag{4.13i}$$

with the coefficients Q_{ij} defined in terms of the engineering constants of the k-th layer as follows

$$\begin{gathered} Q_{11} = \frac{E_1}{1-\nu_{12}\nu_{21}}, \quad Q_{12} = \frac{\nu_{12}E_2}{1-\nu_{12}\nu_{21}}, \quad Q_{22} = \frac{E_2}{1-\nu_{12}\nu_{21}} \\ Q_{66} = G_{12}, \quad Q_{44} = G_{23}, \quad Q_{55} = G_{13} \end{gathered} \tag{4.14}$$

The equations of motion (4.8) and constitutive relations (4.9)-(4.11) can be cast in matrix notation as

$$\mathcal{D}_1^T\mathbf{N} = \mathbf{0}, \quad \mathcal{D}_2^T\mathbf{Q} = q, \quad \mathcal{D}_1^T\mathbf{M} - \mathbf{Q} = \mathbf{0} \tag{4.15}$$

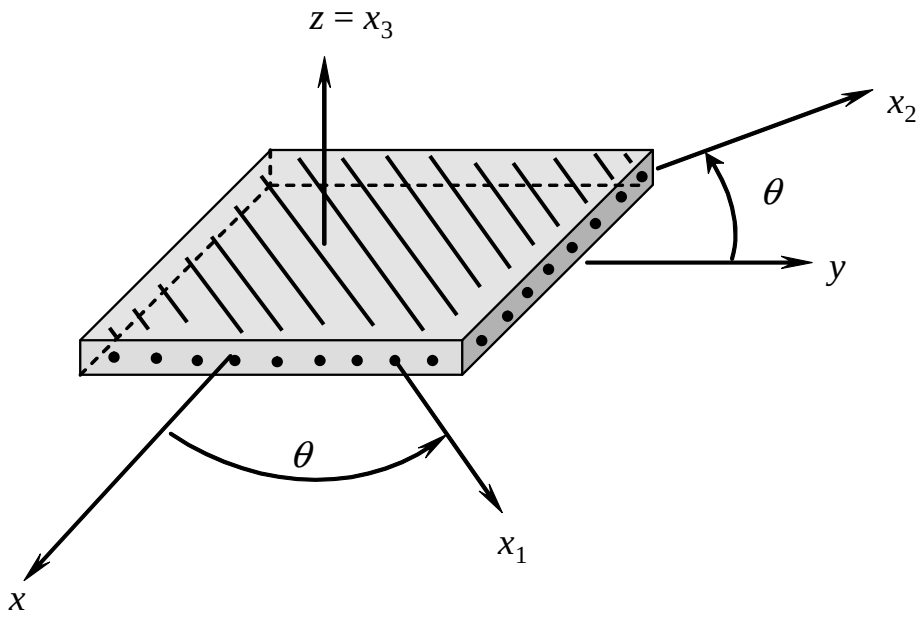

Fig. 17. Material $(x_1^{(k)}, x_2^{(k)}, x_3^{(k)})$ and laminate (x, y, z) coordinates.

$$\left\{ \begin{array}{c} \mathbf{N} \\ \mathbf{M} \end{array} \right\} = \left[\begin{array}{cc} \mathbf{A} & \mathbf{B} \\ \mathbf{B}^T & \mathbf{D} \end{array} \right] \left\{ \begin{array}{c} \varepsilon^0 \\ \varepsilon^1 \end{array} \right\}, \quad \mathbf{Q} = \tilde{\mathbf{A}}\gamma^0 \tag{4.16}$$

To develop the mixed finite element model, Eq. (4.16) is written in the following alternative form

$$\mathbf{N} = \bar{\mathbf{A}}\varepsilon^0 + \bar{\mathbf{B}}\mathbf{M}, \quad \varepsilon^1 = -\bar{\mathbf{B}}^T\varepsilon^0 + \bar{\mathbf{D}}\mathbf{M} \tag{4.17}$$

where

$$\bar{\mathbf{A}} = \mathbf{A} - \mathbf{B}\bar{\mathbf{D}}\mathbf{B}^T, \quad \bar{\mathbf{B}} = \mathbf{B}\bar{\mathbf{D}}\mathbf{B}, \quad \bar{\mathbf{D}} = \mathbf{D}^{-1} \tag{4.18}$$

The set of equilibrium and constitutive equations can be summarized as follows

$$\mathcal{D}_1^T\mathbf{N} = \mathbf{0}, \quad \mathcal{D}_2^T\mathbf{Q} = q, \quad \mathcal{D}_1^T\mathbf{M} - \mathbf{Q} = \mathbf{0}, \quad \varepsilon^1 = -\bar{\mathbf{B}}^T\varepsilon^0 + \bar{\mathbf{D}}\mathbf{M} \tag{4.19}$$

where the vector of in-plane force resultants $\mathbf{N}$ and the vector of shear force resultants

$\mathbf{Q}$ can be expressed in terms of the displacements and moment resultants by using

$$\mathbf{N} = \bar{\mathbf{A}}\varepsilon^0 + \bar{\mathbf{B}}\mathbf{M}, \quad \mathbf{Q} = \tilde{\mathbf{A}}\gamma^0 \tag{4.20}$$

The resulting system of governing equations consists of 8 equations in 8 unknowns $(u_0, v_0, w_0, \phi_x, \phi_y, M_{xx},\ M_{yy}, M_{xy})$.

IV.3. Mixed variational principle

Here we use the inverse procedure to develop a variational principle associated with the set of equations (4.19). The procedure involves multiplying each vectorial equation with a suitable dual variable. For example, the equations of equilibrium of in-plane forces in (4.19) should be pre-multiplied with the vector $\delta\mathbf{u}^T$. Similarly, the second equation, third and last equation in (4.19) should be pre-multiplied with the vectors δw_0, $\delta\phi^T$ and $\delta\mathbf{M}^T$, respectively. Proceeding in this manner, we write,

$$\begin{aligned} 0 = &\int_\Omega \left\{ \delta\mathbf{u}^T \left(-\mathcal{D}_1^T\mathbf{N} - \mathbf{0}\right) + \delta w_0 \left(-\mathcal{D}_2^T\mathbf{Q} + q - 0\right) + \delta\mathbf{\Phi}^T \left(-\mathcal{D}_1^T\mathbf{M} + \mathbf{Q} - \mathbf{0}\right) \right. \\ &\left. + \delta\mathbf{M}^T \left[\varepsilon^1 - \bar{\mathbf{D}}\mathbf{M} + \bar{\mathbf{B}}^T\varepsilon^0 - \mathbf{0}\right] \right\} d\mathbf{x} \\ = &\int_\Omega \left[\left(\delta\varepsilon^0\right)^T \bar{\mathbf{A}}\varepsilon^0 + \left(\delta\varepsilon^0\right)^T \bar{\mathbf{B}}\mathbf{M} + \left(\delta\gamma^0\right)^T \tilde{\mathbf{A}}\gamma^0 + q\delta w_0 + \left(\delta\varepsilon^1\right)^T \mathbf{M} \right. \\ &\left. + \left(\varepsilon^1\right)^T \delta\mathbf{M} - \delta\mathbf{M}^T\bar{\mathbf{D}}\mathbf{M} + \delta\mathbf{M}^T\bar{\mathbf{B}}\varepsilon^0 \right] d\mathbf{x} - \int_\Gamma \mathbf{t}\delta\mathbf{\Delta} ds \end{aligned} \tag{4.21}$$

The boundary term in the above equation can be written as

$$\int_\Gamma \mathbf{t}\delta\mathbf{\Delta} ds = \int_\Gamma (N_n\delta u_n + N_{ns}\delta u_s + M_n\delta\phi_n + M_{ns}\delta\phi_s + Q_n\delta w_0) ds \tag{4.22}$$

where $Q_n, N_n, N_{ns}, M_n, M_{ns}$ are the shear force, normal and tangential in-plane forces and bending moments on the boundary surface with normal $\hat{\mathbf{n}}$:

$$Q_n = Q_x n_x + Q_y n_y$$

$$
\begin{aligned}
N_{nn} &= N_{xx}n_x n_y + 2N_{xy}n_x n_y + N_y n_x n_y \\
N_{ns} &= n_x n_y(N_{yy} - N_{xx}) + N_{xy}(n_x^2 - n_y^2) \\
M_{nn} &= M_{xx}n_x n_y + 2M_{xy}n_x n_y + M_y n_x n_y \\
M_{ns} &= n_x n_y(M_{yy} - M_{xx}) + M_{xy}(n_x^2 - n_y^2)
\end{aligned} \tag{4.23}
$$

Note also that in arriving at the second expression, integration by parts was used. Substituting the membrane, bending and shear strains from Eqns. (4.2)-(4.4) along with their corresponding variations into Eq. (4.21) and collecting the coefficients of the virtual displacements and stress resultants we obtain the following set of equations at the element level:

$$
0 = \int_\Omega \left\{ \frac{\partial \delta u_0}{\partial x}\left(\bar{A}_{11}\varepsilon^0_{xx} + \bar{A}_{12}\varepsilon^0_{yy} + \bar{A}_{16}\gamma^0_{xy} + \bar{B}_{11}M_{xx} + \bar{B}_{12}M_{yy} + \bar{B}_{16}M_{xy}\right) \right. \tag{4.24a}
$$

$$
\left. + \frac{\partial \delta u_0}{\partial y}\left(\bar{A}_{16}\varepsilon^0_{xx} + \bar{A}_{26}\varepsilon^0_{yy} + \bar{A}_{66}\gamma^0_{xy} + \bar{B}_{16}M_{xx} + \bar{B}_{26}M_{yy} + \bar{B}_{66}M_{xy}\right) \right\} dA \tag{4.24b}
$$

$$
\begin{aligned}
0 = \int_\Omega \left\{ \right. & \frac{\partial \delta v_0}{\partial x}\left(\bar{A}_{16}\varepsilon^0_{xx} + \bar{A}_{26}\varepsilon^0_{yy} + \bar{A}_{66}\gamma^0_{xy} + \bar{B}_{16}M_{xx} + \bar{B}_{26}M_{yy} + \bar{B}_{66}M_{xy}\right) \\
& \left. + \frac{\partial \delta v_0}{\partial y}\left(\bar{A}_{12}\varepsilon^0_{xx} + \bar{A}_{22}\varepsilon^0_{yy} + \bar{A}_{26}\gamma^0_{xy} + \bar{B}_{12}M_{xx} + \bar{B}_{22}M_{yy} + \bar{B}_{26}M_{xy}\right) \right\} dA
\end{aligned} \tag{4.24c}
$$

$$
\begin{aligned}
0 = \int_\Omega \left\{ \right. & \frac{\partial \delta w_0}{\partial x}\left[\frac{\partial w_0}{\partial x}\left(\bar{A}_{11}\varepsilon^0_{xx} + \bar{A}_{12}\varepsilon^0_{yy} + \bar{A}_{16}\gamma^0_{xy} + \bar{B}_{11}M_{xx} + \bar{B}_{12}M_{yy} + \bar{B}_{16}M_{xy}\right) \right. \\
& \left. + \frac{\partial w_0}{\partial y}\left(\bar{A}_{16}\varepsilon^0_{xx} + \bar{A}_{26}\varepsilon^0_{yy} + \bar{A}_{66}\gamma^0_{xy} + \bar{B}_{16}M_{xx} + \bar{B}_{26}M_{yy} + \bar{B}_{66}M_{xy}\right) \right] \\
& + \frac{\partial \delta w_0}{\partial y}\left[\frac{\partial w_0}{\partial x}\left(\bar{A}_{16}\varepsilon^0_{xx} + \bar{A}_{26}\varepsilon^0_{yy} + \bar{A}_{66}\gamma^0_{xy} + \bar{B}_{16}M_{xx} + \bar{B}_{26}M_{yy} + \bar{B}_{66}M_{xy}\right) \right. \\
& \left. + \frac{\partial w_0}{\partial y}\left(\bar{A}_{12}\varepsilon^0_{xx} + \bar{A}_{22}\varepsilon^0_{yy} + \bar{A}_{26}\gamma^0_{xy} + \bar{B}_{12}M_{xx} + \bar{B}_{22}M_{yy} + \bar{B}_{26}M_{xy}\right) \right] \\
& + K_s\frac{\partial \delta w_0}{\partial x}\left(\tilde{A}_{55}\gamma^0_{xz} + \tilde{A}_{45}\gamma^0_{yz}\right) + K_s\frac{\partial \delta w_0}{\partial y}\left(\tilde{A}_{45}\gamma^0_{xz} + \tilde{A}_{44}\gamma^0_{yz}\right) \Big\} dA
\end{aligned} \tag{4.24d}
$$

$$
0 = \int_\Omega \left\{ K_s\left(\tilde{A}_{55}\gamma^0_{xz} + \tilde{A}_{45}\gamma^0_{yz}\right)\delta\phi_x + \frac{\partial \delta\phi_x}{\partial x}M_{xx} + \frac{\partial \delta\phi_x}{\partial y}M_{xy} \right\} dA \tag{4.24e}
$$

$$0 = \int_\Omega \left\{ K_s \left(\tilde{A}_{45}\gamma^0_{xz} + \tilde{A}_{44}\gamma^0_{yz} \right) \delta\phi_y + \frac{\partial \delta\phi_y}{\partial x} M_{xx} + \frac{\partial \delta\phi_y}{\partial y} M_{xy} \right\} dA \tag{4.24f}$$

$$0 = \int_\Omega \delta M_{xx} \Big\{ \varepsilon^1_{xx} - \bar{D}_{11} M_{xx} - \bar{D}_{12} M_{yy} - \bar{D}_{16} M_{xy} + \bar{B}_{11}\varepsilon^0_{xx} + \bar{B}_{12}\varepsilon^0_{yy} + \bar{B}_{16}\gamma^0_{xy} \Big\} dA \tag{4.24g}$$

$$0 = \int_\Omega \delta M_{yy} \Big\{ \varepsilon^1_{yy} - \bar{D}_{12} M_{xx} - \bar{D}_{22} M_{yy} - \bar{D}_{26} M_{xy} + \bar{B}_{12}\varepsilon^0_{xx} + \bar{B}_{22}\varepsilon^0_{yy} + \bar{B}_{26}\gamma^0_{xy} \Big\} dA \tag{4.24h}$$

$$0 = \int_\Omega \delta M_{xy} \Big\{ \gamma^1_{xy} - \bar{D}_{16} M_{xx} - \bar{D}_{26} M_{yy} - \bar{D}_{66} M_{xy} + \bar{B}_{16}\varepsilon^0_{xx} + \bar{B}_{26}\varepsilon^0_{yy} + \bar{B}_{66}\gamma^0_{xy} \Big\} dA \tag{4.24i}$$

IV.4. Mixed finite element model

The variational formulation contains, at the most, only the first derivatives of the dependent variables. Therefore, we assume

$$u^e_0(x,y) = \sum_{j=1}^m u_j \psi_j(x,y), \quad v^e_0(x,y) = \sum_{j=1}^m v_j \psi_j(x,y), \quad w^e_0(x,y) = \sum_{j=1}^m w_j \psi_j(x,y)$$
$$\phi^e_x(x,y) = \sum_{j=1}^m \phi^1_j \psi_j(x,y), \quad \phi^e_y(x,y) = \sum_{j=1}^m \phi^2_j \psi_j(x,y) \tag{4.25}$$
$$M^e_{xx}(x,y) = \sum_{j=1}^m M^1_j \psi_j(x,y), \quad M^e_{yy}(x,y) = \sum_{j=1}^m M^2_j \psi_j(x,y), \quad M^e_{xy}(x,y) = \sum_{j=1}^m M^6_j \psi_j(x,y)$$

where ψ_j are the Lagrange interpolation functions. Substituting Eq.(4.25) for the primary variables and the $i-th$ interpolation function for the virtual displacements and virtual stress resultants ($\delta u_0 \sim \psi_i, \delta v_0 \sim \psi_i, ..., \delta M_{xy} \sim \psi_i$) into the variational principle in Eqns. (2.24a) - (2.24i) we obtain the finite element model of the first-order

laminated plate theory

$$\begin{bmatrix} [K^{11}] & [K^{12}] & [K^{13}] & \cdots & [K^{18}] \\ [K^{21}] & [K^{22}] & [K^{23}] & \cdots & [K^{28}] \\ [K^{31}] & [K^{23}] & [K^{33}] & \cdots & [K^{38}] \\ \vdots & \vdots & \vdots & \ddots & \vdots \\ [K^{81}] & [K^{82}] & [K^{83}] & \cdots & [K^{88}] \end{bmatrix} \begin{Bmatrix} \{u^e\} \\ \{v^e\} \\ \{w^e\} \\ \vdots \\ \{M^{6^e}\} \end{Bmatrix} = \begin{Bmatrix} \{F^1\} \\ \{F^2\} \\ \{F^3\} \\ \vdots \\ \{F^8\} \end{Bmatrix} \tag{4.26}$$

where

$$\left[K^{\alpha\beta}\right] = \left[L^{\alpha\beta}\right] + \left[G^{\alpha\beta}\right] \tag{4.27}$$

The linear submatrix $\left[L^{\alpha\beta}\right]$ is symmetric whereas the nonlinear submatrix $\left[G^{\alpha\beta}\right]$ is unsymmetric. The linear coefficients $L_{ij}^{\alpha\beta}$ are defined for $(\alpha, \beta = 1, 2, ..., 8)$ by the following expressions

$$L_{ij}^{11} = \int_{\Omega_e} \left[\frac{\partial \psi_i}{\partial x} \left(\bar{A}_{11} \frac{\partial \psi_j}{\partial x} + \bar{A}_{16} \frac{\partial \psi_j}{\partial y} \right) + \frac{\partial \psi_i}{\partial y} \left(\bar{A}_{16} \frac{\partial \psi_j}{\partial x} + \bar{A}_{66} \frac{\partial \psi_j}{\partial y} \right) \right] dxdy$$

$$L_{ij}^{12} = \int_{\Omega_e} \left[\frac{\partial \psi_i}{\partial x} \left(\bar{A}_{16} \frac{\partial \psi_j}{\partial x} + \bar{A}_{12} \frac{\partial \psi_j}{\partial y} \right) + \frac{\partial \psi_i}{\partial y} \left(\bar{A}_{66} \frac{\partial \psi_j}{\partial x} + \bar{A}_{26} \frac{\partial \psi_j}{\partial y} \right) \right] dxdy$$

$$L_{ij}^{13} = L_{ij}^{14} = L_{ij}^{15} = 0$$

$$L_{ij}^{16} = \int_{\Omega_e} \left(\bar{B}_{11} \frac{\partial \psi_i}{\partial x} + \bar{B}_{61} \frac{\partial \psi_i}{\partial y} \right) \psi_j \, dxdy$$

$$L_{ij}^{17} = \int_{\Omega_e} \left(\bar{B}_{12} \frac{\partial \psi_i}{\partial x} + \bar{B}_{62} \frac{\partial \psi_i}{\partial y} \right) \psi_j \, dxdy$$

$$L_{ij}^{18} = \int_{\Omega_e} \left(\bar{B}_{16} \frac{\partial \psi_i}{\partial x} + \bar{B}_{66} \frac{\partial \psi_i}{\partial y} \right) \psi_j \, dxdy$$

$$L_{ij}^{23} = L_{ij}^{24} = L_{ij}^{25} = 0$$

$$L_{ij}^{22} = \int_{\Omega_e} \left[\frac{\partial \psi_i}{\partial x} \left(\bar{A}_{66} \frac{\partial \psi_j}{\partial x} + \bar{A}_{26} \frac{\partial \psi_j}{\partial y} \right) + \frac{\partial \psi_i}{\partial y} \left(\bar{A}_{26} \frac{\partial \psi_j}{\partial x} + \bar{A}_{22} \frac{\partial \psi_j}{\partial y} \right) \right] dxdy$$

$$L_{ij}^{26} = \int_{\Omega_e} \left(\bar{B}_{61} \frac{\partial \psi_i}{\partial x} + \bar{B}_{21} \frac{\partial \psi_i}{\partial y} \right) \psi_j \, dxdy$$

$$
\begin{aligned}
L_{ij}^{27} &= \int_{\Omega_e} \left(\bar{B}_{62} \frac{\partial \psi_i}{\partial x} + \bar{B}_{22} \frac{\partial \psi_i}{\partial y} \right) \psi_j \, dxdy \\
L_{ij}^{28} &= \int_{\Omega_e} \left(\bar{B}_{66} \frac{\partial \psi_i}{\partial x} + \bar{B}_{26} \frac{\partial \psi_i}{\partial y} \right) \psi_j \, dxdy \\
L_{ij}^{3,3} &= \int_{\Omega_e} \left[\tilde{A}_{55} \frac{\partial \psi_i}{\partial x} \frac{\partial \psi_j}{\partial x} + \tilde{A}_{45} \left(\frac{\partial \psi_i}{\partial x} \frac{\partial \psi_j}{\partial y} + \frac{\partial \psi_i}{\partial y} \frac{\partial \psi_j}{\partial x} \right) + \tilde{A}_{44} \frac{\partial \psi_i}{\partial y} \frac{\partial \psi_j}{\partial y} \right] dxdy \\
L_{ij}^{34} &= \int_{\Omega_e} \left(\tilde{A}_{55} \frac{\partial \psi_i}{\partial x} + \tilde{A}_{45} \frac{\partial \psi_i}{\partial y} \right) \psi_j \, dxdy \\
L_{ij}^{35} &= \int_{\Omega_e} \left(\tilde{A}_{45} \frac{\partial \psi_i}{\partial x} + \tilde{A}_{44} \frac{\partial \psi_i}{\partial y} \right) \psi_j \, dxdy \\
L_{ij}^{36} &= L_{ij}^{37} = L_{ij}^{38} = 0 \\
L_{ij}^{44} &= \int_{\Omega_e} \tilde{A}_{55} \psi_i \psi_j \, dxdy, \quad L_{ij}^{45} = \int_{\Omega_e} \tilde{A}_{45} \psi_i \psi_j \, dxdy \\
L_{ij}^{46} &= \int_{\Omega_e} \frac{\partial \psi_i}{\partial x} \psi_j \, dxdy, \quad L_{ij}^{47} = 0 \\
L_{ij}^{48} &= \int_{\Omega_e} \frac{\partial \psi_i}{\partial y} \psi_j \, dxdy \\
L_{ij}^{55} &= \int_{\Omega_e} \tilde{A}_{44} \psi_i \psi_j \, dxdy, \quad L_{ij}^{56} = 0 \\
L_{ij}^{57} &= \int_{\Omega_e} \frac{\partial \psi_i}{\partial y} \psi_j \, dxdy, \quad L_{ij}^{58} = \int_{\Omega_e} \frac{\partial \psi_i}{\partial x} \psi_j \, dxdy \\
L_{ij}^{66} &= \int_{\Omega_e} -\bar{D}_{11} \psi_i \psi_j \, dxdy, \quad L_{ij}^{67} = \int_{\Omega_e} -\bar{D}_{12} \psi_i \psi_j \, dxdy \\
L_{ij}^{68} &= \int_{\Omega_e} -\bar{D}_{16} \psi_i \psi_j \, dxdy \\
L_{ij}^{77} &= \int_{\Omega_e} -\bar{D}_{22} \psi_i \psi_j \, dxdy, \quad L_{ij}^{78} = \int_{\Omega_e} -\bar{D}_{26} \psi_i \psi_j \, dxdy \\
L_{ij}^{88} &= \int_{\Omega_e} -\bar{D}_{66} \psi_i \psi_j \, dxdy
\end{aligned} \tag{4.28}
$$

The nonlinear coefficients $G_{ij}^{\alpha\beta}$ are given by

$$
\begin{aligned}
G_{ij}^{13} = & \frac{1}{2} \int_{\Omega_e} \left\{ \frac{\partial \psi_i}{\partial x} \left[\frac{\partial \psi_j}{\partial x} \left(\bar{A}_{11} \frac{\partial w_0}{\partial x} + \bar{A}_{16} \frac{\partial w_0}{\partial y} \right) + \frac{\partial \psi_j}{\partial y} \left(\bar{A}_{16} \frac{\partial w_0}{\partial x} + \bar{A}_{12} \frac{\partial w_0}{\partial y} \right) \right] \right. \\
& \left. + \frac{\partial \psi_i}{\partial y} \left[\frac{\partial \psi_j}{\partial x} \left(\bar{A}_{16} \frac{\partial w_0}{\partial x} + \bar{A}_{66} \frac{\partial w_0}{\partial y} \right) + \frac{\partial \psi_j}{\partial y} \left(\bar{A}_{66} \frac{\partial w_0}{\partial x} + \bar{A}_{26} \frac{\partial w_0}{\partial y} \right) \right] \right\} dxdy
\end{aligned}
$$

$$
\begin{aligned}
G_{ij}^{23} =& \frac{1}{2}\int_{\Omega_e}\left\{\frac{\partial\psi_i}{\partial x}\left[\frac{\partial\psi_j}{\partial x}\left(\bar{A}_{16}\frac{\partial w_0}{\partial x}+\bar{A}_{66}\frac{\partial w_0}{\partial y}\right)+\frac{\partial\psi_j}{\partial y}\left(\bar{A}_{66}\frac{\partial w_0}{\partial x}+\bar{A}_{26}\frac{\partial w_0}{\partial y}\right)\right]\right.\\
&\left.+\frac{\partial\psi_i}{\partial y}\left[\frac{\partial\psi_j}{\partial x}\left(\bar{A}_{12}\frac{\partial w_0}{\partial x}+\bar{A}_{26}\frac{\partial w_0}{\partial y}\right)+\frac{\partial\psi_j}{\partial y}\left(\bar{A}_{26}\frac{\partial w_0}{\partial x}+\bar{A}_{22}\frac{\partial w_0}{\partial y}\right)\right]\right\}dxdy\\
G_{ij}^{33} =& \int_{\Omega_e}\left\{\bar{N}_1\frac{\partial\psi_i}{\partial x}\frac{\partial\psi_j}{\partial x}+\bar{N}_2\frac{\partial\psi_i}{\partial y}\frac{\partial\psi_j}{\partial y}+\bar{N}_6\left(\frac{\partial\psi_i}{\partial x}\frac{\partial\psi_j}{\partial y}+\frac{\partial\psi_i}{\partial y}\frac{\partial\psi_j}{\partial x}\right)\right\}dxdy\\
G_{ij}^{36} =& \int_{\Omega_e}\left\{\frac{\partial\psi_i}{\partial x}\left(\bar{B}_{11}\frac{\partial w_0}{\partial x}+\bar{B}_{61}\frac{\partial w_0}{\partial y}\right)\psi_j+\frac{\partial\psi_i}{\partial y}\left(\bar{B}_{61}\frac{\partial w_0}{\partial x}+\bar{B}_{21}\frac{\partial w_0}{\partial y}\right)\psi_j\right\}dxdy\\
G_{ij}^{37} =& \int_{\Omega_e}\left\{\frac{\partial\psi_i}{\partial x}\left(\bar{B}_{12}\frac{\partial w_0}{\partial x}+\bar{B}_{62}\frac{\partial w_0}{\partial y}\right)\psi_j+\frac{\partial\psi_i}{\partial y}\left(\bar{B}_{62}\frac{\partial w_0}{\partial x}+\bar{B}_{22}\frac{\partial w_0}{\partial y}\right)\psi_j\right\}dxdy\\
G_{ij}^{38} =& \int_{\Omega_e}\left\{\frac{\partial\psi_i}{\partial x}\left(\bar{B}_{16}\frac{\partial w_0}{\partial x}+\bar{B}_{66}\frac{\partial w_0}{\partial y}\right)\psi_j+\frac{\partial\psi_i}{\partial y}\left(\bar{B}_{66}\frac{\partial w_0}{\partial x}+\bar{B}_{26}\frac{\partial w_0}{\partial y}\right)\psi_j\right\}dxdy\\
G_{ij}^{31} =& 2G_{ji}^{13},\quad G_{ij}^{32}=2G_{ji}^{23},\quad G_{ij}^{63}=\frac{1}{2}G_{ji}^{36},\quad G_{ij}^{73}=\frac{1}{2}G_{ji}^{37},\quad G_{ij}^{83}=\frac{1}{2}G_{ji}^{38}
\end{aligned}
\tag{4.29}
$$

where

$$\bar{N}_1=\frac{1}{2}\bar{A}_{11}\left(\frac{\partial w_0}{\partial x}\right)^2+\frac{1}{2}\bar{A}_{12}\left(\frac{\partial w_0}{\partial y}\right)^2+\bar{A}_{16}\frac{\partial w_0}{\partial x}\frac{\partial w_0}{\partial y} \tag{4.30a}$$

$$\bar{N}_2=\frac{1}{2}\bar{A}_{12}\left(\frac{\partial w_0}{\partial x}\right)^2+\frac{1}{2}\bar{A}_{22}\left(\frac{\partial w_0}{\partial y}\right)^2+\bar{A}_{26}\frac{\partial w_0}{\partial x}\frac{\partial w_0}{\partial y} \tag{4.30b}$$

$$\bar{N}_6=\frac{1}{2}\bar{A}_{16}\left(\frac{\partial w_0}{\partial x}\right)^2+\frac{1}{2}\bar{A}_{26}\left(\frac{\partial w_0}{\partial y}\right)^2+\bar{A}_{66}\frac{\partial w_0}{\partial x}\frac{\partial w_0}{\partial y} \tag{4.30c}$$

The remaining $G_{ij}^{\alpha\beta}$ are zero. Similarly, the force vectors are defined by

$$
\begin{aligned}
F_i^1 &= \int_{\Gamma^e} N_n\psi_i ds,\quad F_i^2=\int_{\Gamma^e} N_{ns}\psi_i ds,\quad F_i^3=\int_{\Gamma^e} Q_n\psi_i ds\\
F_i^4 &= \int_{\Gamma^e} M_n\psi_i ds,\quad F_i^5=\int_{\Gamma^e} M_{ns}\psi_i ds,\quad F_i^6=F_i^7=F_i^8=0
\end{aligned}
\tag{4.31}
$$

where $Q_n, N_n, N_{ns}, M_n, M_{ns}$ are given in equation (4.23).

In order to solve the corresponding system of nonlinear algebraic equations, the tangent stiffness coefficients are derived.The Newton-Raphson iterative method in-

volves solving equations of the form

$$\begin{bmatrix} [T^{11}] & [T^{12}] & [T^{13}] & \cdots & [T^{18}] \\ & [T^{22}] & [T^{23}] & \cdots & [T^{28}] \\ & & [T^{33}] & \cdots & [T^{38}] \\ & (sym) & & \ddots & \vdots \\ & & & & [T^{88}] \end{bmatrix} \begin{Bmatrix} \{\delta\Delta^1\} \\ \{\delta\Delta^2\} \\ \{\delta\Delta^3\} \\ \vdots \\ \{\delta\Delta^8\} \end{Bmatrix} = - \begin{Bmatrix} \{R^1\} \\ \{R^2\} \\ \{R^3\} \\ \vdots \\ \{R^8\} \end{Bmatrix} \tag{4.32}$$

where the vector Δ^α contains the generalized displacements and stress resultants,i.e.,

$$\begin{gathered} \Delta_i^1 = u_i, \quad \Delta_i^2 = v_i, \quad \Delta_i^3 = w_i, \quad \Delta_i^4 = \phi_i^1, \quad \Delta_i^5 = \phi_i^2 \\ \Delta_i^6 = M_i^1, \quad \Delta_i^7 = M_i^2, \quad \Delta_i^8 = M_i^6 \end{gathered} \tag{4.33}$$

The coefficients of the submatrices $[T^{\alpha\beta}]$ and the components of the residual vector $\{R^\alpha\}$ are defined by

$$T_{ij}^{\alpha\beta} = \frac{\partial R_i^\alpha}{\partial \Delta_j^\beta} = \sum_{\gamma=1}^{8}\sum_{k=1}^{n} \frac{\partial K_{ik}^{\alpha\gamma}}{\partial \Delta_j^\beta}\Delta_k^\gamma + K_{ij}^{\alpha\beta}, \quad R_i^\alpha = \sum_{\gamma=1}^{8}\sum_{k=1}^{n} K_{ik}^{\alpha\gamma}\Delta_k^\gamma - F_i^\alpha \tag{4.34}$$

The explicit form of the tangent stiffness coefficients is given by

$$\begin{aligned} T_{ij}^{\alpha\beta} &= K_{ij}^{\alpha\beta} \quad \text{for } \alpha = 1, 2...8;\ \beta \neq 3 \\ T_{ij}^{13} &= \sum_{\gamma=1}^{8}\sum_{k=1}^{n} \frac{\partial K_{ik}^{1\gamma}}{\partial w_j}\Delta_k^\gamma + K_{ij}^{13} = 2K_{ij}^{13}, \quad T_{ij}^{23} = \sum_{\gamma=1}^{8}\sum_{k=1}^{n} \frac{\partial K_{ik}^{2\gamma}}{\partial w_j}\Delta_k^\gamma + K_{ij}^{23} = 2K_{ij}^{23} \\ T_{ij}^{33} &= \sum_{\gamma=1}^{8}\sum_{k=1}^{n} \frac{\partial K_{ik}^{3\gamma}}{\partial w_j}\Delta_k^\gamma + K_{ij}^{33} = \sum_{k=1}^{n}\Bigg(\frac{\partial K_{ik}^{31}}{\partial w_j}u_k + \frac{\partial K_{ik}^{32}}{\partial w_j}v_k + \frac{\partial K_{ik}^{33}}{\partial w_j}w_k + \frac{\partial K_{ik}^{34}}{\partial w_j}\phi_k^1 \\ &\quad + \frac{\partial K_{ik}^{35}}{\partial w_j}\phi_k^2 + \frac{\partial K_{ik}^{36}}{\partial w_k}M_j^1 + \frac{\partial K_{ik}^{37}}{\partial w_k}M_j^2 + \frac{\partial K_{ik}^{38}}{\partial w_k}M_j^6\Bigg) + K_{ij}^{33} \\ &= \int_{\Omega_e}\Bigg\{\left(\bar{A}_{11}\frac{\partial u_0}{\partial x} + \bar{A}_{16}\frac{\partial u_0}{\partial y}\right)S_{xx} + \left(\bar{A}_{12}\frac{\partial u_0}{\partial x} + \bar{A}_{26}\frac{\partial u_0}{\partial y}\right)S_{yy} \\ &\qquad + \left(\bar{A}_{16}\frac{\partial u_0}{\partial x} + \bar{A}_{66}\frac{\partial u_0}{\partial y}\right)S_{xy} + \left(\bar{A}_{16}\frac{\partial v_0}{\partial x} + \bar{A}_{12}\frac{\partial v_0}{\partial y}\right)S_{xx} \end{aligned}$$

$$+\left(\bar{A}_{26}\frac{\partial v_0}{\partial x}+\bar{A}_{22}\frac{\partial v_0}{\partial y}\right)S_{yy}+\left(\bar{A}_{66}\frac{\partial v_0}{\partial x}+\bar{A}_{16}\frac{\partial v_0}{\partial y}\right)S_{xy} \tag{4.35}$$
$$+\left[\bar{A}_{11}\left(\frac{\partial w_0}{\partial x}\right)^2+\frac{1}{2}\bar{A}_{12}\left(\frac{\partial w_0}{\partial y}\right)^2+2\bar{A}_{16}\frac{\partial w_0}{\partial x}\frac{\partial w_0}{\partial y}\right]S_{xx}$$
$$+\left[\frac{1}{2}\bar{A}_{66}\left(\frac{\partial w_0}{\partial x}\right)^2+\bar{A}_{22}\left(\frac{\partial w_0}{\partial y}\right)^2+2\bar{A}_{26}\frac{\partial w_0}{\partial x}\frac{\partial w_0}{\partial y}\right]S_{yy}$$
$$+\left[\bar{A}_{16}\left(\frac{\partial w_0}{\partial x}\right)^2+\bar{A}_{26}\left(\frac{\partial w_0}{\partial y}\right)^2+\frac{1}{2}\left(\bar{A}_{12}+2\bar{A}_{66}\right)\frac{\partial w_0}{\partial x}\frac{\partial w_0}{\partial y}\right]S_{xy}$$
$$+\left(M^1\bar{B}_{11}+M^2\bar{B}_{12}+M^6\bar{B}_{16}\right)S_{xx}+\left(M^1\bar{B}_{21}+M^2\bar{B}_{22}+M^6\bar{B}_{26}\right)S_{yy}$$
$$+\left(M^1\bar{B}_{61}+M^2\bar{B}_{62}+M^6\bar{B}_{66}\right)S_{yy}+K_{ij}^{33}\Big\}dxdy$$

$$T_{ij}^{43}=K_{ij}^{43},\quad T_{ij}^{53}=K_{ij}^{53},\quad T_{ij}^{63}=\sum_{\gamma=1}^{8}\sum_{k=1}^{n}\frac{\partial K_{ik}^{6\gamma}}{\partial w_j}\Delta_k^{\gamma}+K_{ij}^{63}=2K_{ij}^{63}$$

$$T_{ij}^{73}=\sum_{\gamma=1}^{8}\sum_{k=1}^{n}\frac{\partial K_{ik}^{7\gamma}}{\partial w_j}\Delta_k^{\gamma}+K_{ij}^{73}=2K_{ij}^{73},\quad T_{ij}^{83}=\sum_{\gamma=1}^{8}\sum_{k=1}^{n}\frac{\partial K_{ik}^{8\gamma}}{\partial w_j}\Delta_k^{\gamma}+K_{ij}^{83}=2K_{ij}^{83}$$

where the remaining $T_{ij}^{\alpha\beta}$ are equal to $K_{ij}^{\alpha\beta}$ and

$$S_{xx}=\frac{\partial\psi_i}{\partial x}\frac{\partial\psi_j}{\partial x},\quad S_{yy}=\frac{\partial\psi_i}{\partial y}\frac{\partial\psi_j}{\partial y},\quad S_{xy}=\left(\frac{\partial\psi_i}{\partial y}\frac{\partial\psi_j}{\partial x}+\frac{\partial\psi_i}{\partial x}\frac{\partial\psi_j}{\partial y}\right)$$

The finite element model for laminated beams can be obtained as a special case of the finite element model for laminated plates. The bending of beam structures can be modelled as a one-dimensional problem, consequently the displacements (u, v, w) and moment resultant M_{xx} are taken to be functions of the x-coordinate. The associated displacement field is

$$u(x)=u_0(x)+z\phi_x(x),\quad v(x)=0,\quad w(x)=w_0(x) \tag{4.36}$$

and the corresponding system of equilibrium equations at the element level takes the

form

$$\begin{bmatrix} [K^{11}] & [K^{12}] & [K^{13}] & [K^{14}] \\ [K^{21}] & [K^{22}] & [K^{23}] & [K^{24}] \\ [K^{31}] & [K^{23}] & [K^{33}] & [K^{34}] \\ [K^{41}] & [K^{42}] & [K^{43}] & [K^{44}] \end{bmatrix}^{(e)} \begin{Bmatrix} \{u^e\} \\ \{w^e\} \\ \{\phi_x^e\} \\ \{M_{xx}^e\} \end{Bmatrix} = \begin{Bmatrix} \{F^1\} \\ \{F^2\} \\ \{F^3\} \\ \{F^4\} \end{Bmatrix}^{(e)} \tag{4.37}$$

where the coefficients $K_{ij}^{\alpha}\beta$ are defined by the following expressions

$$\begin{aligned}
K_{ij}^{11} &= \int_{\Omega_e} \bar{A}_{11} \frac{d\psi_i}{dx}\frac{d\psi_j}{dx}\,dx, \quad K_{ij}^{12} = \frac{1}{2}\int_{\Omega_e} \bar{A}_{11}\frac{dw_0}{dx}\frac{d\psi_i}{dx}\frac{d\psi_j}{dx}\,dx \\
K_{ij}^{14} &= \int_{\Omega_e} \bar{B}_{11}\frac{d\psi_i}{dx}\psi_j\,dx, \quad K_{ij}^{13} = K_{ij}^{31} = 0 \\
K_{ij}^{21} &= \int_{\Omega_e} \bar{A}_{11}\frac{dw_0}{dx}\frac{d\psi_i}{dx}\frac{d\psi_j}{dx}\,dx, \quad K_{ij}^{22} = \int_{\Omega_e}\left[\frac{1}{2}\bar{A}_{11}\left(\frac{dw_0}{dx}\right)^2 + \tilde{A}_{55}\right]\frac{d\psi_i}{dx}\frac{d\psi_j}{dx}\,dx \\
K_{ij}^{23} &= \int_{\Omega_e} \tilde{A}_{55}\frac{d\psi_i}{dx}\psi_j\,dx, \quad K_{ij}^{24} = \int_{\Omega_e} \bar{B}_{11}\frac{dw_0}{dx}\frac{d\psi_i}{dx}\psi_j\,dxdy \\
K_{ij}^{32} &= \int_{\Omega_e} \tilde{A}_{55}\frac{d\psi_j}{dx}\psi_i\,dx, \quad K_{ij}^{33} = \int_{\Omega_e} \tilde{A}_{55}\psi_i\psi_j\,dx, \quad K_{ij}^{34} = \int_{\Omega_e}\frac{d\psi_j}{dx}\psi_i\,dx \\
K_{ij}^{41} &= \int_{\Omega_e} \bar{B}_{11}\frac{d\psi_j}{dx}\psi_i\,dx, \quad K_{ij}^{42} = \frac{1}{2}\int_{\Omega_e} \bar{B}_{11}\frac{dw_0}{dx}\frac{d\psi_j}{dx}\psi_i\,dx \\
K_{ij}^{43} &= \int_{\Omega_e}\frac{d\psi_j}{dx}\psi_i\,dx, \quad K_{ij}^{44} = \int_{\Omega_e}\bar{D}_{11}\psi_i\psi_j\,dx
\end{aligned} \tag{4.38}$$

The corresponding linearized system of equations has the form

$$\begin{bmatrix} [T^{11}] & [T^{12}] & [T^{13}] & [T^{14}] \\ & [T^{22}] & [T^{23}] & [T^{24}] \\ & & [T^{33}] & [T^{34}] \\ (sym) & & & [T^{44}] \end{bmatrix}^{(e)} \begin{Bmatrix} \{\delta\Delta^1\} \\ \{\delta\Delta^2\} \\ \{\delta\Delta^3\} \\ \{\delta\Delta^4\} \end{Bmatrix}^{(e)} = -\begin{Bmatrix} \{R^1\} \\ \{R^2\} \\ \{R^3\} \\ \{R^4\} \end{Bmatrix}^{(e)} \tag{4.39}$$

where

$$
\begin{aligned}
&T_{ij}^{11} = K_{ij}^{11}, \quad T_{ij}^{12} = K_{ij}^{12} + \frac{1}{2}\int_{\Omega_e} \bar{A}_{11}\frac{dw_0}{dx}\frac{d\psi_i}{dx}\frac{d\psi_j}{dx}\,dx = 2K_{ji}^{12} \\
&T_{ij}^{13} = T_{ij}^{31} = 0, \quad T_{ij}^{14} = K_{ij}^{14} \\
&T_{ij}^{21} = K_{ij}^{21}, \quad T_{ij}^{23} = K_{ij}^{23}, \quad T_{ij}^{24} = K_{ij}^{24} \\
&T_{ij}^{22} = K_{ij}^{22} + \int_{\Omega_e} \left\{ \bar{A}_{11}\left[\frac{du_0}{dx} + \left(\frac{dw_0}{dx}\right)^2\right] + \bar{B}_{11}M_{xx} \right\} \frac{d\psi_i}{dx}\frac{d\psi_j}{dx}\,dx \\
&T_{ij}^{32} = K_{ij}^{32}, \quad T_{ij}^{33} = K_{ij}^{33}, \quad T_{ij}^{34} = K_{ij}^{34} \\
&T_{ij}^{41} = K_{ij}^{41}, \quad T_{ij}^{43} = K_{ij}^{43}, \quad T_{ij}^{44} = K_{ij}^{44} \\
&T_{ij}^{42} = K_{ij}^{42} + \frac{1}{2}\int_{\Omega_e} \bar{B}_{11}\frac{dw_0}{dx}\frac{d\psi_j}{dx}\psi_i\,dx = 2K_{ji}^{42}
\end{aligned}
\tag{4.40}
$$

CHAPTER V

MIXED PLATE BENDING ELEMENTS: NUMERICAL RESULTS

V.1. Introduction

The mixed finite element model developed herein is employed in the linear and nonlinear bending analysis of a variety of layered composite rectangular plates. The effects of transverse shear deformation, material anisotropy and coupling between stretching and bending on deflections and stresses are investigated. Validation of the present model is carried out by comparing the finite element results with analytical (Navier) solutions based on the first-order shear deformation theory (FSDT) and experimental and numerical solutions available in the literature.

The shear correction coefficient is taken to be 5/6. Only one quadrant of the plate is used as computational domain for plates with biaxial symmetry. The corresponding boundary conditions for cross-ply and angle-ply simply supported rectangular laminates are depicted in Figure 18. Note that the antisymmetric cross-ply and angle-ply laminated plates admit the Navier solutions only for SS-1 and SS-2 boundary conditions, respectively.

The following nondimensionalizations of the quantities are used to present results in graphical and tabular form:

$$\begin{aligned}
\bar{w} &= w(x_A, y_A, 0)\frac{E_2 h^3}{b^4 q_0}10^2, \quad \bar{\sigma}_{xx} = \sigma_{xx}(x_A, y_A, z)\frac{h^2}{b^2 q_0} \\
\bar{\sigma}_{yy} &= \sigma_{yy}(x_A, y_A, z)\frac{h^2}{b^2 q_0}, \qquad \bar{\sigma}_{xy} = \sigma_{xy}(x_D, y_D, z)\frac{h^2}{b^2 q_0} \\
\bar{\sigma}_{xz} &= \sigma_{xz}(x_B, y_B, z)\frac{h}{b q_0}, \qquad \bar{\sigma}_{yz} = \sigma_{yz}(x_C, y_C, z)\frac{h}{b q_0} \\
(\bar{M}_{xx}, \bar{M}_{yy}, \bar{M}_{xy}) &= (M_{xx}, M_{yy}, M_{xy})\frac{10}{q_0 a^2}
\end{aligned} \tag{5.1}$$

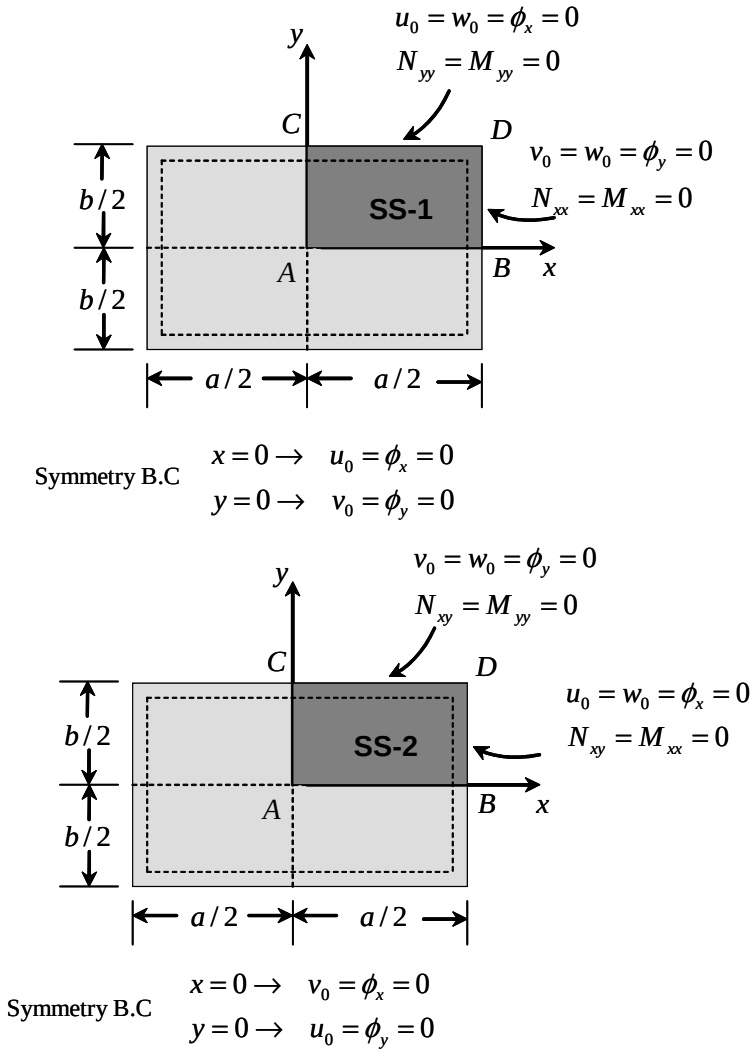

Fig. 18. Boundary conditions in a quadrant of cross-ply (SS-1) and angle-ply (SS-2) laminates.

The location of the maximum normal and shear stresses in the plane of the plate is shown in Figure 18. Note that the location of maximum stress through the plate thickness depends on the lamination scheme. For antisymmetric cross-ply laminates, the maximum values of M_{xx} and M_{yy} occur at point A (see figure 18), and the maximum of M_{xy} takes place at point D. The locations of maximum bending

moments for angle-ply laminates varies with the stacking sequence.

The strains are calculated by differentiating the displacement expansions (4.25) according to the definition given in Equations (4.2)-(4.4). The stresses are then computed at each layer k in the global coordinates using the constitutive equations:

$$\begin{Bmatrix} \sigma_{xx} \\ \sigma_{yy} \\ \sigma_{xy} \\ \sigma_{xz} \\ \sigma_{yz} \end{Bmatrix}^{(k)} = \begin{bmatrix} \bar{Q}_{11} & \bar{Q}_{12} & \bar{Q}_{16} & 0 & 0 \\ \bar{Q}_{12} & \bar{Q}_{22} & \bar{Q}_{26} & 0 & 0 \\ \bar{Q}_{16} & \bar{Q}_{26} & \bar{Q}_{66} & 0 & 0 \\ 0 & 0 & 0 & \bar{Q}_{55} & \bar{Q}_{45} \\ 0 & 0 & 0 & \bar{Q}_{45} & \bar{Q}_{44} \end{bmatrix}^{(k)} \begin{Bmatrix} \epsilon_{xx} \\ \epsilon_{yy} \\ \epsilon_{xy} \\ \epsilon_{xz} \\ \epsilon_{yz} \end{Bmatrix} \tag{5.2}$$

where $\bar{Q}_{ij}$ are the transformed plane-stress reduced stiffness. Both strains and stresses are the most accurate when computed at the reduced $(N-1)\times(N-1)$ Gauss points, where $N \times N$ is the exact Gauss quadrature rule used to evaluate the bending stiffness coefficients. The bending moments are computed directly at the nodal points, along with the displacements and rotations, by solving the assembled system of equilibrium equations.

The effect of the integration rule of the stiffness coefficients on the solution is also investigated. Mixed C^0-plate bending elements based on the first-order shear deformation plate theory are expected to give the thin plate theory solution when the side-to-thickness a/h is very large. When low-order interpolation of the dependent variables is used, the elements become excessively stiff, yielding displacements that are too small compared to the thin plate solution. This effect is known as "shear-locking". When thin plates are analyzed by shear deformable plate elements, the shearing strains are required to vanish. This can be numerically achieved by either using high-order approximation functions or by using reduced integration.

V.2. Linear bending analysis

In all the linear problems considered, the individual layers are assumed to be of equal thickness and made of graphite-epoxy material with

$$\begin{gathered} E_1/E_2 = 25, \quad G_{12}/E_2 = 0.5, \quad G_{23}/E_2 = 0.2 \\ \nu_{12} = 0.25, \quad G_{12} = G_{13}, \quad \nu_{12} = \nu_{13} \end{gathered} \tag{5.3}$$

Figures 19 and 20 illustrate the convergence of the finite element solution for the center deflection w to the analytical solution w^*, for a thin cross-ply (0/90/90/0) laminate subjected to uniformly distributed load (UDL) and sinusoidal loading (SSL). As the the mesh size h is decreased, the percentage error in the normalized maximum deflection decreases for a fixed p-level of 2.

Tables 3 and 4 show results of a p-convergence study for maximum transverse deflection and stresses of simply supported cross-ply (0/90/90/0) and angle-ply (−45/45) laminates subjected to sinusoidal and uniform loading, respectively. The effect of shear locking is mitigated as the expansion order increases and becomes negligible for p-levels of 4. The stiffness terms are evaluated using full integration. It is clear from the results that the rate of convergence is faster for thin plates than for thick plates.

It should also be noted that the errors in the maximum deflections exhibit an exponentially fast decay with increasing p, as shown in Figures 21 and 22. In the previous examples, full integration was used in the evaluation of the stiffness matrix coefficients associated with bending and transverse shear strains.

Next a comparison between the performance of displacement-based plate elements and mixed plate elements is carried out. In the sequel, mixed finite elements derived in the present work will be denoted by the acronym MXFEM, whereas the displacement-based finite elements are denoted by DBFEM.

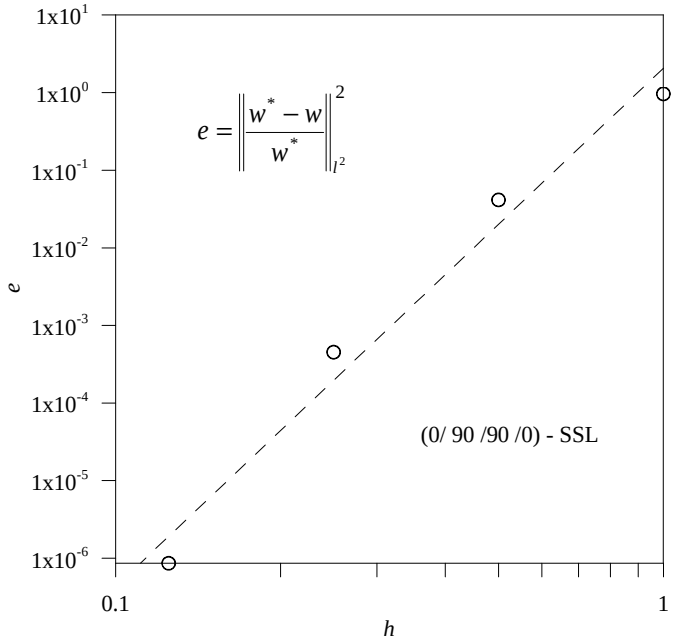

Fig. 19. Convergence of the center deflection w as a function of the mesh size h, for a SS-1 cross-ply (0/90/90/0) square plate under sinusoidal load ($a/h = 100$).

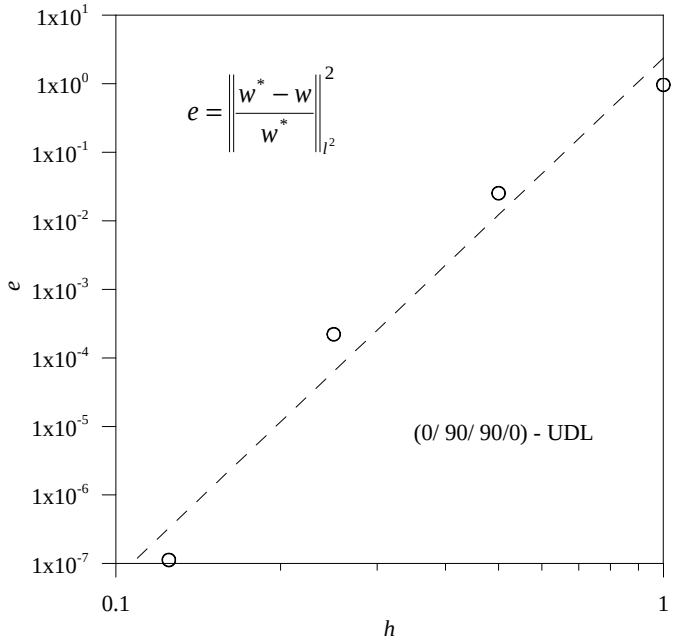

Fig. 20. Convergence of the center deflection w as a function of the mesh size h, for a SS-1 cross-ply (0/90/90/0) square plate under uniform load ($a/h = 100$).

Table 3. p-convergence†of maximum transverse deflection and stresses of a simply supported (SS-1) cross-ply (0/90/90/0) square plate under sinusoidal load for different values of side-to-thickness ratio a/h.

a/h	p	$\bar{w}$	$\bar{\sigma}_{xx}$	$\bar{\sigma}_{yy}$	$\bar{\sigma}_{xy}$	$\bar{\sigma}_{xz}$	$\bar{\sigma}_{yz}$
10	1	0.4530	0.0959	0.0734	0.0048	0.1323	0.0809
	2	0.6529	0.4191	0.2958	0.0208	0.3613	0.1154
	3	0.6634	0.4861	0.3543	0.0234	0.4049	0.1257
	4	0.6627	0.4931	0.3574	0.0239	0.4116	0.1277
Analytical	-	0.6627	0.4889	0.3614	0.0241	0.4160	0.1290
20	1	0.1627	0.0516	0.0296	0.0022	0.1219	0.0914
	2	0.4609	0.4201	0.2224	0.0187	0.3761	0.0981
	3	0.4925	0.5163	0.2939	0.0214	0.4254	0.1061
	4	0.4912	0.5214	0.2927	0.0218	0.4319	0.1074
Analytical	-	0.4912	0.5273	0.2956	0.0221	0.4370	0.1090
100	1	0.0084	0.0032	0.0016	0.0001	0.1076	0.1057
	2	0.3454	0.3390	0.1667	0.0168	0.3845	0.0842
	3	0.4369	0.5469	0.2775	0.0203	0.4351	0.0998
	4	0.4337	0.5341	0.2690	0.0211	0.4397	0.0997
Analytical	-	0.4337	0.5382	0.2704	0.0213	0.4450	0.1010

†Full integration is used to evaluate membrane, bending and shearing stiffness terms.

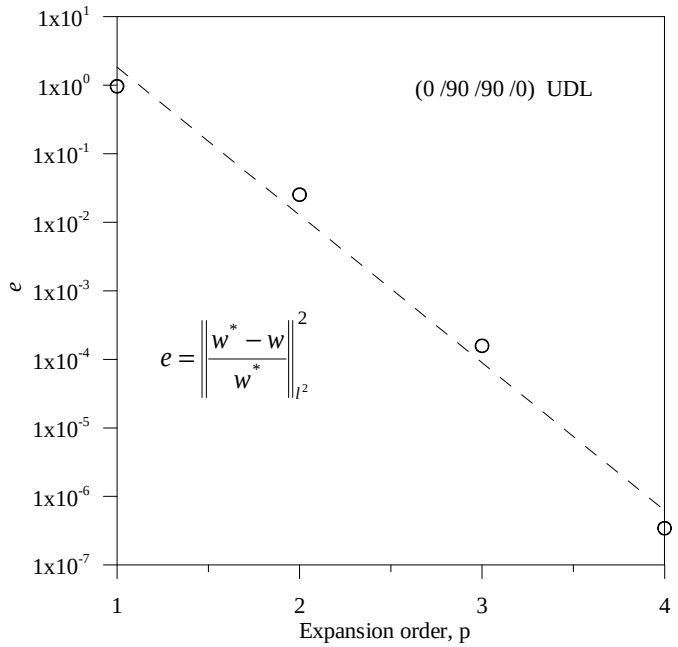

Fig. 21. Convergence of the center deflection w as a function of the expansion order p, for a SS-1 cross-ply (0/90/90/0) square plate under uniform load ($a/h = 100$).

Table 4. p-convergence†of maximum transverse deflection and stresses of a simply supported (SS-2) angle-ply ($-45/45$) square plate under uniform load for different values of side-to-thickness ratio a/h.

a/h	p	$\bar{w}$	$\bar{\sigma}_{xx}$	$\bar{\sigma}_{xy}$	$\bar{\sigma}_{xz}$
10	1	0.7685	0.1224	0.1200	0.1607
	2	1.0560	0.2990	0.3253	0.2689
	3	1.2800	0.3714	0.4215	0.3308
	4	1.2790	0.3740	0.4270	0.3537
Analytical	-	1.2792	0.3476	0.4274	0.3540
20	1	0.2673	0.0512	0.0502	0.1607
	2	0.8366	0.3132	0.3464	0.2747
	3	1.0970	0.3652	0.4243	0.3322
	4	0.3322	0.3707	0.4330	0.3503
Analytical	-	1.0907	0.3496	0.4357	0.3510
100	1	0.0128	0.0026	0.0026	0.1607
	2	0.7032	0.3745	0.3987	0.3361
	3	1.0460	0.3868	0.4246	0.3429
	4	1.0290	0.3696	0.4350	0.3453
Analytical	-	1.0305	0.3504	0.4417	0.3499

†Full integration is used to evaluate membrane, bending and shearing stiffness terms.

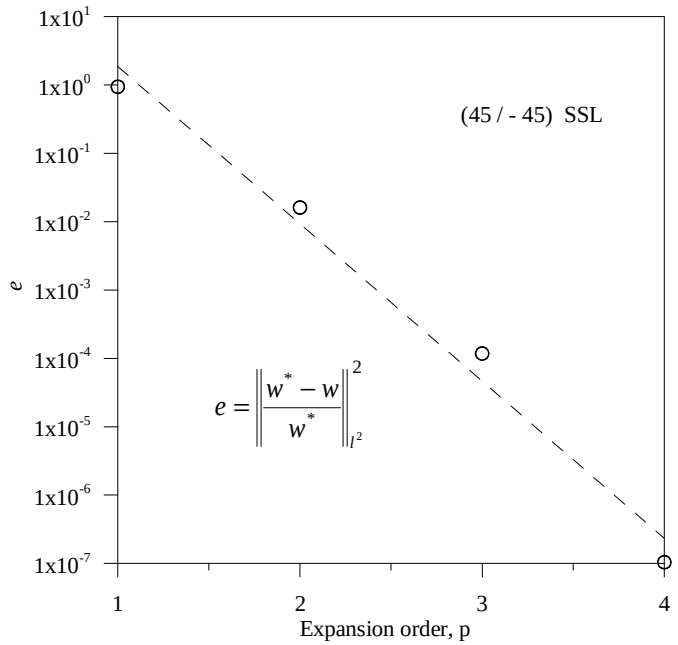

Fig. 22. Convergence of the center deflection w as a function of the expansion order p, for a SS-2 angle-ply (-45/45) square plate under sinusoidal load ($a/h = 100$).

It can be observed from Tables 5 and 6 that the values of deflections predicted by MXFEM elements are close to those predicted by DBFEM elements. However, mixed elements yield more accurate results for bending moments, and hence stresses. The superiority of MXFEM over DBFEM plate elements can be attributed to the inclusion of the bending moments as nodal degrees of freedom. Additionally, the moment boundary conditions are satisfied exactly in mixed finite element models whereas for displacement finite element models the natural boundary conditions are only met in an integral sense.

Table 5. Comparison of displacement-based and mixed finite element results for deflections, bending moments and stresses of a simply supported (SS-2) angle-ply $(-45/45)$ square plate under uniform load.

Mesh Type†	$\bar{w}$	$\bar{M}_{xx}$	$\bar{M}_{xy}$	$\bar{\sigma}_{xx}$	$\bar{\sigma}_{xy}$	$\bar{\sigma}_{xz}$
4L-DBFEM-F	0.1797	0.0659	0.0655	0.0635	0.0665	0.3470
4L-DBFEM-R	1.0269	0.3633	0.3981	0.3643	0.4078	0.3267
2Q-DBFEM-F	1.0221	0.3706	0.4125	0.3806	0.4327	0.3403
2Q-DBFEM-R	1.0320	0.3696	0.4187	0.3788	0.4262	0.3307
4L-MXFEM-F	0.1797	0.0706	0.0720	0.0635	0.0665	0.3472
4L-MXFEM-R	1.0294	0.3605	0.4420	0.3519	0.4072	0.3307
2Q-MXFEM-F	1.0252	0.3320	0.4711	0.3531	0.4316	0.3416
2Q-MXFEM-R	1.0306	0.3821	0.4607	0.3513	0.4371	0.3499
Analytical	1.0305	0.3754	0.4544	0.3504	0.4417	0.3499

†F = full integration; R = reduced integration.

The effect of the integration rule of the stiffness coefficients on the solution is investigated. Two different meshes, a 4×4 mesh of linear elements $(4L)$ and a 2×2 mesh of quadratic elements $(2Q)$ in a quarter plate, are considered. An examination of the numerical results presented in Tables 6 and 7 shows that both MXFEM and DBFEM elements experience shear locking when linear elements and full integration rule are used. Clearly, the effect of shear locking vanishes when using quadratic

Table 6. Comparison of displacement-based and mixed finite element results for deflections, bending moments and stresses of a simply supported (SS-1)cross-ply (0/90/90/0) square plate under sinusoidal load.

Mesh Type †	$\bar{w}$	$\bar{M}_{xx}$	$\bar{M}_{yy}$	$\bar{M}_{xy}$	$\bar{\sigma}_{xx}$	$\bar{\sigma}_{yy}$	$\bar{\sigma}_{xy}$	$\bar{\sigma}_{xz}$	$\bar{\sigma}_{yz}$
4L-DBFEM-F	0.1034	0.1766	0.0339	0.0079	0.1203	0.0604	0.0048	0.2980	0.2210
4L-DBFEM-R	0.4284	0.7414	0.1423	0.0333	0.5048	0.2537	0.0207	0.4280	0.0970
2Q-DBFEM-F	0.4193	0.7264	0.1379	0.0335	0.4946	0.2420	0.0201	0.4310	0.0980
2Q-DBFEM-R	0.4339	0.7672	0.1472	0.0345	0.5224	0.2550	0.0206	0.4300	0.0970
4L-MXFEM-F	0.1037	0.1895	0.0363	0.0085	0.1207	0.0599	0.0048	0.2973	0.2212
4L-MXFEM-R	0.4339	0.8202	0.1573	0.0355	0.5153	0.2561	0.0219	0.4300	0.0992
2Q-MXFEM-F	0.4244	0.7601	0.1479	0.0370	0.5004	0.2510	0.0199	0.4332	0.0988
2Q-MXFEM-R	0.4337	0.7992	0.1543	0.0355	0.5341	0.2690	0.0211	0.4397	0.0997
Analytical	0.4337	0.7905	0.1517	0.0355	0.5382	0.2704	0.0213	0.4450	0.1010

†F = full integration; R = reduced integration.

elements and reduced integration. As discussed earlier, the shear locking can also be removed by increasing the p-level even when full integration is used. However, high-order elements are computationally more expensive. Guided by these observations, a mesh of quadratic elements with reduced integration is employed in the remaining analyses, unless otherwise specified.

Next, we consider the bending of symmetrically laminated beams. When the width of a laminated plate is very small compared to the length and the lamination scheme and loading are such that the displacements are functions of x only, the laminated plate is treated as a beam. The results presented here serve as a basis for understanding the response of more general laminates.

Table 7. Effect of the lamination scheme and transverse shear deformation on the center deflection $\bar{w}$ and normal stress $\bar{\sigma}_{xx}$ of a beam under uniform load†.

	Hinged-Hinged			Clamped-Clamped			Clamped-Free		
$a/h \rightarrow$	100	20	10	100	20	10	100	20	10
0	0.628	0.700	0.925	0.128	0.200	0.425	6.02	6.30	7.19
	0.628	0.700	0.925	0.128	0.200	0.425	6.01	6.30	7.20
90	15.667	15.812	16.375	3.134	3.313	3.875	150.03	150.76	152.91
	15.633	15.813	16.375	3.132	3.312	3.875	150.00	150.75	153.00
$(0/90)_s$	0.713	0.816	1.138	0.146	0.248	0.569	6.82	7.24	8.51
	0.713	0.816	1.137	0.146	0.249	0.570	6.82	7.23	8.52
$(45/-45)_s$	8.956	9.050	9.371	1.792	1.896	2.217	85.85	86.27	87.56
	8.947	9.049	9.371	1.793	1.895	2.217	85.86	86.28	87.56

†The first row contains the finite element values of the nondimensionalized maximum deflections, and the second row contains the corresponding analytical solutions.

Table 8 contains the nondimensionalized maximum transverse deflections of various laminated beams for simply supported (hinged-hinged), clamped (fixed-fixed), and cantilever (clamped-free) boundary conditions. The results are in very good

agreement with the closed-form solutions. The 0^o laminated beam is stiffer in bending than the 90^o beam, and therefore undergoes smaller deflections. This is due to the fact that the stiffness in a laminate is largest in the fiber direction because $E_1 > E_2$.

The effect of lamination scheme and shear deformation on the beam deflections can be seen in Figures 23 to 25. Since the bending stiffness increases with the cube of the distance of the layers from the midplane, $(0/90)_s$ laminates undergo smaller deflections when compared to the $(90/0)_s$ beams. Similarly, due to the placement of the 0^o layers, laminate $(0/45/-45/90)_s$ is much stiffer than laminate $(90/45/-45/0)_s$. Symmetric angle-ply laminated beams $(\theta/-\theta)_s$ have the same stiffness characteristics as $(-\theta/\theta)_s$, and they are less stiff compared to the symmetric cross-ply laminated beams.

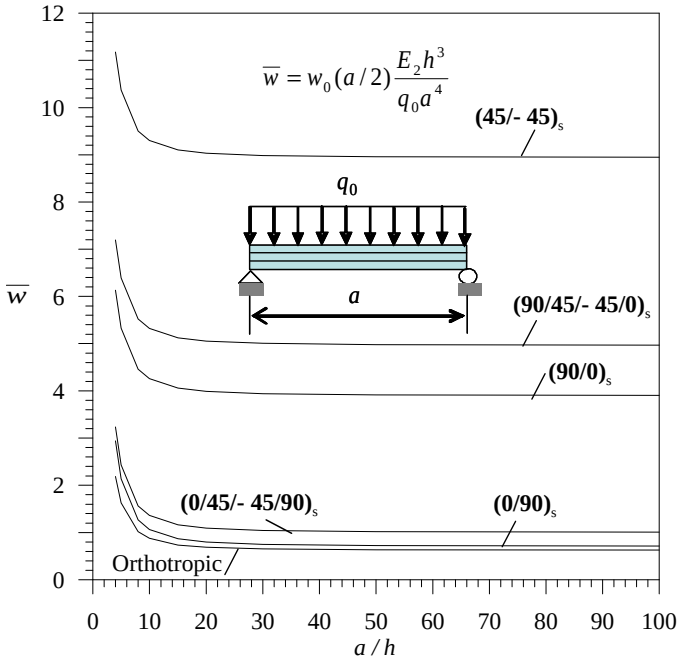

Fig. 23. Convergence of the maximum displacement $\bar{w}$ as a function of Maximum deflection $\bar{w}$ versus length-to-thickness ratio of a simply-supported beam under uniform load.

It can also be observed from the plots that the effect of shear deformation is more significant for beams with length-to-thickness ratios smaller than 10. The effect of shear deformation is to increase the transverse deflection.

The next example deals with a four-layer cross-ply symmetric (0/90/90/0) square laminate subjected to sinusoidal loading (SSL). The plate is assumed to be SS-1 simply-supported (see Figure 18). The maximum deflections at the center of the plate are plotted against the side-to-thickness ratio a/h in Figure 26. It can be observed that the shearing deformation is more pronounced in the range of medium to thick plates ($a/h \leq 20$) and is almost negligible for thin plates, for which both the classical (CLPT) and first order (FSDT) theories yield similar results ($a/h \geq 50$). Very good agreement is found between the analytical solution based on FSDT and the mixed finite element results.

The variations of stresses $\sigma_{xx}, \sigma_{yy}, \sigma_{xy}, \sigma_{xz}, \sigma_{yz}$ through the thickness are shown in Figures 27 through 31. Stresses are computed using the constitutive relations in Eq. (5.1). In-plane stresses vary linearly with the z-coordinate whereas transverse shear stresses are constant, as suggested by the assumed displacement field of the first order theory. The changes in slope observed in plots 27 and 28 represent the change in axial stiffness of each layer. The maximum σ_{xx} takes place at $z = h/2$ whereas the maximum σ_{yy} occurs at $z = h/4$. It is clear that the 0^o layers carry the most axial stress σ_{xx} while the 90^o layers carry the most axial stress σ_{yy}, in proportion to their axial stiffness in the x and y direction. The shear stress σ_{xy} varies linearly with a constant slope, as depicted in Figure 29. This is due to the fact that $\bar{Q}_{16}, \bar{Q}_{26}, \bar{Q}_{66}$ do not change with z for the (0/90/90/0) laminate. In Figures 30 and 31, a comparison between the transverse shear stresses (σ_{xz}, σ_{yz}) calculated via equilibrium equations and constitutive equations is presented. In the case of σ_{xz} the equilibrium equations predict the maximum stress to be at the midplane of the plate,

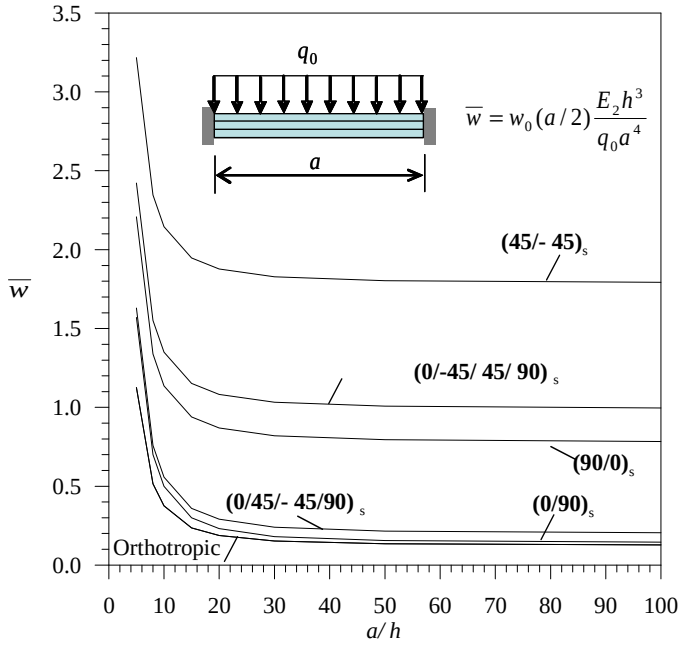

Fig. 24. Maximum deflection $\bar{w}$ versus length-to-thickness ratio of a clamped beam under uniform load.

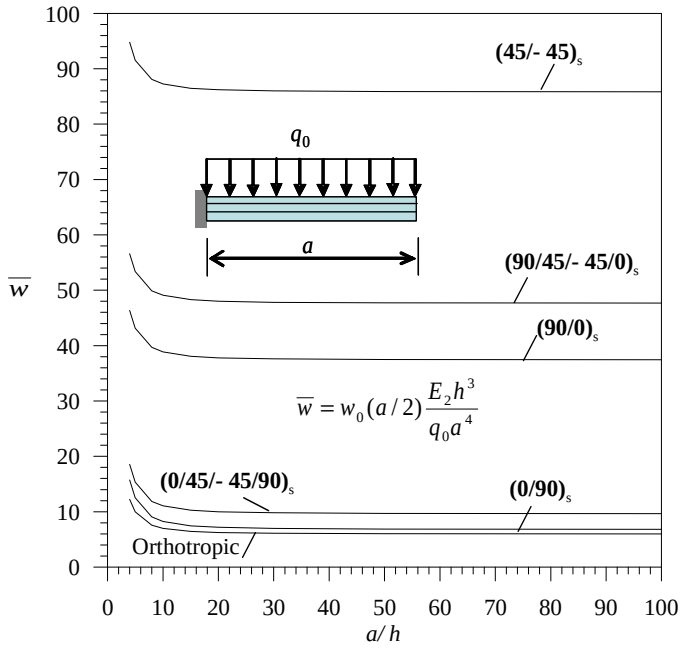

Fig. 25. Maximum deflection $\bar{w}$ versus length-to-thickness ratio of a cantilever beam under uniform load.

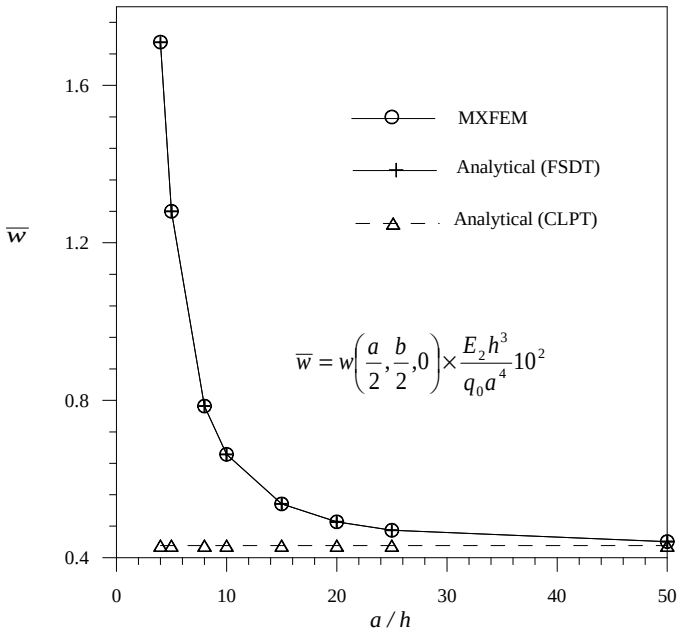

Fig. 26. Effect of shear deformation on the maximum displacement $\bar{w}$ of a SS-1 cross–ply (0/90/90/0) square plate under sinusoidal load.

while the constitutive equations predict maximum stress in the outer layers. It turns out that the constitutive equations yield, qualitatively, the correct stress variation (see the elasticity solution of Pagano [48]). The stresses predicted with MXFEM elements are in excellent agreement with the exact FSDT solutions.

As pointed out by Reddy [45], the effect of the shearing deformation also depends on the material anisotropy of the layers. It can be seen from Figure 32 that deflections decrease with increasing value of E_1/E_2. The difference among the classical and shear deformable theories is more significant as the ratio E_1/E_2 gets larger for a given length-to-thickness ratio. The classical plate theory under-predicts the deflections even at low values of E_1/E_2.

Figure 33 contains plots of maximum center deflection versus side-to-thickness ratio a/h for two- and eight-layer simply supported SS-2 antisymmetric angle-ply

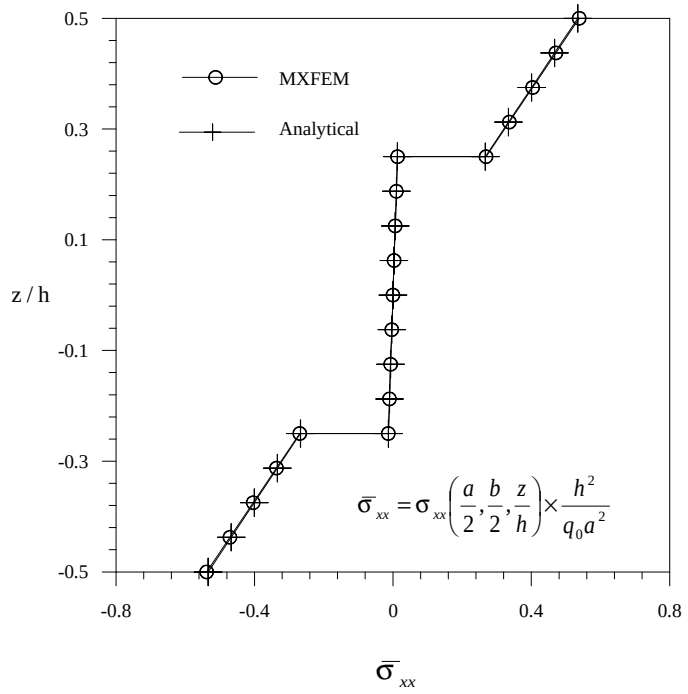

Fig. 27. Variation of maximum normal stress $\bar{\sigma}_{xx}$ through the thickness (z/h) of a SS-1 cross-ply (0/90/90/0) square plate under sinusoidal load.

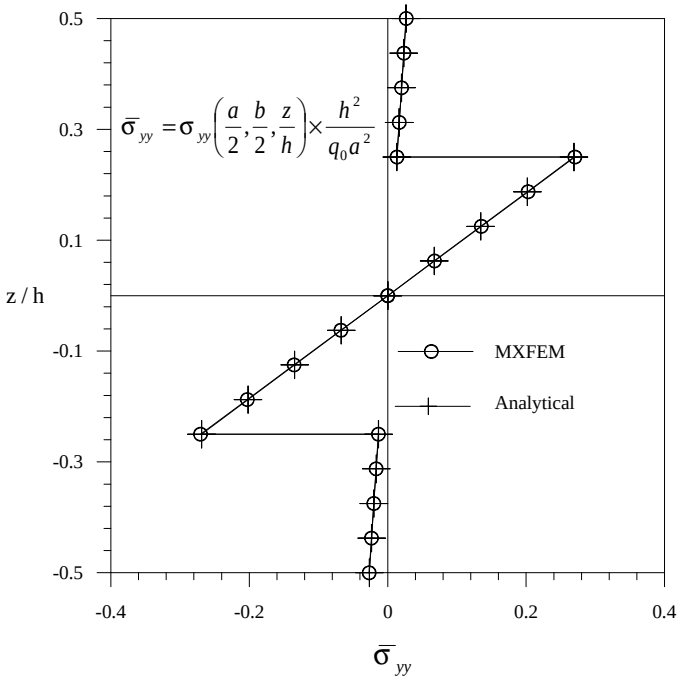

Fig. 28. Variation of maximum normal stress $\bar{\sigma}_{yy}$ through the thickness (z/h) of a SS-1 cross-ply (0/90/90/0) square plate under sinusoidal load.

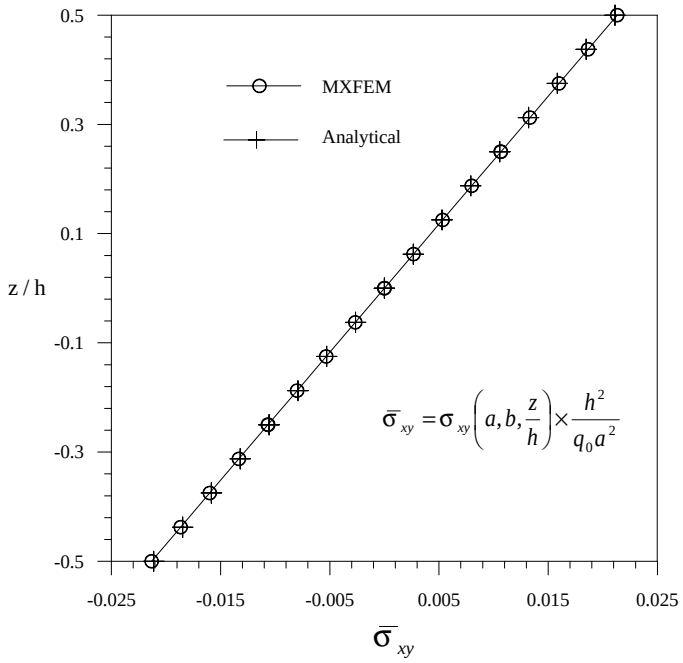

Fig. 29. Variation of maximum shear stress $\bar{\sigma}_{xy}$ through the thickness (z/h) of a SS-1 cross-ply (0/90/90/0) square plate under sinusoidal load.

$(-45/45)$ square plates under uniform loading. A laminated composite, unless symmetrically laminated, is characterized by the coupling between bending and extensional degrees of freedom ($B_{ij} \neq 0$). Antisymmetric angle-ply laminates come under this category. As the number of layers increase, for the same total laminate thickness, the bending-stretching coupling coefficients B_{ij} decrease causing a reduction in the magnitude of deflections. The response of antisymmetric plates does not tend towards the orthotropic plate solution as the coupling effect decreases with increasing number of layers, whereas antisymmetric cross-ply laminates essentially behave as specially orthotropic plates ($B_{ij} = D_{16} = D_{26} = 0$).

The dependence of the coupling effect on the modulus ratio E_1/E_2 for antisymmetric angle-ply laminates is illustrated in Figure 34. It can be seen that the behavior of the antisymmetric angle-ply laminate is similar to the one discussed for cross-ply

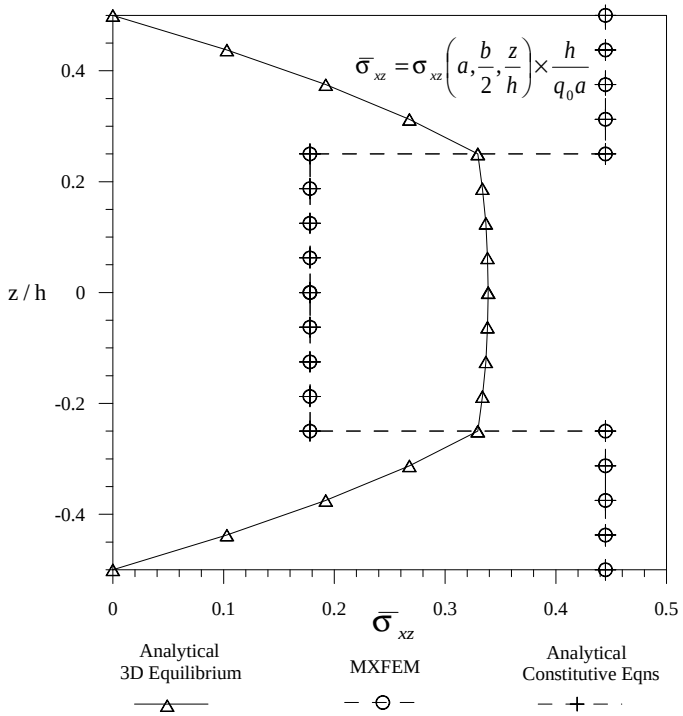

Fig. 30. Variation of maximum transverse shear stress $\bar{\sigma}_{xz}$ through the thickness (z/h) of a SS-1 cross-ply (0/90/90/0) square plate under sinusoidal load.

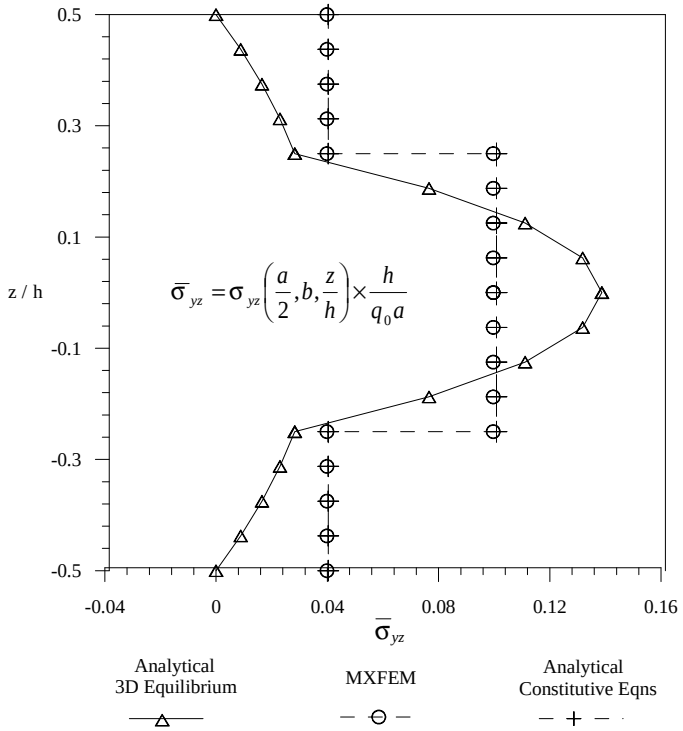

Fig. 31. Variation of maximum transverse shear stress $\bar{\sigma}_{yz}$ through the thickness (z/h) of a SS-1 cross-ply (0/90/90/0) square plate under sinusoidal load.

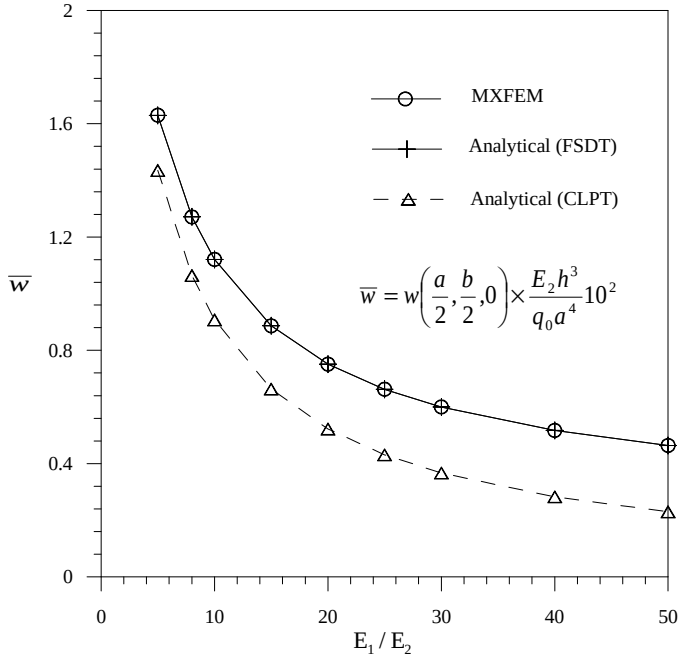

Fig. 32. Effect of material anisotropy on the maximum displacement $\bar{w}$ of a simply supported cross-ply (0/90/90/0) square plate.

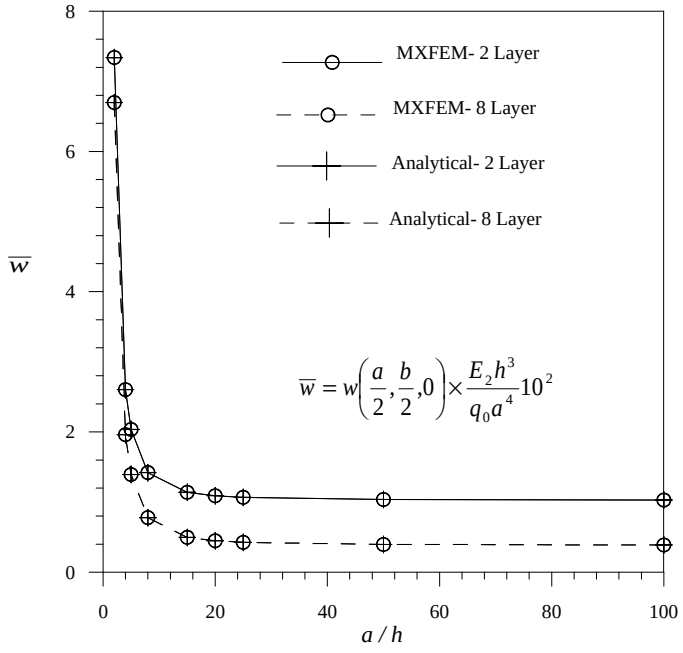

Fig. 33. Effect of shear deformation on the maximum displacement $\bar{w}$ of a SS-2 angle–ply (-45/45) square plate under sinusoidal load.

laminates, i.e., deflections decrease with increasing values of E_1/E_2. The coupling effect becomes negligible for modulus ratios close to unity. As expected, the results for anti-symmetric laminates are very close to the exact solutions.

The results discussed establish two things: First, the mixed finite element model developed herein, based on the first order shear theory, predicts results that are in excellent agreement with the exact solutions. Second, the use of mixed plate elements allow the direct computation of the bending moments at the nodes, which results in better accuracy of moments and hence, stresses. This feature is quite attractive since most design criteria are based on critical stresses.

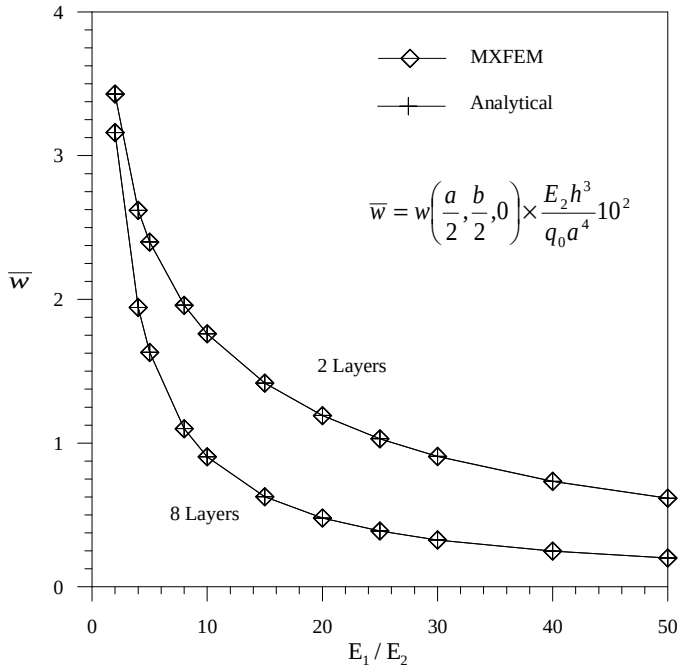

Fig. 34. Effect of material anisotropy and number of layers on the maximum displacement $\bar{w}$ of a simply supported angle-ply $(-45/45)$ square plate.

V.3. Nonlinear bending analysis

Having validated the present mixed model for linear bending analysis, we now turn to geometrically nonlinear analysis of laminated isotropic and anisotropic composite plates. The governing equations that describe the mechanical behavior of FSDT plates subjected to moderate rotations based on the mixed variational principle are given in Equations (4.1) - (4.8). The geometric nonlinearity is included via the von Kàrman strain-displacement relations, which account for the coupling between bending and membrane behavior. This coupling in turn contributes to plate stiffening, and hence results in a decrease in the magnitude of deflections when compared to the results of the linear theory.

Five sets of material properties are used in the numerical tests:

- Material 1: $E_1 = E_2 = 30 \times 10^6$ psi, $\nu = 0.316$
- Material 2 : $E_1 = E_2 = 7.8 \times 10^6$ psi, $\nu = 0.3$
- Material 3 : $E_1 = 3 \times 10^6$psi, $E_2 = 1.28 \times 10^6$psi, $G = 0.37 \times 10^6$psi, $\nu = 0.32$
- Material 4 :$E_1 = 1.8282 \times 10^6$psi, $E_2 = 1.8315 \times 10^6$psi, $G = 3.125 \times 10^5$psi, $\nu = 0.2395$
- Material 5 : $E_1/E_2 = 40$, $G_{12} = G_{13} = 0.6E_2$, $G_{23} = 0.5E_2$, $\nu = 0.25$
- Material 6 : $E_1/E_2 = 25$, $G_{12} = G_{13} = 0.5E_2$, $G_{23} = 0.2E_2$, $\nu = 0.25$

Displacements and stresses are nondimensionalized using the following expressions

$$\begin{aligned} \bar{w} &= \frac{w}{h}, & \bar{\sigma}_{xx} &= \sigma_{xx}\frac{h^2}{b^2 q_0} \\ \bar{\sigma}_{yy} &= \sigma_{yy}\frac{h^2}{b^2 q_0}, & \bar{\sigma}_{xy} &= \sigma_{xy}\frac{h^2}{b^2 q_0} \\ \bar{\sigma}_{xz} &= \sigma_{xz}\frac{h}{b q_0}, & \bar{\sigma}_{yz} &= \sigma_{yz}\frac{h}{b q_0} \end{aligned} \tag{5.4}$$

The equilibrium equations are solved at each load step by using a Newton-Raphson iterative scheme with a convergence tolerance of $\epsilon = 10^{-3}$. Whenever biaxial

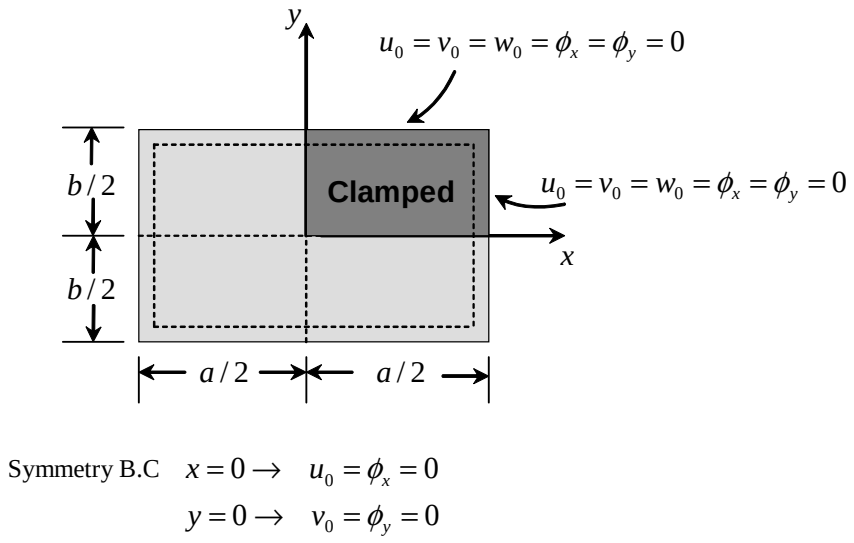

Fig. 35. Boundary conditions in a quadrant of clamped laminates.

symmetry exists, only a quadrant of the plate is modelled. Unless stated otherwise, a uniform mesh of 4×4 nine-node quadratic elements is used in the simulations. For this choice of mesh, full integration 3×3 is used for the evaluation of linear stiffness coefficients whereas reduced integration 2×2 is employed for the nonlinear and shear stiffnesses.

The first example is concerned with a thin ($a/h = 100$) clamped isotropic square plate (Material 1, $a = 300\text{in}, h = 3\text{in}$) under uniformly distributed load. The clamped boundary conditions are shown in Figure 35:

$$\begin{aligned} &u = \phi_x = 0, \quad \text{at} \quad x = 0 \\ &v = \phi_y = 0, \quad \text{at} \quad y = 0 \\ &u = v = w = \phi_x = \phi_y = 0, \quad \text{at} \quad x = a/2, y = b/2 \end{aligned} \tag{5.5}$$

This example is a benchmark problem widely used to verify the geometrically nonlinear capability of thin plate formulations [61]. Mixed finite element results for

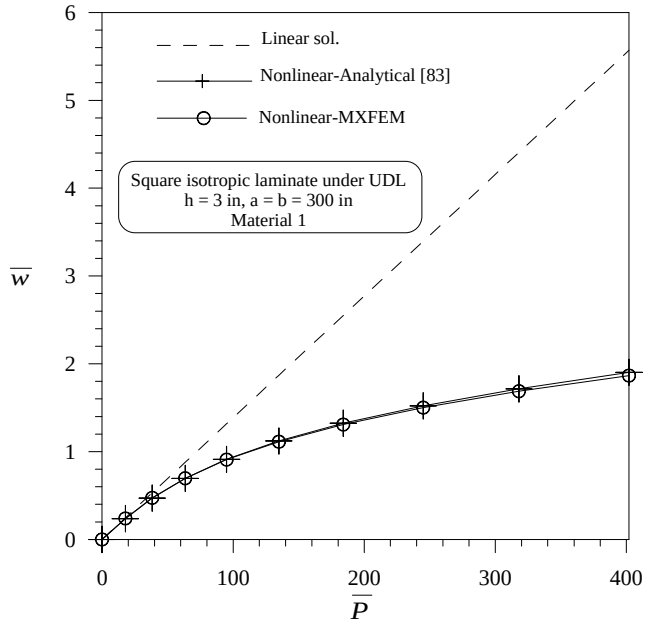

Fig. 36. Center deflection $\bar{w}$ of a clamped isotropic plate under uniformly distributed load (Material 1, $a/h = 100$).

displacements $\bar{w}$ and normal stresses $\bar{\sigma}_{xx}$ are presented in Table 8. The results are in excellent agreement with the thin plate analytical solutions of Levy [83], who solved the problem using a double Fourier series. The geometrically nonlinear behavior of deflections and stresses as a function of the load parameter $\bar{P} = q_0 a^4/E_2 h^4$ is depicted in Figures 36 and 37.

Next, the effect of the boundary conditions in the nonlinear behavior of isotropic and orthotropic square plates under uniform load is studied. Two types of simply supported boundary conditions are considered (see Figures 35 and 38),

$$\begin{aligned} &\text{SS-1}: \quad v_0 = w_0 = \phi_y = 0, \quad \text{at} \quad x = a/2; \quad u_0 = w_0 = \phi_x = 0, \quad \text{at} \quad y = b/2 \\ &\text{SS-3}: \quad u_0 = v_0 = w_0 = 0 \quad \text{at} \quad x = a/2, \quad y = b/2 \end{aligned} \tag{5.6}$$

The geometric and material properties used are

- Isotropic Plate: Material 1,$a = b = 10$in, $h = 1$in
- Orthotropic Plate: Material 3, $a = b = 12$in, $h = 0.138$in

Table 8. Nondimensional center deflection $\bar{w}$ and normal stress $\bar{\sigma}_{xx}$ of a clamped isotropic square plate under uniform loading (Material 1, $a/h = 100$).

Load $\bar{P}$	Analytical†	MXFEM	Linear
	Deflections, $\bar{w}$		
17.8	0.2370	0.2392	0.2465
38.3	0.4710	0.4738	0.5307
63.4	0.6950	0.6965	0.8785
95.0	0.9120	0.9087	1.3163
134.9	1.1210	1.1130	1.8692
184.0	1.3230	1.3080	2.5495
245.0	1.5210	1.5010	3.3947
318.0	1.7140	1.6880	4.4062
402.0	1.9020	1.8660	5.5702
	Normal stresses, $\bar{\sigma}_{xx}$		
17.8	2.600	2.414	2.387
38.3	5.200	5.022	5.138
63.4	8.000	7.649	8.510
95.0	11.100	10.254	12.745
134.9	13.300	12.850	18.099
184.0	15.900	15.420	24.686
245.0	19.200	18.060	32.869
318.0	21.900	20.741	42.664
402.0	25.100	23.423	53.933

† (see Levy [83])

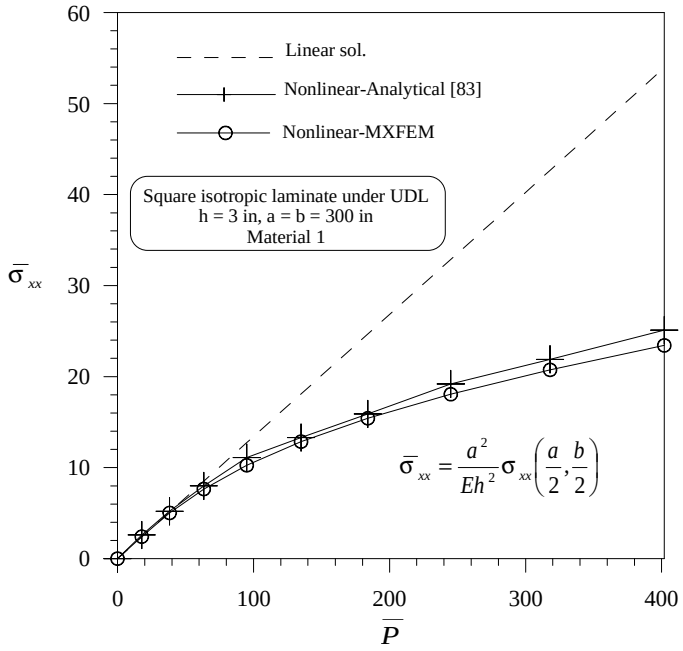

Fig. 37. Maximum normal stress σ_{xx} of a clamped isotropic plate under uniformly distributed load (Material 1, $a/h = 100$).

Tables 9 and 10 contain the nondimensionalized deflections $\bar{w}$ and normal stresses $\bar{\sigma}_{xx}$ as a function of the load parameter $\bar{P}$, for the two boundary conditions (see also Figures 39 to 42).

It is clear that SS-3 provides more edge restraint than SS-1 and therefore produces lower transverse deflections. The figures also show the results obtained using a plate element based on a nonlinear displacement finite element model (see Reddy [25]). The agreement between both models is excellent in all cases.

In Figures 43 and 44, the present finite element results are compared with the experimental results of Zaghloul and Kennedy [84]. In Figure 43, a plot of the maximum center deflection versus the intensity of the uniform load q_0 for a simply supported square plate (Material 3) is presented. The dimensions of the plate are: $a = b = 12\text{in}, h = 0.138\text{in}$.

Table 9. Effect of the boundary conditions on the center deflection $\bar{w}$ and normal stress $\bar{\sigma}_{xx}$ of an isotropic square plate under uniform loading (Material 2, $a/h = 10$).

	Deflection, $\bar{w}$				Normal Stress, $\bar{\sigma}_{xx}$			
	SS-1		**SS-3**		**SS-1**		**SS-3**	
$\bar{P}$	DBFEM†	MXFEM	DBFEM	MXFEM	DBFEM	MXFEM	DBFEM	MXFEM
6.25	0.2813	0.2813	0.2790	0.2798	1.779	1.775	1.861	1.848
12.50	0.5186	0.5186	0.4630	0.4638	3.396	3.387	3.305	3.280
25.00	0.8673	0.8674	0.6911	0.6918	5.882	5.859	5.320	5.277
50.00	1.3149	1.3150	0.9575	0.9581	9.162	9.108	8.002	7.934
75.00	1.6239	1.6250	1.1333	1.1340	11.462	11.379	9.984	9.898
100.00	1.8683	1.8690	1.2688	1.2690	13.307	13.196	11.634	11.534
125.00	2.0751	2.0770	1.3809	1.3810	14.890	14.751	13.085	12.973
150.00	2.2556	2.2580	1.4774	1.4780	16.293	16.130	14.398	14.276
175.00	2.4177	2.4210	1.5629	1.5630	17.572	17.384	15.610	15.479
200.00	2.5657	2.5690	1.6399	1.6400	18.755	18.545	16.743	16.603
225.00	2.7023	2.7070	1.7103	1.7110	19.863	19.631	17.813	17.666
250.00	2.8296	2.8360	1.7753	1.7760	20.898	20.656	18.831	18.675

†See Reddy [25].

Table 10. Effect of the boundary conditions on the center deflection $\bar{w}$ and normal stress $\bar{\sigma}_{xx}$ of an orthotropic square plate under uniform loading.

	Deflection, $\bar{w}$				Normal Stress, $\bar{\sigma}_{xx}$			
	SS-1		**SS-3**		**SS-1**		**SS-3**	
q_0 (psi)	DBFEM†	MXFEM	DBFEM	MXFEM	DBFEM	MXFEM	DBFEM	MXFEM
0.05	0.0819	0.0819	0.0819	0.0822	1.034	1.033	1.056	1.046
0.10	0.1623	0.1627	0.1580	0.1591	2.070	2.068	2.116	2.096
0.20	0.3181	0.3179	0.2277	0.2891	4.092	4.087	4.058	4.018
0.40	0.5906	0.5906	0.4710	0.4722	7.716	7.704	7.103	7.024
0.60	0.8130	0.8134	0.5971	0.5987	10.702	10.681	9.406	9.294
0.80	0.9978	0.9980	0.6949	0.6959	13.169	13.137	11.284	11.146
1.00	1.1551	1.1550	0.7746	0.7754	15.255	15.212	12.894	12.733
1.20	1.2920	1.2920	0.8420	0.8430	17.050	16.996	14.316	14.136
1.40	1.4138	1.4140	0.9014	0.9025	18.631	18.564	15.602	15.404
1.60	1.5239	1.5240	0.9551	0.9555	20.044	19.966	16.783	16.569
1.80	1.6239	1.6250	1.0029	1.0040	21.324	21.234	17.880	17.652
2.00	1.7174	1.7170	1.0471	1.0480	22.495	22.394	18.909	18.667

†See Reddy [25].

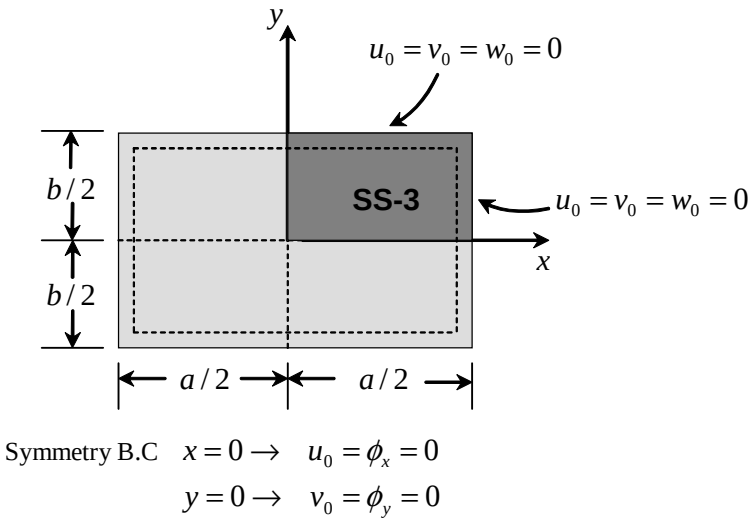

Fig. 38. Boundary conditions in a quadrant of simply supported (SS-3) laminates.

The agreement between the present solution and the experimental values is very good. It is clear that, even for thin plates, the shear deformation effect is significant in the nonlinear range.

The load-deflection curve of a clamped symmetric (0/90/90/0) cross-ply plate (Material 4) under uniform load is presented in Figure 44. For this case, a small discrepancy between the numerical and experimental results is observed. This difference can be attributed to possible errors in the simulation of the actual support (boundary conditions) and material properties used in the experiment.

The effect of number of layers and the lamination scheme on the center deflection is investigated in Figures 45 and 46, for two- and eight-layer laminates. Clamped square plates with $a/h = 10$ and Material 5 are used in the analysis.

Table 11 contains numerical values of the maximum center deflection $\bar{w}$ for increasing values of load parameter $\bar{P}$.

It can be seen that increasing the number of layers reduces the nonlinear effects in both cross-ply and angle-ply cases, resulting in straightening of the nonlinear curve

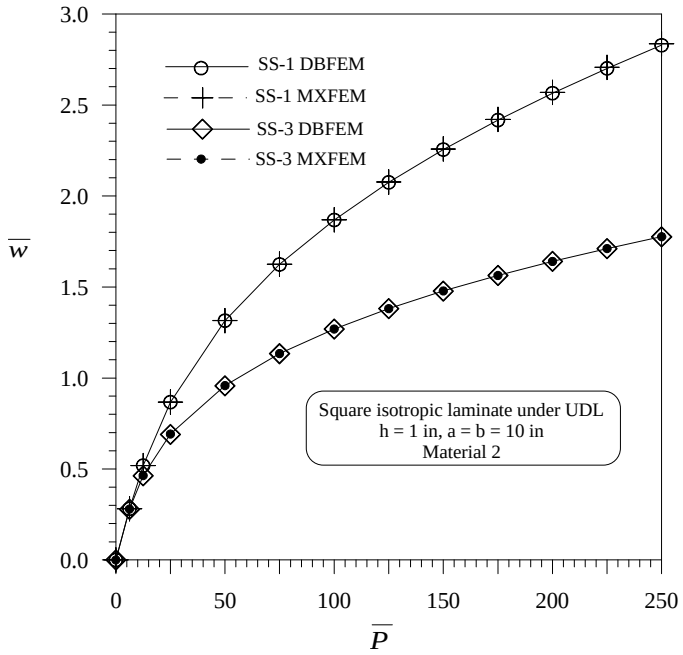

Fig. 39. Effect of boundary conditions on the center deflection $\bar{w}$ of an isotropic square plate under uniform load (Material 2, $a/h = 10$).

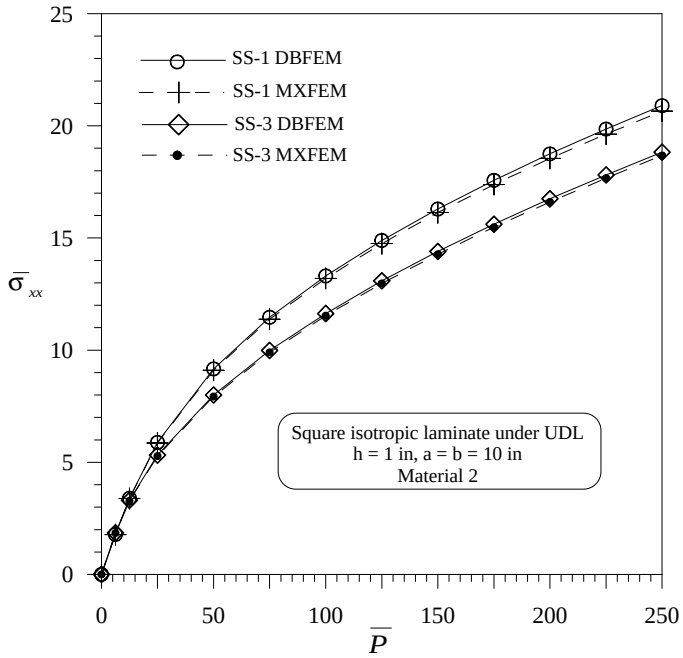

Fig. 40. Effect of boundary conditions on the maximum normal stress $\bar{\sigma}_{xx}$ of an isotropic square plate under uniform load (Material 2, $a/h = 10$).

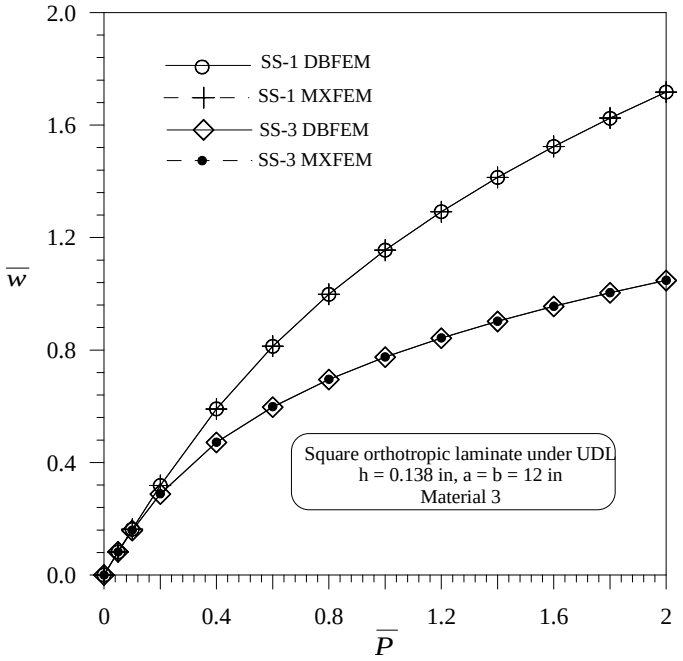

Fig. 41. Effect of boundary conditions on the center deflection $\bar{w}$ of an orthotropic square plate under uniform load (Material 3, $a = b = 12in, h = 0.138in$).

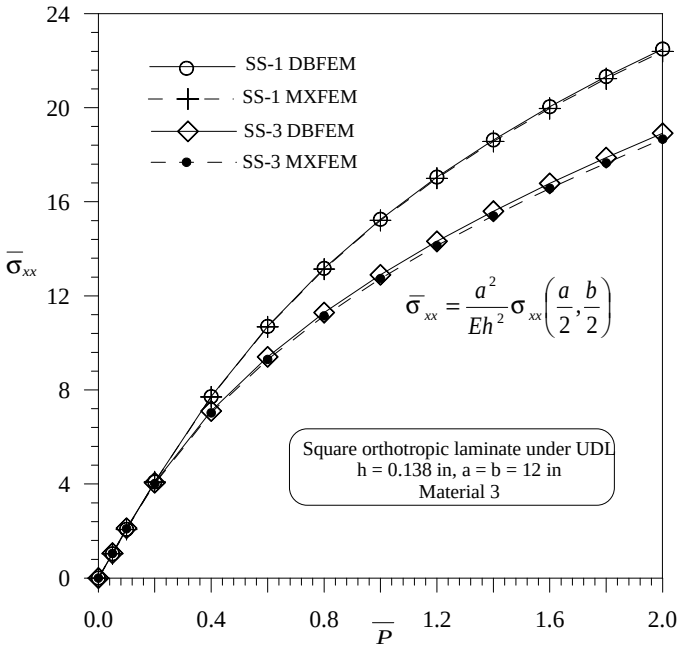

Fig. 42. Effect of boundary conditions on $\bar{\sigma}_{xx}$ of an orthotropic square plate under uniform load (Material 3, $a = b = 12in, h = 0.138in$).

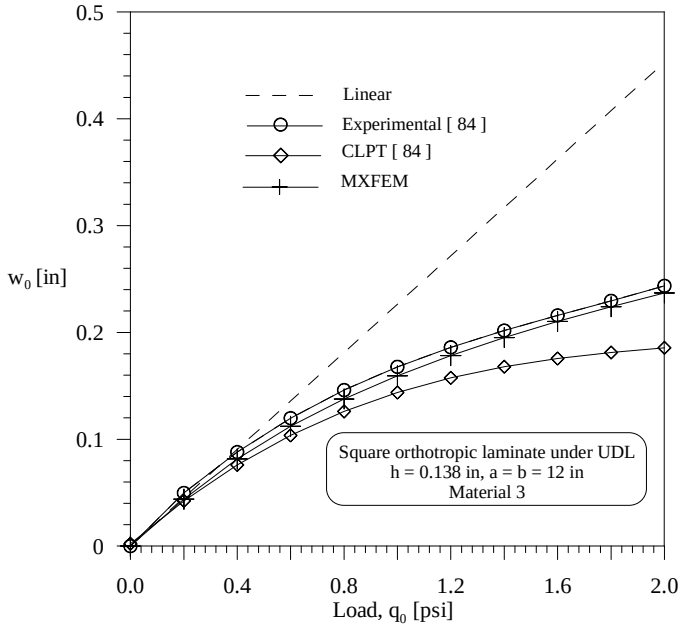

Fig. 43. Comparison of the mixed finite element results and experimental results for $\bar{w}$ as a function of $\bar{P}$. Simply supported square plate under uniform load (Material 3).

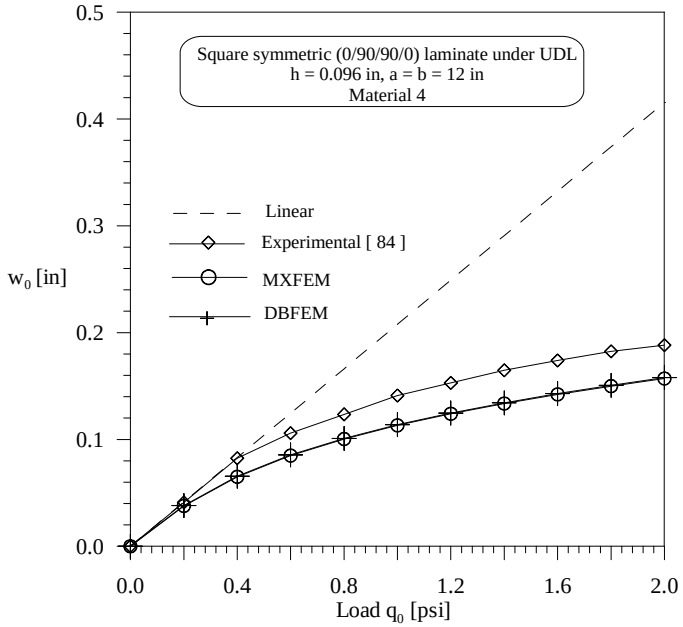

Fig. 44. Comparison of the mixed finite element results and experimental results for $\bar{w}$ as a function of $\bar{P}$. Clamped square plate under uniform load (Material 4).

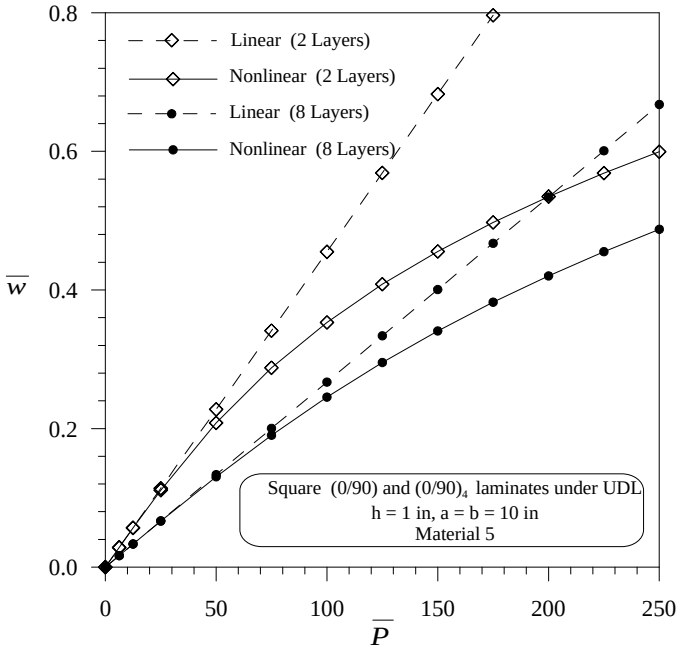

Fig. 45. Effect of the number of layers on a clamped cross-ply square plate under uniform load (Material 5, $a/h = 10$).

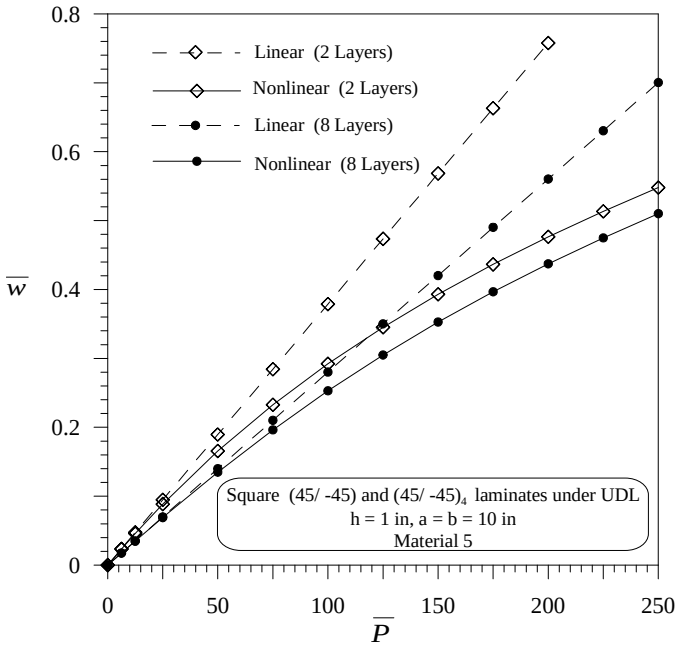

Fig. 46. Effect of the number of layers on a clamped angle-ply square plate under uniform load (Material 5, $a/h = 10$).

Table 11. Effect of the number of layers nl on the center deflection $\bar{w}$ of antisymmetric cross-ply and angle-ply clamped square plates under uniform loading.

	$(0/90/0...)$		$(45/-45/45...)$	
Load $\bar{P}$	nl=2	nl=8	nl=2	nl=8
6.25	0.0284	0.0167	0.0233	0.0175
12.5	0.0567	0.0333	0.0458	0.0348
25.0	0.1112	0.0664	0.0886	0.0690
50.0	0.2082	0.1304	0.1657	0.1349
75.0	0.2877	0.1903	0.2329	0.1963
100.0	0.3531	0.2453	0.2923	0.2530
125.0	0.4082	0.2953	0.3452	0.3050
150.0	0.4557	0.3408	0.3930	0.3528
175.0	0.4975	0.3823	0.4365	0.3967
200.0	0.5348	0.4202	0.4765	0.4373
225.0	0.5686	0.4552	0.5135	0.4749
250.0	0.5995	0.4875	0.5480	0.5101

closer to the linear solution. Also, angle-ply laminates exhibit less degree of nonlinearity compared to the cross-ply laminates, and eight-layer laminates are stiffer than two-layer laminates.

Figure 47 shows load-deflection curves of clamped antisymmetric cross-ply (0/90) and angle-ply $(45/-45)$ laminates for $a/h = 10$ and $a/h = 100$. It can be observed that the degree of nonlinearity in thick plates is more pronounced than in thin plates, due to the the effect of shear deformation.

Next, we consider the nonlinear bending response of a symmetric (0/90/90/0) cross-ply laminated plate (Material 4) with $a = b = 12\text{in}, h = 0.096\text{in}$. As expected, the maximum deflections are obtained for SS-3 (see Figure 48). Increasing the restrictions on degrees of freedom at the boundary causes a stiffening of the structure which translates into a reduction in the nonlinearity of the response.

The present mixed formulation is also employed in the nonlinear analysis of

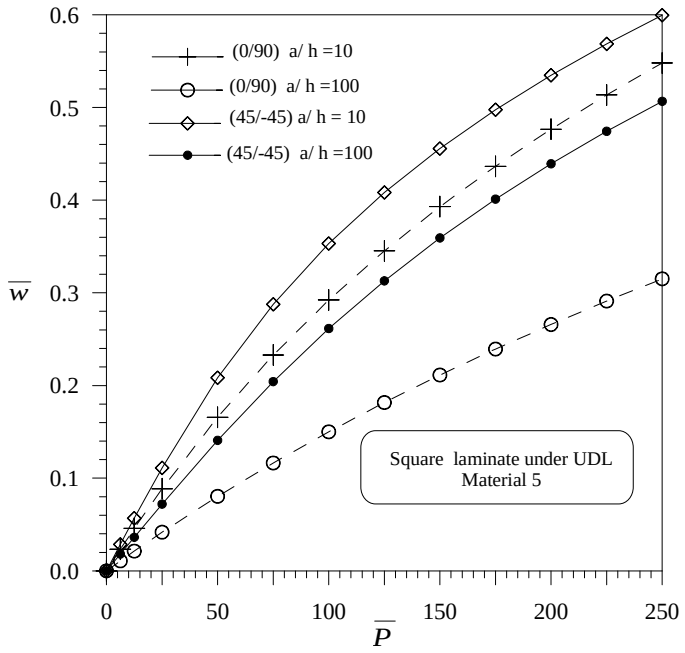

Fig. 47. Effect of the length-to-thickness ratio a/h on the center deflection $\bar{w}$ of clamped antisymmetric cross-ply and angle-ply laminates (Material 5).

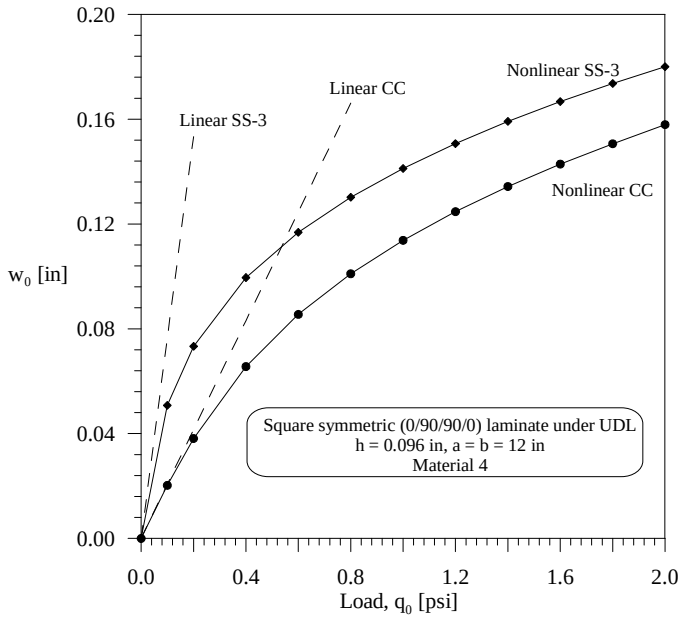

Fig. 48. Effect of the boundary conditions on the center deflection $\bar{w}$ for a symmetric-cross-ply (0/90/90/0) laminated plate (Material 4).

beam structures. The first one-dimensional example deals with a beam made of an isotropic material (Material 1, $a/h = 100$) subjected to uniform loading for different various conditions. Table 12 contains the nondimensionalized maximum deflections

Table 12. Center deflection $\bar{w}$ of an isotropic beam under uniform load for various boundary conditions.

	Hinged-Hinged		Pinned-Pinned		Clamped-Clamped	
$\bar{P}$	DBFEM†	MXFEM	DBFEM	MEXFEM	DBFEM	MXFEM
1	0.5208	0.5196	0.3685	0.3682	0.1035	0.1035
2	1.0417	1.0400	0.5454	0.5459	0.2025	0.2026
3	1.5625	1.5620	0.6640	0.6642	0.2943	0.2942
4	2.0833	2.0840	0.7555	0.7543	0.3778	0.3779
5	2.6042	2.6070	0.8312	0.8303	0.4534	0.4534
6	3.1250	3.1350	0.8964	0.8956	0.5220	0.5217
7	3.6458	3.6530	0.9540	0.9526	0.5845	0.5843
8	4.1667	4.1850	1.0058	1.0050	0.6418	0.6414
9	4.6875	4.6890	1.0531	1.0520	0.6946	0.6942
10	5.2083	5.1970	1.0967	1.0960	0.7436	0.7434

†See Reddy [25].

for increasing values of the load parameter $\bar{P}$. Results compare very well to those obtained by Reddy [25] using a displacement-based finite element model.

Lastly, we consider the nonlinear bending behavior of two-layer angle-ply $(45/-45)$ and two-layer cross-ply $(0/90)$ composite beams with pinned-pinned and clamped-clamped ends. The mechanical properties used are those of Material 6, and the slenderness ratio is assumed to be $a/h = 10$.

Figure 49 shows the variation of $\bar{w}$ with the load parameter $\bar{P}$ for the pinned-pinned case. It may be observed that the behavior of the cross-ply $(0/90)$ laminate changes with the direction of the load. For positive loading the nonlinearity is of softening type for small loads and of hardening type for larger loads.

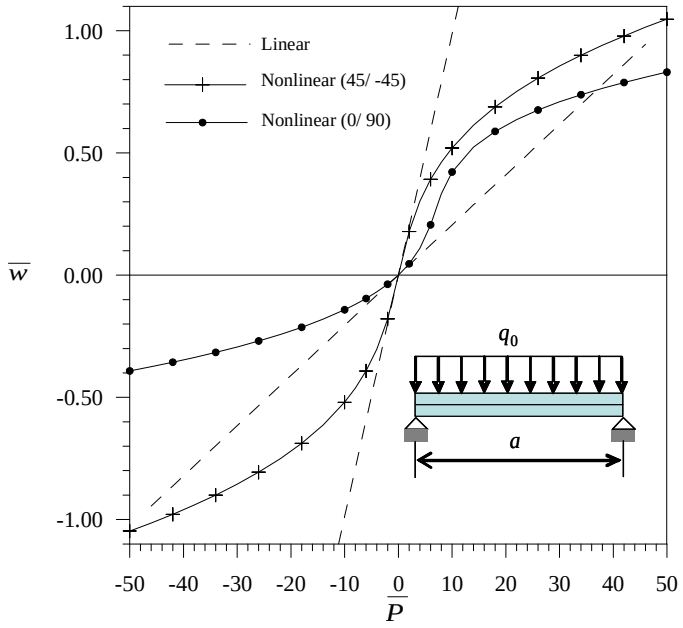

Fig. 49. Load-deflection curves for cross-ply (0/90) and angle-ply (45/ − 45) pinned-pinned composite beams under uniform load (Material 6, $a/h = 10$).

The nonlinear axial force N_{xx} for a beam can be expressed as,

$$N_{xx} = A_{11}\left[\frac{du_0}{dx} + \frac{1}{2}\left(\frac{dw_0}{dx}\right)^2\right] + B_{11}\frac{d\phi_x}{dx}, \quad B_{11} < 0 \tag{5.7}$$

It is clear that for small values of the positive load, the term containing the stretch-bending coupling coefficient B_{11} in Equation 5.7 is larger than the A_{11} expression, and therefore the axial load N_{xx} is compressive. This causes a "softening" in the structure which explains the nonlinear transverse deflections being larger than the linear deflections (see Figure 49). As the load increases, the A_{11} expression becomes predominant (the quadratic term increases), the axial force N_{xx} becomes positive and the beam stiffens. For a negative load, $B_{11}\frac{d\phi_x}{dx}$ is positive, and the two terms in N_{xx} add up yielding a larger axial force and therefore a stiffer structure.

For the antisymmetric angle-ply (45/ − 45) laminate, the nonlinear deflections have the same magnitude regardless of the load direction, and the nonlinearity is

always of hardening type. For these laminates the bending-extension coupling B_{11} is zero. It may also be observed that two-layered angle-ply beams are more flexible than two-layer cross-ply beams.

Figure 50 depicts the variation of $\bar{w}$ with the load parameter $\bar{P}$ for the fixed-fixed case. It is shown that the nonlinear behavior of both cross-ply and angle-ply beams is the same for positive and negative loads, irrespective of the lay-up.

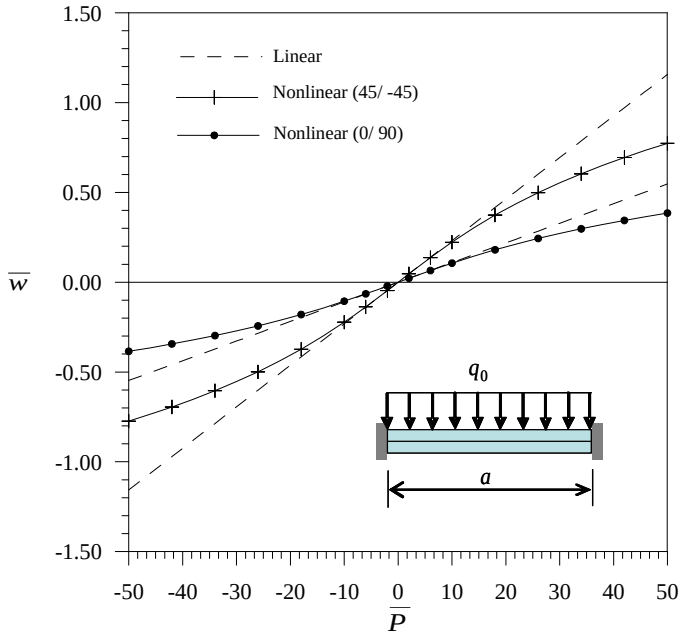

Fig. 50. Load-deflection curves for cross-ply (0/90 and angle-ply $(45/-45)$ clamped–clamped composite beams under uniform load (Material 6, $a/h = 10$).

The various numerical examples discussed above demonstrate the validity of the present mixed finite element model for nonlinear bending analysis of isotropic and composite beams and plates. It is also shown that geometric nonlinear effects could be very significant even at small loads, depending on the lamination scheme, geometry and boundary conditions.

CHAPTER VI

SUMMARY, CONCLUSIONS, AND RECOMMENDATIONS

VI.1. Summary and conclusions

Two different finite element models for geometrically nonlinear analysis of frame and plate structures are developed in the present study. These are

1. A corotational frame finite element for large-rotations problems of planar frame structures.

2. A mixed shear flexible finite element for moderately large rotations problems of layered anisotropic plates.

The first of the aforementioned finite element models is based on a corotational description of the motion of a unified beam element which has embedded the kinematics assumptions of classical and refined beam theories. The corotational finite element model presented herein is new in the sense that it contains all known beam theories in one element. The following characteristics of the element must be noted:

- The kinematic assumptions of the Euler-Bernoulli theory, the Timoshenko theory, as well as the simplified Reddy beam theory are incorporated into the model.

- The governing equations are written in a local 'corotated' frame that undergoes arbitrarily large rotations, and with respect to which the small strain-displacement relationships can be used.

- The corotational beam element has three degrees of freedom per node which consists of two displacements and one rotation.

- The axial displacement is approximated using Lagrange functions, whereas Hermite cubic interpolation is used for the transverse displacement, and interdependent quadratic interpolation for the rotation.

- The geometric nonlinearity is fully introduced by the coordinate transformation between the local and global nodal degrees of freedom.

- The shear-locking is resolved by using appropriate approximation functions for the generalized displacements, i.e. Lagrange interpolation of the axial displacement, Hermite cubic interpolation of the transverse displacement, and interdependent quadratic interpolation of the rotation.

- This 'corotational' concept makes possible the application of linear beam finite elements in nonlinear bending analysis. Several numerical examples are carried out to demonstrate the large-rotation capability and accuracy of the model.

The numerical performance of the element is characterized by the following properties:

- Convergence of the solution with mesh refinement is verified for cases of moderate and severe severe geometric nonlinearity (large rotations).

- The element is free of membrane and shear-locking.

- The accuracy of the present model is assessed by comparison with closed-form solutions and numerical solutions available in the literature. Highly accurate solutions are obtained in all cases.

- The corotational beam element performs well when applied in problems of severe geometric nonlinearity (large rotations).

The second finite element model presented herein is based on a mixed formulation of the first-order shear deformation theory for laminated composite plates. The features of the developed finite element model are:

- The formulation accounts for constant transverse shear stress through thickness, and the geometric nonlinearity is included via the von Kàrman strains.
- The finite element model is constructed using independent approximations of the generalized displacements and bending moments, and therefore, only C^0-interpolation of all field variables is required.
- The finite element consists of eight degrees of freedom per node which include three displacements, two rotations and three moment resultants: $(u, v, w, \phi_x, \phi_y, M_{xx}, M_{yy}, M_{xy})$.
- Higher-order nodal expansions of the fields variables are employed.

Concerning the numerical performance of the element, the following remarks can be made:

- The present element provides the best compromise between computational cost, formulation simplicity and accuracy of the global response of thin to moderately thick laminates when compared to other mixed and displacement-based finite element models based on classical or high-order theories.
- Convergence, with mesh refinement (h-convergence) and increase of the expansion order (p-convergence), of the numerical solution to the analytical solution is verified.
- High-order elements with full integration, and low-order elements with reduced integration are shown to be locking-free.

- The accuracy and consistency of in-plane and transverse displacements and stresses is demonstrated by comparison with exact, experimental and displacement-based finite element results.

- It is shown that the element is flexible and capable of analyzing both linear and geometrically nonlinear bending problems of laminated anisotropic plates.

- The use of mixed plate elements allows the direct computation of the bending moments at the nodes, which results in better accuracy of moments and hence, stresses. This feature is quite attractive since most design criteria are based on critical stresses.

- The moment boundary conditions are satisfied exactly in mixed finite element models whereas for displacement finite element models the natural boundary conditions are only met in an integral sense.

In summary, the main contributions of the present study are

- The derivation of the corotational frame element is greatly simplified in comparison to other formulations in the literature. The incorporation of the unified linear beam model in the development of the corotational beam does not exist in the literature. The advantage of the unified element is that the shear deformation is automatically accounted for without the intervention of the user. The element does not have the need for a shear correction factor. Most importantly, the element does not suffer from shear or membrane locking.

- The mixed plate bending element with generalized displacements and moments as degrees of freedom and higher-order nodal expansions is novel with the present study. The element locking may be eliminated by using sufficiently large p or lower p with reduced integration.

VI.2. Recommendations

Few recommendations for further study are in order. The mixed finite element model developed herein can be modified to include material nonlinearities and thermal stress effects. The constitutive equations can also be generalized to include functionally graded materials. It is also of interest to extend the formulation to buckling and transient analysis of laminated composite plates. Since the recovery of accurate transverse stress profiles is of crucial importance in the study of delamination mechanisms, it is suggested the inclusion of the shear stress resultants as nodal degrees of freedom. In this case, care should be exercised to avoid singularities in the stiffness matrix.

The corotational frame finite element developed in this work can be extended to shear-deformable plates and shells. A brief description of the methodology proposed for the derivation of a corotational plate element is presented in the Appendix to help those who wish to undertake the extension.

REFERENCES

[1] Martinez CE, Urthaler Y, Goncalves R. Nonlinear finite element analysis of submarine pipelines during installation. *Proceedings of the ASME Pressure Vessels and Piping Conference* 1999; **385**:187-194.

[2] Crisfield MA, Yazdchi M. Non-linear dynamic behaviour of flexible marine pipes and risers. *International Journal for Numerical Methods in Engineering* 2002; **54**:1265-1308.

[3] Felippa CA, Haugen B. A unified formulation of small-strain corotational finite elements: I Theory. *Computer Methods in Applied Mechanics and Engineering* 2005; **194**:2285-2335.

[4] Martin HC. On the derivation of stiffness matrices for the analysis of large deflection and stability problems. *Proceedings of the Conference on Matrix Methods in Structural Mechanics* 1965; 697-716.

[5] Ebner AM, Uciferro JJ. A theoretical and numerical comparison of elastic nonlinear finite element methods. *Computers and Structures* 1972; **2**:1043-1061.

[6] Oran C. Tangent stiffness in plane frames. *Journal of the Structural Division* 1973; **99**:973-985.

[7] Oran C, Kassimali A. Large deformation of framed structures under static and dynamic loads. *Computers and Structures* 1976; **6**:539-547.

[8] Hsiao KM, Hou FY. Nonlinear finite element analysis of elastic frames. *Computers and Structures* 1987; **26**:693-701.

[9] Bathe K, Bolourchi S. Large displacement analysis of three-dimensional beam structures. *International Journal for Numerical Methods in Engineering* 1979; **14**:961-986.

[10] Gattass M, Abel JF. Equilibrium considerations of the updated lagrangian formulation of beam-columns with natural concepts. *International Journal for Numerical Methods in Engineering* 1987; **24**:2119-2141.

[11] Guo Ying Q, Batoz J. Displacement fields and large deformation analysis of 3-D beams. *Lecture notes in Engineering*. Dalian Inst of Technology, China, 1987; 406-417.

[12] Behdinan K, Stylianou MC, Tabarrok B. Static and dynamic analysis of flexible beams: a consistent updated Lagrangian formulation. *Transactions of the Canadian Society for Mechanical Engineering* 1997; **21**:141-177.

[13] Pai PF, Anderson TJ, Wheater EA. Large-deformation tests and total-Lagrangian finite-element analyses of flexible beams. *International Journal of Solids and Structures* 2000; **37**:2951-2980.

[14] Argyris JH. Recent advances in matrix methods of structural analysis. *Progress in Aeronautical Sciences*, Ferri, A, Küchemann, D, Smolderen, J (eds), Pergamon Press, New York, 1964.

[15] Belytschko T, Hsieh BJ. Non-linear transient finite element analysis with convected co-ordinates. *International Journal for Numerical Methods in Engineering* 1973; **7**:255-271.

[16] Argyris JH, Balmer H, Doltsinis J, Dunne PC, Haase M, Mullerand M, Scharpf DW. Finite element method-the natural approach. *Computer Methods in Applied*

Mechanics and Engineering 1979; **17/18**:1-106.

[17] Belytschko T, Glaum LW. Applications of higher order corotational stretch theories to nonlinear finite element analysis. *Computers and Structures* 1979; **10**:175-182.

[18] Crisfield MA, Cole G. Co-rotational beam elements for two-and three-dimensional non-linear analysis. *Proc. IUTAM/IACM Symp. on Discretization Methods in Structural Mechanics* 1989; **4**:115-124.

[19] Crisfield MA. A consistent co-rotational formulation for non-linear, three-dimensional, beam-elements. *Computer Methods in Applied Mechanics and Engineering* 1990; **81**:131-150.

[20] Iura M, Suetake Y. Accuracy of co-rotational formulation for 3-D Timoshenko's beam. *Computer Modeling in Engineering and Sciences* 2003; **4**:249-258.

[21] Martinez CE. A theoretical and numerical evaluation of nonlinear beam elements. *MSc. Thesis*, Massachusetts Institute of Technology, Boston, MA, 1997.

[22] Urthaler Y, Reddy JN. A corotational finite element formulation for the analysis of planar beams. *Communications in Numerical Methods in Engineering* 2005; **21**:553-570.

[23] Simo JC. Finite strain beam formulation: the three-dimensional dynamic problem-Part I. *Computer Methods in Applied Mechanics and Engineering* 1985; **49**:55-70.

[24] Yang T Y. Matrix displacement solution to elastica problems of beams and frames. *International Journal of Solids and Structures* 1973; **9**:829-842.

[25] Reddy JN. *An Introduction to Nonlinear Finite Element Analysis*. Oxford University Press: Oxford, U.K., 2004.

[26] Reddy JN. *An Introduction to the Finite Element Method* (3rd edn). McGraw-Hill: New York, 2006.

[27] Wempner G. Finite elements, finite rotations and small strains of flexible shells. *International Journal of Solids and Structures* 1969; **5**:117-153.

[28] Crisfield MA. *Non-Linear Finite Element Analysis of Solids and Structures, Volume 1: Essentials*. John Wiley: New York, 1991.

[29] Timoshenko SP. On the correction for shear of the differential equation for transverse vibrations of prismatic bars. *Philosophical Magazine* 1921; **41**:744-746.

[30] Heyliger PR, Reddy JN. A higher-order beam finite element for bending and vibration problems. *Journal of Sound and Vibration* 1988; **126**:309-326.

[31] Reddy JN. On locking free shear deformable finite elements. *Computer Methods in Applied Mechanics and Engineering* 1997; **149**:113-132.

[32] Reddy JN. Unified finite elements based on the classical and shear deformation theories of beams and axisymmetric circular plates. *Communications in Numerical Methods in Engineering* 1997; **13**:495-510.

[33] Reissner E, Stavsky Y. Bending and stretching of certain types of aeolotropic elastic plates. *Journal of Applied Mechanics* 1961; **28**:402-405.

[34] Stavsky Y. Bending and stretching of laminated aeolotropic plates. *Journal of Engineering Mechanics* 1961; **87**:31-56.

[35] Whitney JM. The effect of transverse shear deformation on the bending of laminated plates. *Journal of Composite Materials* 1969; **3**:534-547.

[36] Reissner E. On the theory of bending of elastic plates. *Journal of Mathematical Physics* 1944; **23**:184-191.

[37] Reissner E. The effect of transverse shear deformation on the bending of elastic plates. *Journal of Applied Mechanics* 1945; **12**:69-77.

[38] Mindlin R. Influence of rotatory inertia and shear on flexural motions of isotropic, elastic plates. *Journal of Applied Mechanics* 1951; **18**:31-38.

[39] Yang P, Norris C, Stavsky Y. Elastic wave propagation in heterogeneous plates. *International Journal of Solids and Structures* 1966; **2**:665-684.

[40] Whitney J, Pagano N. Shear deformation in heterogeneous anisotropic plates. *Journal of Applied Mechanics* 1970; **37**:1031-1036.

[41] Reddy JN. A simple higher-order theory for laminated composite plates. *Journal of Applied Mechanics* 1984; **51**:745-752.

[42] Reddy JN. Refined nonlinear theory of plates with transverse shear deformation. *International Journal of Solids and Structures* 1984; **20**:881-896

[43] Reddy JN, Sandidge D. Mixed finite element models for laminated composite plates. *Journal of Engineering for Industry* 1986; **109**:39-45.

[44] Wang CM, Reddy JN, Lee KH. *Shear Deformable Beams and Plates: Relationships with Classical Solutions*. Elsevier: Oxford, U.K., 2000.

[45] Reddy JN. *Mechanics of Laminated Composite Plates and Shells: Theory and Analysis* (2nd edn). CRC Press: Boca Raton, Florida, 2004.

[46] Pagano NJ. Exact solutions for rectangular bidirectional composites and sandwich plates. *Journal of Composite Materials* 1970; **4**:20-34.

[47] Srinivas S, Rao AK. Bending, vibration and buckiling of simply supported thick orthotropic rectangular plates and laminates. *International Journal of Solids and Structures* 1970; **6**:1463-1481.

[48] Pagano NJ, Hatfield SJ. Elastic behavior of multilayered bi-directional composites. *AIAA Journal* 1972; **10**:931-933.

[49] Reddy JN, Chao WC. A comparison of closed form and finite element solutions of thick laminated rectangular plates using first-order shear deformation theory. *Nuclear Engineering and Design* 1997; **64**:153-167.

[50] Khdeir A, Reddy JN, Librescu L. Analytical solution of a refined shear deformation theory for rectangular composite plates. *International Journal of Solids and Structures* 1987; **23**:1447-1463.

[51] Auricchio F, Sacco E. Partial-mixed formulation and refined models for the analysis of composite laminates within an FSDT. *Composite Structures* 1999; **46**:103-113.

[52] Fares ME. Non-linear bending analysis of composite laminated plates using a refined first-order theory. *Composite Structures* 1999; **46**:257-266.

[53] Reddy JN. On computational models for composite laminates. *International Journal of Numerical Methods in Engineering* 1989; **27**:361-382.

[54] Noor AK, Burton WS, Bert CW. Computational models for sandwich panels and shells. *Applied Mechanics Reviews* 1996; **49**:155-199.

[55] Carrera E. Developments, ideas and evaluations based upon the Reissner's mixed variational theorem in the modelling of multilayered plates and shells. *Applied Mechanics Reviews* 2001; **54**:301-330.

[56] Carrera E, Demasi L, Manganello M. Assesment of plate elements on bending and vibrations of composite structures. *Mechanics of Advanced Materials and Structures* 2002; **9**:333-357.

[57] Reddy JN. *Energy Principles and Variational Methods in Applied Mechanics* (2nd edn). John Wiley: New York, 2002.

[58] Hughes TJR, Tezduyar TE. Finite elements based upon Mindlin plate theory with particular reference to four-node bilinear isoparametric element. *Journal of Applied Mechanics* 1981; **48**:587-596.

[59] Briossilis D. The C^0 structural finite elements reformulated. *International Journal of Numerical Methods in Engineering* 1993; **36**:541-561.

[60] Carrera E. C^0 Reissner-Mindlin multilayered plate elements including zig-zag and interlaminar stress continuity. *International Journal of Numerical Methods in Engineering* 1996; **39**:1797-1820.

[61] Putcha NS. A mixed shear flexible finite element for geometrically nonlinear analysis of laminated plates. *PhD Dissertation*, Texas AM University, College Station, TX, 1984.

[62] Herrmann LR. Finite element bending analysis of plates. *Journal of Engineering Mechanics Division,ASCE* 1967; **93**:13-26.

[63] Hellan K. Analysis of elastic plates in flexure by simplified finite element method. *Acta Polytechnica Scandinavica – Civil Engineering and Building Construction*

Series 1967; **46**.

[64] Morley LSD. A triangular equilibrium element with linear varying bending moments for plate bending problems. *Journal of the Royal Aeronautical Society* 1967; **71**:715-719.

[65] Cook RD. Eigenvalue problems with a mixed plate element. *AIAA Journal* 1969; **7**:982-983.

[66] Visser W. A refined mixed type plate bending element. *AIAA Journal* 1969; **7**:1801-1802.

[67] Mau ST, Tong P, Pian TH. Finite element solutions for laminated thick plates. *Journal of Composite Materials* 1972; **6**:304-311.

[68] Reddy JN, Tsay CS. Stability and vibration of thin rectangular plates by simplified mixed finite elements. *Journal of Sound and Vibrations* 1977; **55**:289-302.

[69] Tsay CS, Reddy JN. Bending, stability and free vibration of thin orthotropic plates by simplified mixed finite elements. *Journal of Sound and Vibrations* 1977; **59**:307-311.

[70] Putcha NS, Reddy JN. A mixed shear flexible finite element for the analysis of laminated plates. *Computers Methods in Applied Mechanics and Engineering* 1984; **44**:213-227.

[71] Pinsky PM, Jasti RV. A mixed finite element for laminated composite plates based on the use of bubble functions. *Engineering Computations* 1989; **6**:316-330.

[72] Bathe KJ, Dvorkin EN. A four-node plate bending element based on Mindlin/Reissner plate theory and mixed interpolation. *International Journal for Numerical Methods in Engineering* 1985; **21**:367-383.

[73] Pontaza JP, Reddy JN. Mixed plate bending elements based on least-squares formulation. *International Journal for Numerical Methods in Engineering* 2004; **60**:891-922.

[74] Auricchio F, Sacco E, Vairo G. A mixed FSDT finite element for monoclinic laminated plates. *Computers and Structures* 2006; **84**:624-639.

[75] Auricchio F, Sacco E. A mixed-enhanced finite element for the analysis of laminated composite plates. *International Journal for Numerical Methods in Engineering* 1999; **44**:1481-1504.

[76] Putcha NS, Reddy JN. A refined mixed shear flexible finite element for the nonlinear analysis of laminated plates. *Computers and Structures* 1986; **22**:529-538.

[77] Singh G, Venkateswara G, Iyengar NGR. Nonlinear bending of thin and thick unsymmetrically laminated composite beams using refined finite element model. *Computers and Structures* 1992; **42**:471-479.

[78] Babuska I. The p and h-p versions of the finite element method. The state of the art. *Finite Elements: Theory and Application*, Dwoyer, DL, Hussaini, MY, Voigt, RG (eds), Springer-Verlag: New York, 1988.

[79] Chinosi C, Sacchi G, Scapolla T. Hierarchic conforming elements for plate bending problems. *Computational Mechanics* 1991; **8**:181-191.

[80] Scapolla T, Della Croce L. Hierarchic and mixed-interpolated finite elements for Reissner-Mindlin problems. *Communications in Numerical Methods in Engineering* 1995; **11**:549-562.

[81] Bisshop KE, Drucker DC. Large deflections of cantilever beams. *Quarterly of Applied Mathematics* 1945; **3**:272-275.

[82] Rohde FV. Large deflections of a cantilever beam with uniformly distributed load. *Quarterly of Applied Mathematics* 1953; **11**:337-338.

[83] Levy S. Square plate with clamped edges under normal pressure producing large deflections. *Tech. Report, National Advisory Committee for Aeronautics*, Washington, DC, 1942.

[84] Zaghloul SA, Kennedy JB. Nonlinear behavior of symmetrically laminated plates. *Journal of Applied Mechanics* 1975; **42**:234-236.

[85] Onate E, Zarate F. Rotation-free triangular plate and shell elements. *International Journal for Numerical Methods in Engineering* 2000; **47**:557-603.

[86] Rankin CC, Brogan FA. An element independent corotational procedure for the treatment of large rotations. *ASME J. Pressure Vessel Technology* 1986; **108**:165-174.

APPENDIX A

COROTATIONAL FORMULATION OF PLATE BENDING ELEMENTS

Extension of the present formulation to the analysis of plate elements will further demonstrate the numerical accuracy and computational efficiency of the co-rotational technique. In order to simplify the co-rotational formulations previously reported in the literature, a rotation-free linear triangular thin plate, developed by Onate and Zarate [85] can be incorporated into the derivation. The aforementioned plate element has three deflections as the only nodal degrees of freedom, resulting in a very simple and inexpensive element. Certain refinements and extensions may be worth pursuing along the course of future research, namely, the derivation of a co-rotational shell element and the inclusion of laminated composite materials into the constitutive model.

Consider an individual plate element as shown in Figure 51. The undeformed configuration of the element is denoted by C_0 whereas the deformed configuration is denoted by C_n. For a triangular plate element, the x-y plane is taken as the plane that passes through the three corner nodes. The origin is chosen to be the centroid of the element. The x-axis coincides with the line joining the local 1-2 edge (see [3,86]). The z-axis is the normal to the plane and the remaining axis defines a cartesian right-handed system. Thus, the local frame in the undeformed configuration is defined by the triad $(\tilde{\mathbf{i}}_1, \tilde{\mathbf{i}}_2, \tilde{\mathbf{i}}_3)$ as follows

$$\tilde{\mathbf{i}}_1 = \frac{\mathbf{x_2^0} - \mathbf{x_1^0}}{\mid \mathbf{x_2^0} - \mathbf{x_1^0} \mid} \tag{A.1}$$

$$\tilde{\mathbf{v}}_2 = \frac{\mathbf{x_3^0} - \mathbf{x_1^0}}{\mid \mathbf{x_3^0} - \mathbf{x_1^0} \mid} \tag{A.2}$$

$$\tilde{\mathbf{i}}_3 = \tilde{\mathbf{i}}_1 \times \tilde{\mathbf{v}}_2 \tag{A.3}$$

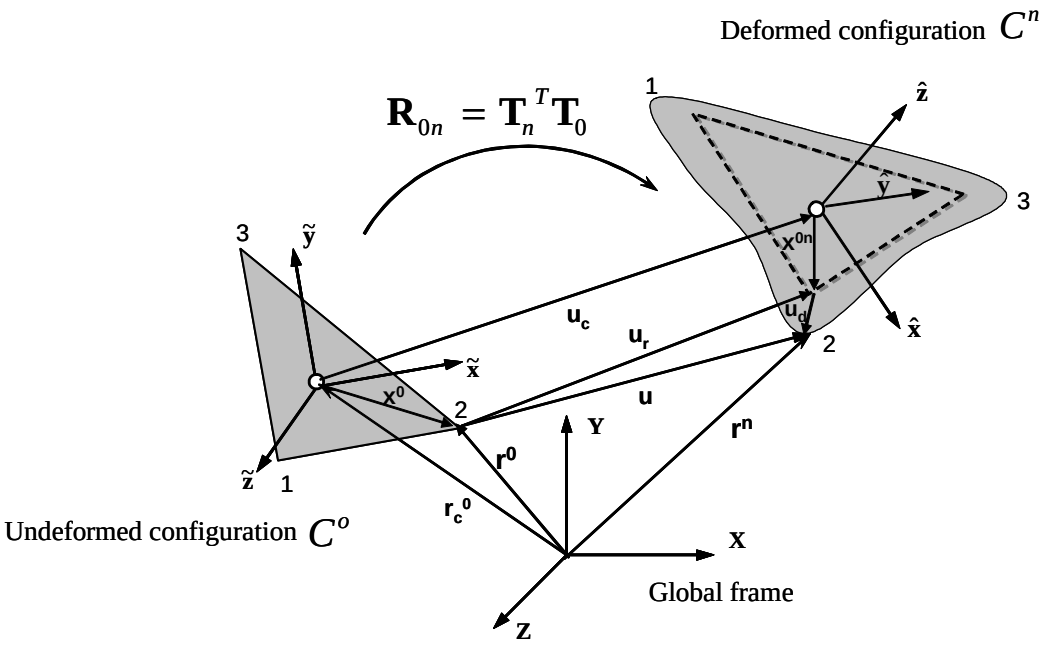

Fig. 51. Undeformed and deformed configurations of a triangular plate element in a co-rotated frame.

$$\tilde{\mathbf{i}}_2 = \tilde{\mathbf{i}}_3 \times \tilde{\mathbf{i}}_1 \tag{A.4}$$

where the superscript 0 refers to quantities measured in the undeformed reference configuration. The transformation of a vector $\mathbf{x}$ referred to the global system to the same vector expressed in the initial local system can be written

$$\tilde{\mathbf{x}} = \mathbf{T}_0 \mathbf{x} \tag{A.5}$$

where

$$\mathbf{T_0} = \left\{ \begin{array}{c} \tilde{\mathbf{i}}_1^T \\ \tilde{\mathbf{i}}_2^T \\ \tilde{\mathbf{i}}_1^T \end{array} \right\} \tag{A.6}$$

Similarly, the the local frame in the deformed configuration is defined by the triad

$(\hat{\mathbf{i}}_1, \tilde{\hat{i}}_2, \hat{\mathbf{i}}_3)$ as follows

$$\hat{\mathbf{i}}_1 = \frac{\mathbf{x_2^n} - \mathbf{x_1^n}}{\mid \mathbf{x_2^n} - \mathbf{x_1^n} \mid} \tag{A.7}$$

$$\hat{\mathbf{v}}_2 = \frac{\mathbf{x_3^n} - \mathbf{x_1^n}}{\mid \mathbf{x_3^n} - \mathbf{x_1^n} \mid} \tag{A.8}$$

$$\hat{\mathbf{i}}_3 = \hat{\mathbf{i}}_1 \times \hat{\mathbf{v}}_2 \tag{A.9}$$

$$\hat{\mathbf{i}}_2 = \hat{\mathbf{i}}_3 \times \hat{\mathbf{i}}_1 \tag{A.10}$$

In this case, the transformation of a vector $\mathbf{x}$ to the local deformed system is defined by

$$\hat{\mathbf{x}} = \mathbf{T}_n \mathbf{x} \tag{A.11}$$

where

$$\mathbf{T_n} = \left\{ \begin{array}{c} \hat{\mathbf{i}}_1^T \\ \hat{\mathbf{i}}_2^T \\ \hat{\mathbf{i}}_1^T \end{array} \right\} \tag{A.12}$$

The corresponding transformation of a vector from the initial or reference configuration to the deformed configuration is defined by the rotation tensor $\mathbf{R}_{0n}$. It can be shown that

$$\mathbf{R}_{0n} = \mathbf{T}_n^T \mathbf{T}_0 \tag{A.13}$$

Consider node 2 of the triangular plate of Figure 51 that moves from the initial position $\mathbf{r}^0$ to its deformed position $\mathbf{r}^n$. The nodal displacement vector is given by

$$\mathbf{u} = \mathbf{r}^n - \mathbf{r}^0 \tag{A.14}$$

This displacement can be split, in accordance with the co-rotational approach, into a rigid body and a deformational component

$$\mathbf{u} = \mathbf{u}_r + \mathbf{u}_d \tag{A.15}$$

The rigid body displacement $\mathbf{u}_r$ and the deformational displacement $\mathbf{u}_d$ are given by the following relations

$$\begin{aligned} \mathbf{u}_r &= \mathbf{r}^{0n} - \mathbf{r}^0 \\ \mathbf{u}_d &= \mathbf{r}^n - \mathbf{r}^{0n} \end{aligned} \tag{A.16}$$

where

$$\begin{aligned} \mathbf{r}_0 &= \mathbf{r}_c^0 + \mathbf{x}^0 \\ \mathbf{r}_{0n} &= \mathbf{r}_c^0 + \mathbf{u}_c + \mathbf{R}_{0n}\mathbf{x}^0 \end{aligned} \tag{A.17}$$

The position vector $\mathbf{x}^0$ contains the coordinates of the node in the initial configuration relative to the element centroid. Combining these equations gives

$$\mathbf{u}_d = \mathbf{u} - \mathbf{u}_c - (\mathbf{R}_{0n} - \mathbf{I})\mathbf{x}^0 \tag{A.18}$$

The deformational translation referred to the local co-rotated coordinate system becomes

$$\hat{\mathbf{u}}_d = \mathbf{T}_n \mathbf{u}_d \tag{A.19}$$

Let us consider the plate of Figure 51 in the deformed co-rotated configuration. The functional for this problem can be written as the algebraic sum of the strain energy U stored in the body and the work V done by the external forces on the body

$$\Pi = U - V \tag{A.20}$$

where

$$U = \int_\Omega \left[\frac{1}{2} \left(\hat{\boldsymbol{\kappa}}^T \mathbf{D} \hat{\boldsymbol{\kappa}} + \hat{\boldsymbol{\epsilon}}^{0^T} \mathbf{A} \hat{\boldsymbol{\epsilon}}^0 \right) + (\mathbf{L}\hat{w} - \hat{\boldsymbol{\kappa}})^T \hat{\mathbf{m}} + \left(\mathbf{L}^0 \hat{\mathbf{u}}^0 - \hat{\boldsymbol{\epsilon}}^0 \right)^T \hat{\mathbf{f}}^0 \right] d\hat{x} d\hat{y}$$

where $\hat{\boldsymbol{\kappa}}$ is the vector of bending curvatures, $\hat{\mathbf{m}}$ is the vector of bending moments, and vectors $\hat{\epsilon}^0$ and $\hat{\mathbf{f}}^0$ are their membrane related counterparts, respectively. Kirchhoff's

hypothesis are assumed to hold so that the following relations are valid

$$\hat{\boldsymbol{\kappa}} = \mathbf{L}\hat{w}, \quad \hat{\mathbf{m}} = \mathbf{D}\hat{\boldsymbol{\kappa}} \tag{A.21}$$

$$\mathbf{L} = \left[-\frac{\partial^2}{\partial \hat{x}^2}, -\frac{\partial^2}{\partial \hat{y}^2}, -2\frac{\partial^2}{\partial \hat{x}\partial \hat{y}} \right]^T \tag{A.22}$$

Similarly, for the in-plane terms we have

$$\hat{\boldsymbol{\epsilon}}^0 = \mathbf{L}^0\hat{\mathbf{u}}^0, \quad \hat{\mathbf{f}}^0 = \mathbf{A}\hat{\boldsymbol{\epsilon}}^0 \tag{A.23}$$

$$\mathbf{L}^0 = \begin{bmatrix} \dfrac{\partial}{\partial \hat{x}} & 0 \\ 0 & \dfrac{\partial}{\partial \hat{y}} \\ \dfrac{\partial}{\partial \hat{y}} & \dfrac{\partial}{\partial \hat{x}} \end{bmatrix} \tag{A.24}$$

with the in-plane displacement vector defined as $\hat{\mathbf{u}}^0 = [\hat{u}, \hat{v}]^T$ and the extensional stiffness matrix, $\mathbf{A}$, and bending stiffness matrix, $\mathbf{D}$, for an isotropic material defined as

$$\mathbf{A} = \frac{Eh}{(1-\nu^2)} \begin{bmatrix} 1 & \nu & 0 \\ \nu & 1 & 0 \\ 0 & 0 & \dfrac{1-\nu}{2} \end{bmatrix}, \quad \mathbf{D} = \frac{Eh^3}{12\,(1-\nu^2)} \begin{bmatrix} 1 & \nu & 0 \\ \nu & 1 & 0 \\ 0 & 0 & \dfrac{1-\nu}{2} \end{bmatrix} \tag{A.25}$$

where E and ν are the Young's modulus and Poisson's ratio, respectively, and h is the thickness of the plate. Taking the first variation of the functional in Eq. A.20 and equating the result to zero, the following set of governing equations is obtained

Constitutive equations

$$\int_\Omega \left[\delta\hat{\boldsymbol{\kappa}}^T \left(\mathbf{D}\hat{\boldsymbol{\kappa}} - \hat{\mathbf{m}} \right) + \delta\hat{\boldsymbol{\epsilon}}^{0^T} \left(\mathbf{A}\hat{\boldsymbol{\epsilon}}^0 - \hat{\mathbf{f}}^0 \right) \right] d\hat{x}d\hat{y} = 0 \tag{A.26}$$

Strain-displacement equations

$$\int_\Omega \left[\delta\hat{\mathbf{m}}^T \left(\mathbf{L}\hat{w} - \hat{\boldsymbol{\kappa}} \right) + \delta\hat{\mathbf{f}}^{0^T} \left(\mathbf{L}^0\hat{\mathbf{u}}^0 - \hat{\boldsymbol{\epsilon}}^0 \right) \right] d\hat{x}d\hat{y} = 0 \tag{A.27}$$

Equilibrium equations

$$\int_{\Omega} \left[(\mathbf{L}\delta\hat{w})^T \hat{\mathbf{m}} + \left(\mathbf{L}^0 \delta\hat{\mathbf{u}}^0\right)^T \hat{\mathbf{f}}^0 - \delta V \right] d\hat{x}d\hat{y} = 0 \tag{A.28}$$

The virtual work δV done by the distributed transverse load q, the in-plane normal stress $\hat{\sigma}_{nn}$, in-plane tangential stress $\hat{\sigma}_{ns}$, and transverse shear stress $\hat{\sigma}_{nz}$ is given by

$$\delta V = \int_{\Omega} q\delta\hat{w}d\hat{x}d\hat{y} + \oint_{\Gamma} \int_{-\frac{h}{2}}^{\frac{h}{2}} \left[\hat{\sigma}_{nn}\delta\hat{u}_n + \hat{\sigma}_{ns}\delta\hat{u}_s + \hat{\sigma}_{nz}\delta\hat{w}\right] dzds \tag{A.29}$$

where $\hat{u}_n$, $\hat{u}_s$ and $\hat{w}$ are the displacements along the normal, tangential and transverse directions in the co-rotated frame, respectively.

Equations (A.26)-(A.28) are the basis of the finite element/finite volume discretization to be presented next.

Let us consider an arbitrary discretization of the plate into standard three-node triangles, as shown in Figure 52.

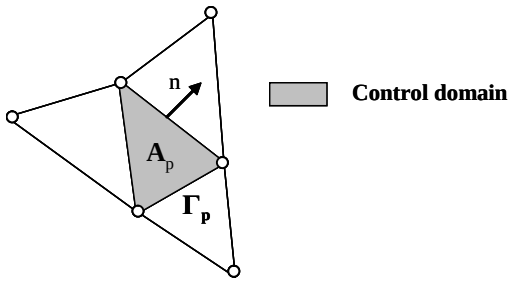

Fig. 52. Control volume scheme for the triangular plate.

The curvature and bending moments are described by constant field within appropriate non-overlapping control domains. The constant curvature and bending moments within each control domain are expressed in terms of the nodal transverse

displacements. From the bending terms of Eqs. (A.26) and (A.27) it follows that

$$\hat{\mathbf{m}}_p = \mathbf{D}_p \hat{\boldsymbol{\kappa}}_p \tag{A.30}$$

$$\hat{\boldsymbol{\kappa}}_p = \frac{1}{A_p} \int_{\Gamma_p} \mathbf{T} \nabla \hat{w} d\Gamma \tag{A.31}$$

where subscript 'p' refers to the p-th control domain, $\mathbf{D}_p$ is the average constitutive matrix over a control domain and

$$\mathbf{T} = \begin{bmatrix} 0 & -n_{\hat{x}} \\ -n_{\hat{y}} & 0 \\ -n_{\hat{x}} & -n_{\hat{y}} \end{bmatrix}, \quad \nabla = \begin{Bmatrix} \dfrac{\partial}{\partial \hat{x}} \\ \\ \dfrac{\partial}{\partial \hat{y}} \end{Bmatrix} \tag{A.32}$$

Applying the Divergence Theorem to the bending term of Eq. (A.28) and substituting Eqs. (A.30) and (A.31) in the resulting expression, gives

$$\sum_p \left(\int_{\Gamma_p} [\mathbf{T} \nabla \hat{w}]^T d\Gamma \right) \frac{1}{A_p} \mathbf{D}_p \int_{\Gamma_p} \mathbf{T} \nabla \hat{w} d\Gamma + \int_{\Omega} \left[\left(\mathbf{L}^0 \delta \hat{\mathbf{u}}^0 \right)^T \hat{\mathbf{f}}^0 - \delta V \right] d\hat{x} d\hat{y} = 0 \tag{A.33}$$

The final step is to discretize the displacement field. Both transverse displacements and in-plane displacements are interpolated using standard linear Lagrangian functions.

$$u = \sum_{i=1}^{3} N_i u_i \tag{A.34a}$$

$$v = \sum_{i=1}^{3} N_i v_i \tag{A.34b}$$

$$w = \sum_{i=1}^{3} N_i w_i \tag{A.34c}$$

Substituting Eq. (A.34a) into (A.33) gives the final system of algebraic equations in the co-rotated system

$$\hat{\mathbf{K}}^e \hat{\mathbf{u}}^e = \hat{\mathbf{f}}^e \tag{A.35}$$

where the vector $\hat{\mathbf{u}}^e$ contains the nodal displacements of the element. The components of the nodal force vector $\hat{\mathbf{f}}^e$ in equation A.35 are then transformed into the global coordinate system via the transformation matrix $\mathbf{T}_n$.

$$\mathbf{f}^e = \mathbf{T}_n^T \hat{\mathbf{f}}^e \tag{A.36}$$

The global stiffness matrix is obtained by assembling the stiffness contributions from the different finite elements. The resulting nonlinear system of equations can be solved by a Newton-Raphson procedure. A flow chart for the co-rotational procedure applied to the plate elements is presented in Figure 53.

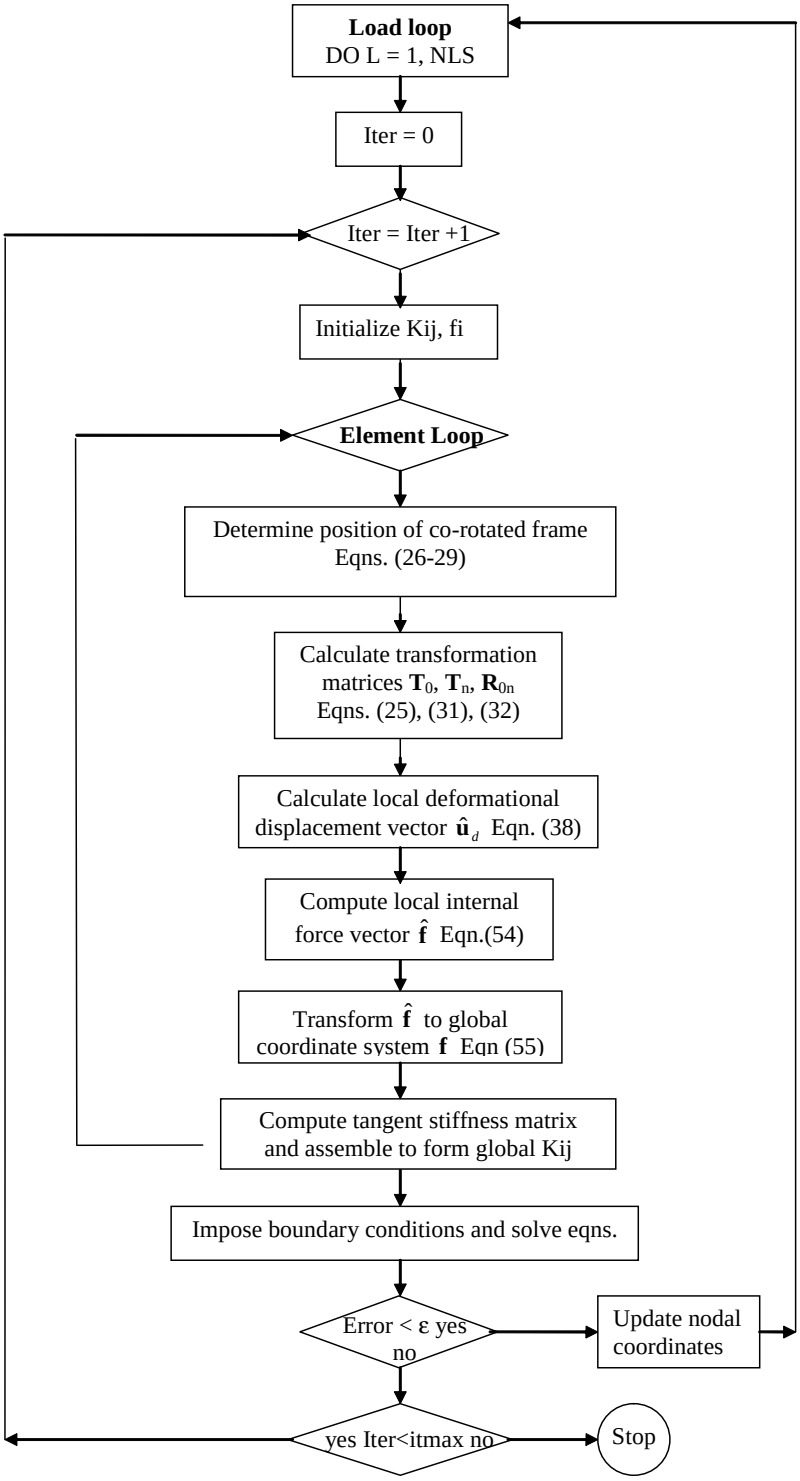

Fig. 53. A computer flow chart for the nonlinear co-rotational finite element analysis of rotation-free plates.

VITA

Yetzirah Yksya Urthaler Lapeira
Department of Mechanical Engineering
c/o Dr. J.N. Reddy
Texas A& M University
College Station, TX 77843-3123

The author was born in Caracas, Venezuela. She completed her high-school at Liceo Parroquial Nuestra Senora del Rosario, Venezuela. In 1990 she joined Universidad Simon Bolivar, Venezuela, and graduated with honors as a Mechanical Engineer in 1995 and a B.S. degree. After that, she served for six years as a Faculty member in the Department of Mechanical Engineering at Universidad Simon Bolivar. She obtained her Master of Science in Mechanical Engineering in 2000 from the same school. In January 2002, she joined the Department of Mechanical Engineering at Texas A&M University . She received a Doctor of Philosophy degree in May 2007. During the course of her graduate studies, she worked as a Teaching and Research Assistant under the supervision of Dr. JN Reddy. She is member of the American Society of Mechanical Engineers, the Society of Women Engineers and the Honor Society Phi Kappa Phi. After graduation, she would like to pursue an academic career.